CANADIAN THESES ON MICROFICHE

THÈSES CANADIENNES SUR MICROFICHE

National Library of Canada
Collections Development Branch

Canadian Theses on
Microfiche Service

Ottawa, Canada
K1A 0N4

Bibliothèque nationale du Canada
Direction du développement des collections

Service des thèses canadiennes
sur microfiche

NOTICE

The quality of this microfiche is heavily dependent upon the quality of the original thesis submitted for microfilming. Every effort has been made to ensure the highest quality of reproduction possible.

If pages are missing, contact the university which granted the degree.

Some pages may have indistinct print especially if the original pages were typed with a poor typewriter ribbon or if the university sent us an inferior photocopy.

Previously copyrighted materials (journal articles, published tests, etc.) are not filmed.

Reproduction in full or in part of this film is governed by the Canadian Copyright Act, R.S.C. 1970, c. C-30. Please read the authorization forms which accompany this thesis.

AVIS

La qualité de cette microfiche dépend grandement de la qualité de la thèse soumise au microfilmage. Nous avons tout fait pour assurer une qualité supérieure de reproduction.

S'il manque des pages, veuillez communiquer avec l'université qui a conféré le grade.

La qualité d'impression de certaines pages peut laisser à désirer, surtout si les pages originales ont été dactylographiées à l'aide d'un ruban usé ou si l'université nous a fait parvenir une photocopie de qualité inférieure.

Les documents qui font déjà l'objet d'un droit d'auteur (articles de revue, examens publiés, etc.) ne sont pas microfilmés.

La reproduction, même partielle, de ce microfilm est soumise à la Loi canadienne sur le droit d'auteur, SRC 1970, c. C-30. Veuillez prendre connaissance des formules d'autorisation qui accompagnent cette thèse.

THIS DISSERTATION
HAS BEEN MICROFILMED
EXACTLY AS RECEIVED

LA THÈSE A ÉTÉ
MICROFILMÉE TELLE QUE
NOUS L'AVONS REÇUE

Canada

NL 339 (r. 85/09)

0-315-19543-6

National Library of Canada | Bibliothèque nationale du Canada

Canadian Theses Division | Division des thèses canadiennes

Ottawa, Canada
K1A 0N4

201

67451

PERMISSION TO MICROFILM — AUTORISATION DE MICROFILMER

• Please print or type — Écrire en lettres moulées ou dactylographier

Full Name of Author — Nom complet de l'auteur

Elizabeth Anne Stubley

Date of Birth — Date de naissance	Country of Birth — Lieu de naissance
28 July 1956	Canada

Permanent Address — Résidence fixe

9-7604 29 Ave.,
Edmonton, Alberta,
T6K 3X2.

Title of Thesis — Titre de la thèse

A Fourier Transform Spectrometer as a Measurement System for Emission From an Inductively Coupled Plasma.

University — Université

University of Alberta

Degree for which thesis was presented — Grade pour lequel cette thèse fut présentée

Ph.D.

Year this degree conferred — Année d'obtention de ce grade	Name of Supervisor — Nom du directeur de thèse
1983	Dr. G. Horlick

Permission is hereby granted to the NATIONAL LIBRARY OF CANADA to microfilm this thesis and to lend or sell copies of the film.

The author reserves other publication rights, and neither the thesis nor extensive extracts from it may be printed or otherwise reproduced without the author's written permission.

L'autorisation est, par la présente, accordée à la BIBLIOTHÈQUE NATIONALE DU CANADA de microfilmer cette thèse et de prêter ou de vendre des exemplaires du film.

L'auteur se réserve les autres droits de publication; ni la thèse ni de longs extraits de celle-ci ne doivent être imprimés ou autrement reproduits sans l'autorisation écrite de l'auteur.

Date	Signature
22 August 1983	Elizabeth Anne Stubley

NL-91 (4/77)

THE UNIVERSITY OF ALBERTA

A FOURIER TRANSFORM SPECTROMETER AS A MEASUREMENT SYSTEM FOR EMISSION FROM AN INDUCTIVELY COUPLED PLASMA

by

(C) ELIZABETH ANNE STUBLEY

A THESIS

SUBMITTED TO THE FACULTY OF GRADUATE STUDIES AND RESEARCH

IN PARTIAL FULFILMENT OF THE REQUIREMENTS FOR THE DEGREE

DOCTOR OF PHILOSOPHY

DEPARTMENT OF CHEMISTRY

EDMONTON, ALBERTA

FALL 1983

THE UNIVERSITY OF ALBERTA

RELEASE FORM

NAME OF AUTHOR ELIZABETH ANNE STUBLEY

TITLE OF THESIS A FOURIER TRANSFORM SPECTROMETER AS A MEASUREMENT SYSTEM FOR EMISSION FROM AN INDUCTIVELY COUPLED PLASMA

DEGREE FOR WHICH THESIS WAS PRESENTED Ph.D.

YEAR THIS DEGREE GRANTED 1983

Permission is hereby granted to THE UNIVERSITY OF ALBERTA LIBRARY to reproduce single copies of this thesis and to lend or sell such copies for private, scholarly or scientific research purposes only.

The author reserves other publication rights, and neither the thesis nor extensive extracts from it may be printed or otherwise reproduced without the author's written permission.

(Signed) Elizabeth Anne Stubley

PERMANENT ADDRESS:

9-7604 29 Avenue
Edmonton, Alberta
T6K 3X2

DATED August 15, 1983

THE UNIVERSITY OF ALBERTA

FACULTY OF GRADUATE STUDIES AND RESEARCH

The undersigned certify that they have read, and recommend to the Faculty of Graduate Studies and Research, for acceptance, a thesis entitled A FOURIER TRANSFORM SPECTROMETER AS A MEASUREMENT SYSTEM FOR EMISSION FROM AN INDUCTIVELY COUPLED PLASMA

submitted by ELIZABETH ANNE STUBLEY

in partial fulfilment of the requirements for the degree of DOCTOR OF PHILOSOPHY.

Gary Horlick
.....
G. Horlick, Supervisor

F. F. Cantwell
.....
F.F. Cantwell

A.H. Kalantar
.....
A.H. Kalantar

E. H. Pinnington
.....
E.H. Pinnington

.....
S. Pons

Thomas M. Niemczyk
.....
T.M. Niemczyk, External Examiner

DATE August 5, 1983

To Hillar

ABSTRACT

With the increasing prominence of the inductively coupled plasma (ICP), large amounts of spectrochemical information can be simultaneously obtained. Conventional measurement systems, including the direct reader and the scanning monochromator, are capable of measuring only a small portion of this information.

The Fourier transform spectrometer (FTS) with its excellent simultaneous multielement measurement capabilities, should allow more complete utilization of the spectrochemical information generated by the ICP. In this laboratory, a Michelson interferometer has been developed, over the past fifteen years, specifically for measurements in the ultraviolet and visible regions of the spectrum. As a tool for the measurement of emission from the ICP, both the qualitative and quantitative capabilities of the FTS system have been examined in this thesis.

The spectral characteristics of the ICP in the near-IR spectral region (0.7 to 3.0 μm) have been examined with the FTS as the measurement system. This region has previously been unexplored with the ICP and was found to have some usefulness for the analysis of nonmetals such as sulphur, carbon, oxygen and the halogens.

In the ultraviolet and visible spectral regions, containing most prominent emission lines for metals, the FTS measurement system was found to have excellent spectral response, ranging from the far ultraviolet, 180 nm, to the near-IR spectral region. However, quantitatively the FTS system is limited by dynamic range limitations and increased background noise due to other emission lines in the spectrum. To improve the quantitative abilities of FTS, a new instrument, a windowed slew-scan Fourier transform spectrometer (WSS-FTS), has been developed. This instrument consists of a slew-scanning monochromator with wide entrance and exit slits coupled to the Michelson interferometer. Accurate wavelength identification, resolution and simultaneous multielement measurement within a particular spectral window is provided by the interferometer while the monochromator provides a flexible method of selecting different spectral windows. Use of WSS-FTS reduces the dynamic range limitations imposed by strong emission lines and also reduces the signal-to-noise limitations.

With WSS-FTS as the measurement system, detection limits measured were found to be comparable to those measured with a commercial ICP instrument, available in this laboratory.

Windowed slew-scan Fourier transform spectromeery should prove to be a viable alternative to conventional measurement systems for emission from the ICP in the future.

ACKNOWLEDGEMENTS

I would like to extend my thanks and appreciation to Professor Gary Horlick for making this research an enjoyable experience. I would also like to thank Dr. Roger Ng and William Pettit for their help in the initial stages of this study. Special thanks are extended to Vassilios Karanassios whose help in understanding the AIM 65 was indispensable.

I acknowledge the efforts of the members of both the Electronics and Machine Shops whose help in the development of the instruments used in this thesis is appreciated.

To Annabelle Wiseman, for an excellent job in typing this thesis, I extend my appreciation.

Finally, financial assistance from the Department of Chemistry, University of Alberta, is gratefully acknowledged.

TABLE OF CONTENTS

CHAPTER		PAGE
I.	INTRODUCTION	1
	A. The Inductively Coupled Plasma	1
	B. The Ideal Spectrochemical Measurement System	3
	C. The Direct Reader	5
	D. The Slew-Scanning Monochromator	6
	E. Variations on the Direct Reader	8
	F. Variations on the Slew-Scanning Monochromator	11
	G. The Echelle Spectrometer	13
	H. ICP-MS	14
	I. Fourier Transform Spectroscopy	15
	1. Historical Background	16
	2. FTS - Advantages and Disadvantages	19
	J. Conclusion	29
II.	THE MICHELSON INTERFEROMETER: INSTRUMENTATION, DESCRIPTION AND MODIFICATIONS	31
	A. Introduction	31
	B. Data Acquisition	31
	C. New Mirror Drive System	34
	D. Microprocessor Generated Control Signals	39

CHAPTER PAGE

E. Optical Modifications..... 50

1. Detector Assembly..... 50

2. Mirrors..... 51

3. Beamsplitter Assembly..... 52

F. Laser Reference Channel..... 57

III. AN INVESTIGATION OF ICP EMISSION IN THE NEAR- AND MID-INFRARED SPECTRAL REGIONS..... 65

A. Introduction..... 65

B. The Experimental System..... 72

C. Results and Discussion..... 77

1. Aliasing..... 77

2. ICP Emission Spectra in the Near-IR.... 80

3. Spectra of Species Containing the Elements C, H, O and S..... 90

i) Sulphur Dioxide..... 90

ii) Xylene..... 94

iii) Dimethylsulphoxide (DMSO)..... 98

4. Halogen Containing Species..... 100

i) Chlorinated Hydrocarbons..... 101

ii) Dibromomethane..... 111

5. Metals..... 113

6. Mid-Infrared Region..... 113

D. Conclusions..... 117

CHAPTER		PAGE
IV.	SULPHUR ANALYSIS IN THE NEAR-IR REGION.....	121
	A. Introduction.....	121
	B. Experimental.....	123
	C. Results and Discussion.....	124
	D. Conclusions.....	131
V.	FTS IN THE ULTRAVIOLET AND VISIBLE SPECTRAL REGIONS	134
	A. Introduction.....	134
	B. Experimentation.....	135
	C. Results and Discussion.....	138
	1. Multielement Spectra.....	138
	2. Analytical Determination of Zinc in the Presence of Magnesium.....	148
	3. The Effect of Magnesium Concentration on the Standard Deviation of the Background Spectrum.....	153
	4. Detection Limits of the Multielement Solution.....	159
	D. Conclusions.....	163
VI.	WINDOWED SLEW-SCAN FOURIER TRANSFORM SPECTROMETRY.....	166
	A. Bandpass Limiting in the Interferometer....	166
	1. Optical Bandpass Limiting.....	167

CHAPTER PAGE

i) Sequential Optical Bandpass Limiting..... 167

ii) Simultaneous Optical Bandpass Limiting..... 168

iii) Random Access Optical Bandpass Limiting..... 169

B. The Monochromator as an Optical Bandpass Limiting Device..... 169

C. Windowed Slew-Scanning Capabilities..... 188

1. Emission from a Multielement Solution.. 188

2. Emission at Wavelengths Below 200 nm... 202

D. Background Subtraction with WSS-FTS..... 209

E. Effect of Mg on the Determination of Zinc.. 219

F. Quantitative Analysis with WSS-FTS..... 226

G. Conclusions..... 231

VII. SUMMARY 237

*****

FOOTNOTE..... 245

BIBLIOGRAPHY..... 246

APPENDIX A: AIM 65 CONTROL PROGRAM FOR THE INTERFEROMETER..... 256

LIST OF TABLES

TABLE		PAGE
1.	Cd hollow cathode lamp emission lines.....	55
2.	Cu, Zn, Sn, Pb hollow cathode lamp emission lines (above 240 nm).....	59
3.	Cu, Zn, Sn, Pb hollow cathode lamp emission lines (below 240 nm).....	60
4.	Plasma running conditions.....	73
5.	Interferometer opto-electronic components.....	75
6.	Major argon lines.....	83
7.	Atomic oxygen emission lines in the near-IR region.....	88
8.	Major nitrogen lines.....	91
9.	Major sulphur lines.....	93
10.	Major carbon lines.....	97
11.	Individual peaks of C-Cl fragment band.....	104
12.	Major atomic chlorine lines.....	106
13.	Bond lengths and force constants for several chloromethanes.....	110
14.	Major atomic bromine lines.....	114
15.	Major europium lines.....	116
16.	Potentially useful analytical lines	120
17.	Sulphur detection limits (ppm-S).....	129

TABLE PAGE

18. Emission lines observed in multielement spectrum with solar blind PMT..... 141
19. Emission lines in multielement spectra with 1P28 PMT..... 142
20. Emission lines observed in Zn and Mg spectrum... 149
21. Detection limits for zinc in the presence of magnesium..... 152
22. Standard deviations of the background as a function of magnesium concentration..... 157
23. Detection limits measured for the multielement solution..... 160
24. Detection limits measured with a commercial ICP instrument..... 162
25. Aliasing regions for ÷8 and ÷16 clocking rates..... 184
26. Emission lines measured by WSS-FTS..... 202
27. Emission lines observed below 200 nm..... 206
28. Standard deviations of the background as a function of magnesium concentration with WSS-FTS..... 225
29. Detection limits as measured with WSS-FTS..... 228
30. A comparison of detection limits obtained by conventional FTS and WSS-FTS..... 232

TABLE PAGE

31. Comparison between detection limits obtained by WSS-FTS and by a commercial ICP instrument... 234

LIST OF FIGURES

FIGURE		PAGE
1.	Block diagram of the Michelson interferometer system	32
2.	Schematic diagram of the Michelson interferometer	33
3.	Electronic diagram for the moving mirror drive system	36
4.	Laser analog signal under (a) PLL control (scope time base: 2 ms/division) and (b) new drive circuit control (scope time base: 0.5 ms/division)	38
5.	Schematic diagram of the control signals' timing sequence	41
6.	Schematic diagram of the AIM 65 control system	43
7.	Interferometer electronics with the AIM 65 and the PDP-11/10 computer	44
8.	Efficiency of the ultraviolet beamsplitter, as measured by its transmission characteristics	53
9.	Emission spectrum of a cadmium hollow cathode lamp	54

FIGURE PAGE

10. Emission spectrum of a multielement hollow cathode lamp containing the elements copper, lead, tin and zinc..... 56

11. Expanded spectrum showing the wavelength region below 240 nm for the multielement hollow cathode lamp illustrated in Figure 10.... 58

12. Digitized interferogram of a He-Ne laser source..... 62

13. Partial spectrum obtained from the interferogram of the laser source illustrated in Figure 12..... 64

14. Block diagram of the ICP-Fourier transform spectrometer system..... 76

15. Schematic spectrum of the near infrared spectral region: (a) the unaliased spectrum and (b) the aliased spectrum..... 79

16. Spectrum of background emission from the argon ICP as measured by the PbS detector..... 81

17. Spectrum of background emission from the argon ICP as measured by the PbSe detector..... 82

18. Emission spectrum of an ICP discharge using a tall torch..... 85

19. Spectrum of background emission from the 10% O_2/Ar ICP as measured by the PbS detector..... 87

FIGURE PAGE

20. Spectrum of background emission from the 30% N_2/Ar ICP as measured by the PbS detector..... 89

21. Emission spectrum of sulphur dioxide in the ICP..... 92

22. Emission spectrum of xylene in the ICP as measured by the PbS detector..... 95

23. Emission spectrum of xylene in the ICP as measured by the PbSe detector..... 96

24. Emission spectrum of dimethylsulphoxide in the ICP..... 99

25. Emission spectrum of 100% dichloromethane in the ICP..... 102

26. Expanded portion of the CH_2Cl_2 spectrum of Figure 25 showing the region between 3500 and 4500 cm^{-1}..... 103

27. Emission spectrum of carbon tetrachloride in the ICP..... 107

28. Emission spectrum of dibromomethane in the ICP..... 112

29. Emission spectrum of a 10000 ppm Europium solution in the ICP..... 115

30. Spectrum of the sulphur triplet as measured by the PDA spectrometer..... 125

FIGURE PAGE

31. Calibration curve for sulphur as dimethylsulphoxide with the silicon photodiode as the detector..... 127

32. Emission spectrum of the multielement solution as measured by the solar blind PMT..... 139

33. Emission spectrum of the multielement solution as measured by the 1P28 PMT..... 140

34. Emission spectrum of a 100 ppm zinc and magnesium solution..... 146

35. Calibration curves for zinc in the presence of varying magnesium concentrations: (a) 0 ppm Mg, (b) 100 ppm Mg and (c) 500 ppm Mg..... 151

36. Standard deviations of the baseline point 116 as a function of magnesium concentration..... 156

37. Block diagram of the ICP-windowed slew-scan Fourier transform spectrometer measurement system..... 173

38. Throughput parameters in the interferometer..... 175

39. Emission spectra as measured by FTS and WSS-FTS: (a) multielement spectrum (Figure 32), (b) 214 nm window - 4096 point transform and (c) 214 nm window - 256 point transform..... 179

40. Windowed slew-scan capabilities of WSS-FTS..... 180

FIGURE PAGE

41. Emission spectra of the spectral windows: (a) 202 nm, (b) 215 nm and (c) 228 nm..... 190

42. Emission spectra of the 250 nm spectral window: (a) 4096 point transform and (b) 256 point transform..... 192

43. Emission spectra of the 259 nm window: (a) 256 point transform and (b) 4096 point transform..... 194

44. Emission spectra of the spectral windows: (a) 280 nm and (b) 285 nm..... 195

45. Emission spectra of the spectral windows: (a) 310 nm, (b) 308 nm and (c) 325 nm..... 197

46. Emission spectra of the 396 nm spectral window: (a) 2 mm slits and (b) 100 μm slits..... 199

47. Emission spectra of the spectral windows: (a) 455 nm, (b) 590 nm and (c) 766 nm..... 201

48. Emission spectrum of 10000 ppm phosphorus in the 185 nm spectral window..... 205

49. Emission spectra of DMSO in the spectral windows: (a) 193 nm, (b) 190 nm, (c) 180 nm and (d) 922 nm..... 207

50. Background subtraction of the hydroxyl band in the 325 nm window: (a) unsubtracted

FIGURE PAGE

spectrum, (b) background spectrum and (c) subtracted spectrum..... 211

51. Background subtraction in the 250 nm spectral window: (a) unsubtracted spectrum, (b) background spectrum and (c) subtracted spectrum..... 213

52. Background subtraction in the 215 nm spectral window, 4096 point spectra: (a) unsubtracted spectrum, (b) background spectrum and (c) subtracted spectrum..... 215

53. Background subtraction in the 215 nm spectral window, 256 point spectra: (a) subtracted spectrum and (b) unsubtracted spectrum..... 217

54. Background subtraction in the 231 nm spectral window: (a) unsubtracted spectrum, (b) background spectrum and (c) subtracted spectrum..... 218

55. Zero-order emission spectrum of a 100 ppm zinc and magnesium solution..... 220

56. Emission spectrum of a 100 ppm zinc and magnesium solution in the 214 nm spectral window..... 221

57. Standard deviations of the baseline point 116 in the presence of varying magnesium

FIGURE PAGE

concentrations: (a) without monochromator and (b) with monochromator..... 223

58. Schematic diagram of a WSS-FTS instrument with a modified monochromator..... 242

59. Schematic diagram of a WSS-FTS instrument incorporating only a grating and collimating optics..... 243

60. Flow chart for the initial portion of the program to generate the control signals for the PDP-11/10..... 258

61. Flow chart for the program used to generate the control signals for the PDP-11/10..... 259

CHAPTER I

INTRODUCTION

A. The Inductively Coupled Plasma

Since the first commercial instrument was introduced in 1974 [1], the inductively coupled plasma (ICP) has steadily increased in prominence as a source for atomic spectrochemical measurement systems. Although the mechanisms of excitation and of other processes occurring in the ICP are not completely understood [2-6], the characteristics and analytical usefulness of the ICP have been well documented [7-10]. Its high temperatures [2,11,12], in the range of 6000 K, and unique energetics allow the excitation from the ground state to higher energy states for most elements. The temperature in the plasma is sufficiently high to ensure complete dissociation of almost all molecules introduced into the plasma and to prevent formation of metal oxides in the analytical viewing region, two of the most common interferences in flame spectroscopy [13,14]. In addition to the observation of neutral atom emission, it is possible to observe ion emission for some elements. The

ICP has good sensitivity for most elements, both metallic and non-metallic, and has a wide linear dynamic range, between five to six orders of magnitude change in concentration in most cases.

Until recently, one of the limitations of the ICP was that samples were restricted to those in solution form. Samples were introduced into the plasma as aqueous, or less frequently, organic aerosols. Several techniques have been developed to eliminate this problem. The first involves the use of a graphite rod electrothermal vaporization device to introduce either liquid [15] or solid [16] samples into the plasma. More novel approaches have involved laser vaporization of metallic solids [17] and direct insertion [18,19] into the ICP using standard DC arc graphite cups. The increased feasability for introducing solid samples into the ICP without pretreatment has extended considerably the range of possible applications.

The ICP is consequently capable of generating large quantities of spectrochemical information about a particular sample. A major branch of active research in the ICP area concerns the development of an optimum or "best" measurement system to analyze and process this spectrochemical information. The approach taken in this thesis has been to couple a Michelson interferometer-based

Fourier transform spectrometer (FTS) to the ICP. Before considering this type of spectrometer, a discussion of the ideal spectrochemical measurement system as it specifically pertains to the ICP, and of current measurement systems, is warranted.

B. The Ideal Spectrochemical Measurement System

The ideal spectrochemical measurement system is capable of providing quantitative and qualitative information for all elements simultaneously in any type of sample. Response should be linear at all concentration levels, be directly proportional to the concentration of each element and be independent of the sample matrix. In other words, the system should have a wide linear dynamic range for all spectral intensity measurements. Background subtraction is an important parameter for the ideal measurement system. Often there is matrix induced background emission at the wavelength of interest for an element. The measurement system should be able to measure emission intensity at the elemental line and at wavelengths around that line to be able to determine the presence of background emission problems. Resolution is another important characteristic of the ideal spectrochemical measurement system. Resolution should be sufficiently high to ensure natural linewidths. The

ability to change the resolution to suit the particular application would be a desirable characteristic of the ideal measurement system. This ability could be termed zoom resolution.

Because of the high excitation energies available in the ICP, spectral line interferences [20] are a major problem. Often it is not possible to obtain sufficient resolution to totally eliminate spectral overlaps. The ideal measurement system should therefore allow easy choice of an alternate analytical line for a particular element. Ideally, it should be possible to measure the emission intensity at any or several lines of a particular element. Often a tradeoff exists - a less sensitive emission line must be used to avoid spectral interferences at more sensitive lines for that element.

Although not of prime importance, time resolution is an advantageous characteristic of a measurement system, especially in the area of direct solid insertion into the ICP.

In addition to the above characteristics, it is desirable to have the ideal measurement system computerized in order to provide a permanent record of the desired spectrochemical information. Ideally, it should also be inexpensive and require minimal upkeep and maintenance.

Conventionally, two main approaches have been utilized to date: a) the direct reader and b) the scanning monochromator. Each system has its individual advantages and disadvantages.

C. The Direct Reader

With as many as 60 channels [21] on current direct reader measurement systems, its simultaneous multielement detection capabilities are unmatched. However, initial alignment of the instrument is usually performed in the factory and once the position of the exit slits and hence the wavelength for each channel has been determined, these positions are fixed. The choice of the analytical wavelength for each element, and indeed of the desired elements themselves, must be based on the type of sample that one expects to analyze. If a spectral overlap occurs, the analytical wavelength cannot be easily changed to eliminate or avoid the interference. Both background and analyte spectral information at wavelengths between the individual channels are difficult to measure. It is impossible to analyze for elements other than those initially programmed into the instrument. However, as mentioned earlier, up to 60 channels and consequently 60 wavelengths can be simultaneously measured. The number of channels in a direct reader is limited only by the number

of exit slits that can be physically positioned in the focal plane.

Although lacking in flexibility, the direct reader does have potential for time resolution and is invaluable for routine analysis.

D. The Slew-Scanning Monochromator

The slew-scanning monochromator system has no simultaneous multielement detection capabilities. In contrast to the direct reader, information over the entire wavelength region of interest can be measured by simply scanning the monochromator. There is no restriction on the number or type of elements that can be analyzed. The problem of spectral line interferences is less serious than for the direct reader since an alternate analytical wavelength for a particular element can be rapidly implemented. Only one wavelength can be monitored at a time, leading to an increased data acquisition period for a multielement analysis.

The biggest problem with the scanning monochromator is wavelength alignment. Wavelength scanning is accomplished by rotating the grating. The precision with which the grating can be positioned is limited by the mechanical drive that rotates the grating, necessitating wavelength alignment each time the grating is repositioned.

From an historical point of view, the spectrograph, which utilizes photographic plate detection, should be mentioned. Reading the plates is a very tedious procedure and fully quantitative results are difficult to obtain.

In initial research involving the ICP, the measurement system was almost exclusively the direct reader. In fact, until recently the direct reader, with its excellent simultaneous multielement analysis capabilities has dominated the field. In the last few years, however, the ability to rapidly and accurately change analytical wavelengths and to more fully utilize all available spectrochemical information has become increasingly important.

One trend, developed by commercial ICP instrument manufacturers, has been to incorporate a scanning monochromator as well as a direct reader into their instruments. In addition to the channels in the direct reader, then, one wavelength either for an alternate element or an alternate analytical wavelength for an identical element can be simultaneously measured.

Recently, several approaches to utilizing more fully the spectrochemical information available from the ICP have been developed. These include variations of the direct reader and of the slew-scanning monochromator as well as more novel approaches, for example, the coupling

of a mass spectrometer (MS) to the ICP and the FTS system developed in this laboratory.

E. Variations on the Direct Reader

Before actually examining variations on the direct reader measurement system, it is of interest to question why the direct reader, which was the work horse of industry for many years, is losing its position as the primary tool for the measurement of ICP emission intensities. Initially in most laboratories, only one type of analysis was performed. For example, in the metallurgical industry, the alloy content of steel is important. Once interference-free lines for elements of interest have been determined, there is little need to change wavelengths or to examine background emission at wavelengths other than that of the elemental lines. However, as the ICP gained in prominence, the range of applications also expanded. In an analytical laboratory, the sample types can be quite diverse, ranging from sea water with its high salt content, to digested coal or bitumen to blood or urine samples. The requirements for both standards and measurement conditions are dependent on the sample matrix and on the desired spectrochemical information. It has, therefore, become increasingly important to have a more flexible measurement system available.

As previously mentioned, one of the major limitations of the direct reader is its inability to measure emission intensities at wavelengths between the individual channels. This information is necessary to provide background matrix correction. Initial variations on the direct reader, therefore, have attempted to improve background correction, with some success.

The first change to the direct reader was the implementation of refractor plates in the focal plane to allow alternate measurement of the elemental line emission intensity and the emission intensities at wavelengths close to the elemental line. A further improvement to this system was the introduction of a moving entrance slit. By scanning the position of the entrance slit, it is possible to measure emission over a small spectral window centered around the analytical line of interest, facilitating background correction.

In an effort to provide alternate line selection, some researchers have modified the direct reader to include a relocatable output channel, commonly referred to as the roving detector. This output channel can be positioned at any point in the focal plane of the direct reader, enhancing the flexibility of the measurement system. An extension of the roving detector has led to the development of a rather impractical instrument by a

research group in South Africa [22]. This instrument, resembling an octopus, consists of the standard optical configuration for the direct reader. However, instead of the fixed exit slits and PMT assemblies of the conventional direct reader, the exit slits and PMT assemblies are mounted at the end of an individual arm or carriage. Each arm can then be positioned at any point in the focal plane. Positioning of each arm is time consuming and tedious. By moving one carriage through the focal plane, it is possible to use this instrument as a scanning monochromator. Although this instrument does perform analyses and does have the capability of checking for spectral interferences and of line selection, it would be impossible to produce this instrument on a large scale, both for complexity and financial considerations. It does illustrate the importance that is currently being placed on a very flexible measurement system.

More practically [23,24], a direct-reader measurement system has been developed in this laboratory that incorporates the capabilities of the conventional direct reader with the ability to choose alternate lines and to measure background spectrochemical information. In this system, the photomultiplier tubes have been replaced by several short linear silicon photodiode arrays (PDA's). The prototype has six 128 element PDA's mounted in a 1.5 m

spectrometer. Each array covers an approximately 1.7 nm window. If each element of the array is considered as a channel, a 768 channel direct reader has been developed. As well as spectral lines, information is provided on the spectral background and spectral interferences within the 1.7 nm window. Alternate line selection and background correction are thus greatly facilitated. The arrays must be fixed in the focal plane and the number of arrays is again limited by the number that can be physically positioned in the focal plane.

F. Variations on the Slew-Scanning Monochromator

Although the slew-scanning monochromator can measure emission intensity at any wavelength, it has no simultaneous multielement detection capabilities. Modifications to the slew-scanning monochromator have been aimed at improving these capabilities.

One approach has been to introduce multiple exit slits with a moving entrance slit into the monochromator, that is, approaching a direct reader-type system. This allows the measurement of more than one wavelength at a time. Scanning is accomplished by rotating the grating, as in the conventional slew-scanning monochromator, for large wavelength changes, while the moving entrance slit allows for positioning of the elemental line at each exit slit.

The introduction of electronic image sensors such as the silicon photodiode array [25,26] have prompted the development of windowed slew-scanning measurement instruments. When the PDA or other image sensor is positioned in the focal plane, simultaneous multielement detection is possible within the spectral window covered by the PDA. The width of the spectral window is dependent on the number of pixels in the array and on the focal length of the monochromator. Both background and analyte spectral information for the entire spectral window is more readily attained than for either the direct reader or the conventional monochromator. Scanning between different spectral windows is again accomplished by rotating the grating and consequently wavelength alignment is still a problem. An additional consideration is that the silicon photodiode array is a factor of ten less sensitive than the photomultiplier tubes normally used in direct readers and scanning monochromators.

Other windowed slew-scanning spectrometers, similar to the PDA spectrometer, have been developed. One instrument developed in Japan [27] incorporates a silicon intensified target (SIT) detector with a one meter monochromator. Multielement analysis is accomplished by rapidly scanning between 5 nm spectral windows. Precise wavelength alignment is provided under computer software

control using a mercury lamp and a stepper motor to achieve wavelengths other than those of the mercury lines.

G. The Echelle Spectrometer

The echelle spectrometer has seen limited use as a measurement system for ICP emission, although a commercial instrument based on the echelle is available. Both linear and area image sensors have proved useful for the echelle spectrometer. With a linear array, one spectral order can be measured simultaneously. The array can then be repositioned to measure a different order. Area sensors, for example the charge-coupled device [28,29], allow the simultaneous measurement of more than one spectral order. Currently, 256 by 256 element arrays (65536 pixels) are available. The trend, for the echelle spectrometer, has been to go to bigger and better image sensors - in the mega-pixel range [30]. Although this type of sensor has the capability of acquiring enormous amounts of information, the amount of memory space (even for 65536 pixels) required to store the information becomes quickly exorbitant. In addition, even at a high clocking rate, data acquisition is bound to be time-consuming.

H. ICP-MS

One of the most exciting and potentially useful instruments for measuring atomic spectrochemical information does not involve detection of optical emission from the ICP. Rather, the technique of mass spectrometry measures the concentration of the ions produced in the ICP by atomic weight rather than by emission wavelengths. The coupling of a quadropole mass spectrometer to an ICP was first proposed in 1975 by Gray [31]. Since its introduction, interest in the ICP-MS system has rapidly escalated [32-35]. A commercial instrument [35] was introduced at the 1983 Pittsburgh Conference of Analytical Chemistry and Applied Spectroscopy. This technique is exceptionally useful for two areas of analysis: 1) Isotope ratios can be directly and rapidly determined for elements in solution [36], greatly facilitating the technique of isotope dilution. Techniques currently in use are tedious and time consuming. With the ICP-MS system, isotope ratios can be determined in a matter of minutes.

2) Matrices with highly complex emission spectra produce much simpler spectra with the MS system. Consider, for example, the optical emission spectrum of steels. The spectrum is dominated by the emission lines of iron. The elimination of spectral line interferences

due to iron in the determination of trace elements in steel is difficult. However, with the use of the mass spectrometer, the spectrum of iron consists of a small number of lines for the different iron isotopes. The spectral interferences found in optical emission spectroscopy have virtually been eliminated with this system.

This technique is still in its infancy and holds great potential for enhancing the utility of the ICP as an analytical tool.

I. Fourier Transform Spectroscopy

Fourier transform spectroscopy is a viable alternative to the optical atomic emission measurement systems currently in use with the ICP. Although research in this area has been ongoing in this group for the last fifteen years [37-39], it is only in the last few years that other research groups have developed an interest in FTS in wavelength regions other than the mid- and far-infrared. Classically, the supposed S/N disadvantage, to be discussed in more detail in Chapter V, with the inteferometer in the UV and visible regions have discouraged researchers from exploring this area. Before discussing the merits and problems of FTS, with respect to the ICP in particular, a brief historical perspective of

FTS in the ultraviolet and visible spectral regions will be presented.

1. Historical Background

Historically, the Michelson inteferometer has been used, at wavelengths shorter than 1.0 μm, only to determine accurately the wavelength of a particular emission line [40-43]. In these applications, the incident light is monochromatic or at most, two wavelengths, one being used as a reference wavelength. In most of these applications, visibility curves, similar to the first work reported by Michelson [42,44] were measured. Wavelength differences could be determined from these curves and consequently, if the reference wavelength is accurately known, the wavelength of interest can be accurately determined. No Fourier transformations were performed.

For astronomical studies, in which the incident or source (atmospheric) radiation is weak [45,46], FTS has been used successfully to obtain molecular spectra of the atmosphere in the wavelength region 300 nm to 2 μm. Because of the weak incident radiation, interferometers have generally employed a stepping mechanism for driving the moving mirror. In this mode, the drive is moved forward one step, the signal at that point is then integrated over a period of time and the process is

repeated. High resolution, in the one meter optical path difference range, is required in atmospheric studies. Most interferometers used in these studies have either been designed by Connes [45] or are modified versions [46] of the Connes instrument. In this type of instrument, the optics have been designed so that the optical path difference is actually four times the mirror drive length. In other words, for a one meter optical path difference, the moving mirror only needs to move 25 cm. This simplifies design and construction of the moving mirror drive system.

Again using a step-and-integrate mode for the interferometer, Davis [47], in 1977, measured the reflectivity of several semiconductor surfaces in the visible region, using a tungsten lamp as the source. Difficulties were encountered in accurately and reproducibly driving the moving mirror. Although his group was successful in determining the reflectivity of several germanium surfaces, this line of research was not pursued.

Until 1982, with the exception of this research group, the few applications of FTS in the UV and visible regions were molecular in nature. However, in the last year, interest in utilizing the FTS as an atomic emission measurement system has begun to escalate. Buijs [48,49]

introduced at the 1983 Pittsburgh Conference a commercial FTS capable of determining wavelengths as short as 250 nm. To sample the interferogram, the frequency of the standard He-Ne laser reference for the interferometer has been multiplied by a factor of eight. In preliminary reports [48], the spectra of several hollow cathode lamps and of microwave discharge emission sources have been measured.

In addition, at the Kitt Peak National Observatory [50-53], an ICP has been coupled to a high resolution one meter FTS. This FTS system [50], originally designed for atmospheric measurements, is a modified version of the Connes interferometer. Both molecular emission [53], primarily NH, OH and cyanogen bands, and atomic emission spectra [51,52] were obtained for the wavelength region 290 nm to 2 μm. In order to view only a small spatial zone in the ICP, the image of the ICP was magnified by a factor of five before collimation. The high resolution of the instrument was more than sufficient to allow complete resolution of the emitted atomic spectral lines. Both natural linewidths and shapes were determined. In the ICP, natural linewidths are dominated by Doppler and Stark broadening [54]. It was reported that for atomic emission measurements with the ICP an optical path difference of approximately two cm would be sufficient to obtain natural line widths.

The results obtained, both with the Kitt Peak FTS and with the interferometer developed in this laboratory, demonstrate the usefulness of the FTS system in the UV and visible regions.

2. FTS - Advantages and Disadvantages

Before discussing FTS in the ultraviolet and visible regions of the spectrum, a brief description of FTS in the mid-infrared is warranted. Complete reviews of this area can be found in the literature [55,56]. Several factors play an important role in mid-infrared FTS. The first is the throughput advantage first described by Jacquinot [57], which arises from the fact that all light incident upon the interferometer is simultaneously detected. Consequently, in comparison with a monochromator with identical resolution, the signal observed at the detector will be greater in the interferometer system.

The ability to observe the whole spectral region of interest simultaneously with the FTS measurement system is unmatched by any of the direct reader or monochromator-based measurement systems. The spectral region measured is limited only by the detector response and the efficiency limits of the optical components of the interferometer. Additional restrictions, either by optical or electronic filtering of the incident radiation,

can be imposed to limit the observed spectral window. In addition to the simultaneous measurement capabilities, the resolution of the FTS system is determined ultimately only by the maximum optical path difference or distance the moving mirror in the interferometer has travelled. Unlike the direct reader or monochromator, the resolution of the instrument can be easily adapted to the application by changing the length of the mirror drive. The tradeoff involved is that the number of points in the acquired interferogram will increase as the resolution is increased and consequently so will the computation time and memory space necessary for the signal processing.

Wavelength accuracy, a large problem with both the monochromator and direct reader, is inherent in the interferometer. A very accurate and precise wavelength axis is provided by the He-Ne laser reference in the interferometer. The accuracy of this axis is limited only by the accuracy with which the wavelength of the laser, 0.6328 μm, is known, and by the alignment of the optics in the interferometer.

All of the above characteristics are directly transferable to FTS in the UV and visible regions of the spectrum. There is one other advantage, Fellgett's advantage, which is applicable in the mid-IR region, but whose application in the UV-visible region is questionable. Fellgett's advantage [55] arises in a

detector-noise limited situation, typical of detectors [58] utilized in the IR region. Fellgett's advantage states that in comparison to the scanning monochromator, a signal-to-noise (S/N) advantage exists for the interferometer that is proportional to the square root of the number of resolution elements in the spectrum. However, in the UV and visible spectral regions, the detector, usually a photomultiplier tube or photodiode, is not normally the noise limiting factor. With the ICP in this region, the noise limiting factor is either shot noise [59], for which there is neither a S/N advantage nor disadvantage, or source flicker noise, for which there is a S/N disadvantage which classically has been defined as inversely proportional to the square root of the number of resolution elements. These results are derived using the assumption that noise in FTS is evenly distributed over the entire spectrum and have been well documented in the literature [59-65].

It is of importance, though, to understand the noise characteristics of the ICP in the ultraviolet and visible regions of the spectrum. Consider first a single emission line of one element as observed with a monochromator. The noise limiting factor in the ICP is dependent on the concentration of that element, or on the intensity of the emission line. At high concentrations, source flicker

noise plays a dominant role. In this instance, the noise is directly proportional to the signal intensity. At lower concentrations, shot noise, proportional to the square root of the signal, is dominant. At concentrations close to the detection limit either shot noise or detector noise is dominant depending on both the type of detector and the signal intensity.

Only at very low concentration levels for all elements then, would the classical Fellgett's advantage be apparent. In the other two situations for any one element, no advantage and possibly a disadvantage would be observed, according to theory.

The situation here is not quite that straightforward for more than one reason: 1) Detector noise is random; that is, there is no frequency dependence and consequently in an FTS system, the noise will be evenly distributed over the entire spectrum. This assumption has been made for both the shot noise and flicker noise limited cases. However, in both of these cases, the noise is proportional to the signal, which is at a particular frequency, and one might, therefore, expect to find some frequency dependency of that noise. This would mean, contrary to original expectations, that these types of noise could be completely or partly localized on the peak similar to results observed with dispersive-based instruments. In

preliminary noise studies [66] (Chapter V) with the FTS in our laboratory, some localization of noise on spectral peaks has indeed been observed, although the picture is certainly not completely clear.

2) In addition to the above considerations, Hirschfeld [61] and others [63] have described a "distributive multiplex" gain for the case of sparse narrow linewidth emission spectra - a situation quite plausible for the ICP. This S/N advantage decreases with an increase in the number of emission lines in the spectrum.

It is clear that further research into the areas of noise distribution in FTS and methods to circumvent the disadvantage, if it exists, is warranted.

Along the same line, one other problem in FTS, both in the mid-IR and in the UV-visible region is dynamic range limitations. This limitation occurs for a very weak signal in the presence of an intense one. The intensity of the weak signal, because the dynamic range is limited by the strong signal, falls below the resolution of the analog-to-digital converter (ADC) required to acquire the interferogram. The weak signal consequently cannot be distinguished from the noise in the baseline of the spectrum.

In comparison then to the direct reader and monochromator, the FTS measurement system has an unparalleled accurate and precise wavelength axis, and measures background and analyte emission simultaneously, facilitating both background subtraction and determination of spectral line interferences. In the case of spectral line interferences, an alternate line can easily be used for analysis - often without having to rerun the sample. On the other hand, dynamic range limitations and a possible S/N disadvantage are problems which must be considered in an FTS measurement system for the UV and visible regions of the spectrum. As well, time resolution is very difficult with the interferometer which requires a stable source for the duration of at least one complete scan. This currently limits the time resolution in our system to, at best, five seconds. Often signal averaging, either in the interferogram or spectral domain, is necessary, eliminating any possibility of time resolution.

As a qualitative tool, for the reasons discussed above, the FTS system is far superior to other methods of measurement. In this thesis, the FTS system has been used to characterize background and analyte emission (Chapter III) from the ICP in the previously uninvestigated near-IR spectral region (0.7 to 3.0 μm).

As mentioned previously, resolution with an FTS system is ultimately determined by the maximum optical path difference, or the distance the moving mirror has travelled. The trend, in both commercial and research instruments, has been to go to "bigger and better" instruments - that is, increasing the available resolution. Increasing the path length results in a proportional increase in the number of points required for the interferogram for the identical data acquisition rate. For example, with the one meter Kitt Peak interferometer [50], one million point interferograms were acquired. The memory space necessary just to store the interferogram is of course correspondingly large. As well, the computation time necessary to process and transform the interferogram is high. The question arises as to whether it is really necessary to have such high resolutions. In the ICP results described earlier, a two cm path length would be sufficient for the determination of atomic emission spectra. At the same data acquisition rate, this would still involve a 20000 point interferogram. There is an alternative approach - that is, keep the same resolution but decrease the number of points in the interferogram. This creates a phenomenon known as aliasing or undersampling of the interferogram. To sample an interferogram properly, the sampling

frequency must be twice that of the highest frequency component in the interferogram. In that case, all frequencies in the resultant spectrum will be correct. If a lower sampling frequency is used, frequencies greater than half the sampling frequency fold back or are aliased into the correctly sampled region, in a precisely predetermined fashion. With line spectra, it is relatively straightforward to identify the correct wavelengths for the aliased lines. Aliasing has been used to advantage in this laboratory and in others [67,68]. When working in the UV region, where frequencies are as high as 50000 cm^{-1} (200 nm), to sample without aliasing requires very high sampling rates and consequently the number of points in the interferogram as well as computation time and memory space rapidly escalates. Limiting the electronic and optical bandpass into the interferometer also limits the possible aliased wavelengths. Aliasing is used extensively in this thesis and will be further discussed in Chapters III and VI. It is possible then, to increase resolution in the interferometer without increasing the number of data points in the acquired interferogram by increasing the sampling interval and thus tolerating further aliasing. The less complex the spectrum is, or the smaller the frequency bandpass into the interferometer, the smaller is the aliasing problem.

The FTS measurement system provides information about the entire spectral region of interest. Often the analytical information desired is only a small portion of the information encoded in the interferogram. The conventional approach is to perform the Fourier transformation on the interferogram to produce a spectrum. The desired qualitative and quantitative information can then be extracted from the spectrum. This process can be quite time-consuming if only a small amount of spectrochemical information is required.

A second approach is the correlation technique [69-71]. In the correlation process, the entire spectrum obtained from the interferogram is not observed. Instead, the desired information is extracted directly from the interferogram. For example, consider the quantitative determination of nickel in an aqueous sample. A "mask" interferogram of the nickel analytical wavelength would be produced and correlated with the sample interferogram to yield a single number representing the nickel concentration in the sample. If nickel is not present in the sample, a correlation value of close to zero would be found. In the instance where nickel is present, the magnitude of the correlation value is directly proportional to the concentration. This process eliminates the more time-consuming Fourier transformation

and has been used with some success in this laboratory [70,71].

A third approach is to limit the optical bandpass into the interferometer to a small region around the spectral position of the desired information. At the same time, the possibility of dynamic range limitations and a multiplex disadvantage due to emission in other spectral regions will be diminished. Often, especially for quantitative work, information about the whole spectrum is not necessary - rather a few selected spectral windows would be sufficient. The spectral window should be broad enough to include background and spectral line interferences but narrow enough to exclude nonessential spectral information. For a narrow, defined optical bandpass, the amount of aliasing becomes unimportant. Very short interferograms, without degrading the resolution of the interferometer, can be acquired, reducing computation time and memory space requirements. At the same time, the ability to selectively change the analytical wavelength for a particular element must not be impaired. A measuring system in which the interferometer is coupled with a slew-scanning monochromator and which incorporates all of the above features will be described in Chapter VI.

J. Conclusion

The potential of the FTS as a measurement tool for ICP emission has been discussed in this chapter. The FTS system can provide simultaneous qualitative and quantitative information over a wide spectral region.

The qualitative capabilities of the FTS system are illustrated in Chapter III of this thesis. The near-infrared spectral emission (0.7 to 3.0 μm) of the ICP has been characterized for both analyte and background emission in this chapter. Several potentially useful analytical lines for nonmetal elements have been observed in the near-IR region. The potential of the near-IR region for the quantitative analysis of elements such as sulphur is presented in Chapter IV.

In Chapter V, the spectral response of the interferometer in the ultraviolet and visible regions of the spectrum is presented. Several limitations of the quantitative capabilities of the FTS system led to the development of a new measurement system which keeps the advantageous characteristics of the interferometer and concurrently enhances it quantitative performance. This system and its characteristics, both qualitative and quantitative, are presented in Chapter VI.

Before presenting the measurement capabilities of an interferometer-based instrument, a brief description of

the interferometer will be presented in Chapter II. The interferometer used in this thesis has been and still is being developed in this laboratory. Several modifications, including microprocessor generated control signals, have been made to optimize the performance of the interferometer. These modifications are presented in the next chapter.

CHAPTER II

THE MICHELSON INTERFEROMETER: INSTRUMENTATION DESCRIPTION AND MODIFICATIONS

A. Introduction

The Michelson inteferometer in use in our laboratory has been, and still is, undergoing the evolution process. During the course of this work, significant modifications have been made, both in optical components of the interferometer and in the associated electronics. These modifications will be discussed in this chapter.

The interferometer system has been described in detail in the literature [38,39,72] and consequently will not be completely described in this thesis. To aid in understanding the modifications presented in this chapter, a block diagram of the interferometer system (Figure 1) and a schematic of the interferometer itself (Figure 2) have been included.

B. Data Acquisition

Data acquisition is accomplished with a PDP-11/10 minicomputer. Both the acquisition programs and the

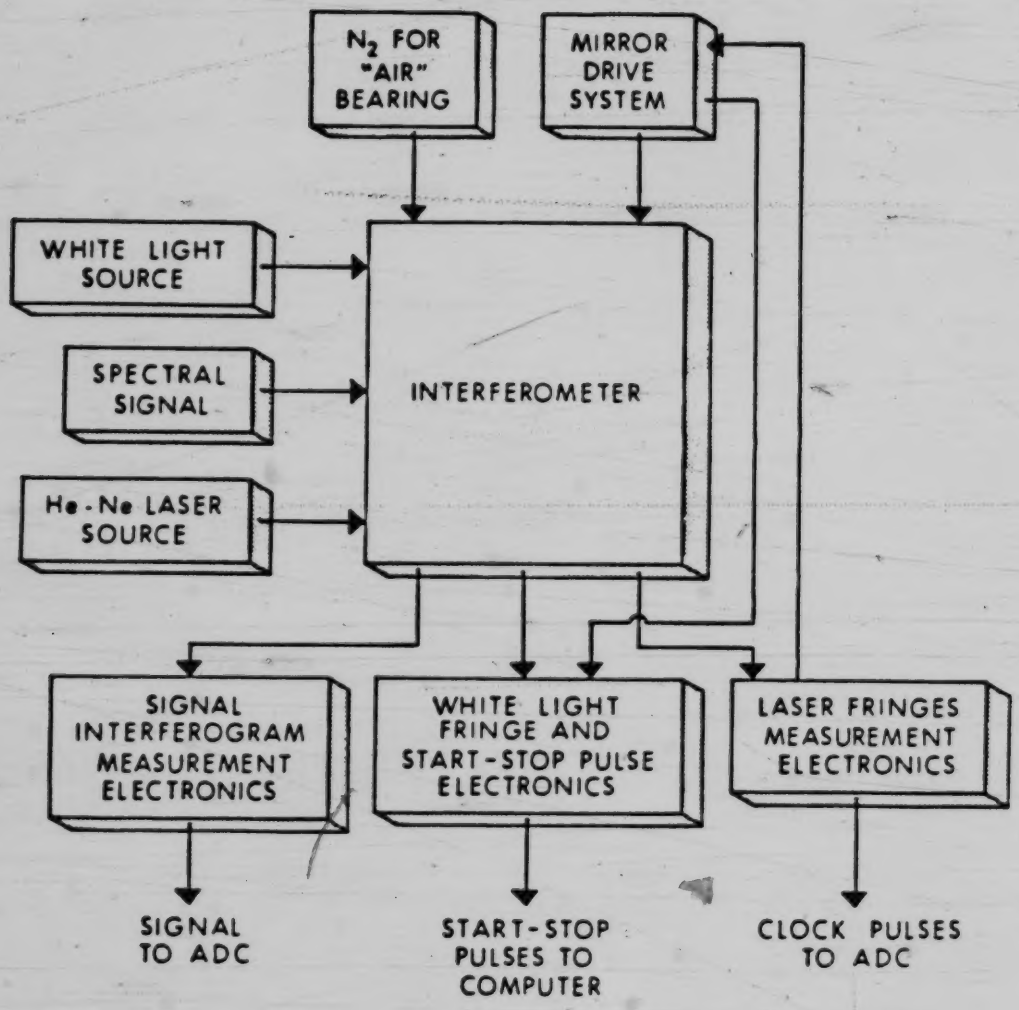

Figure 1. Block diagram of the Michelson interferometer system.

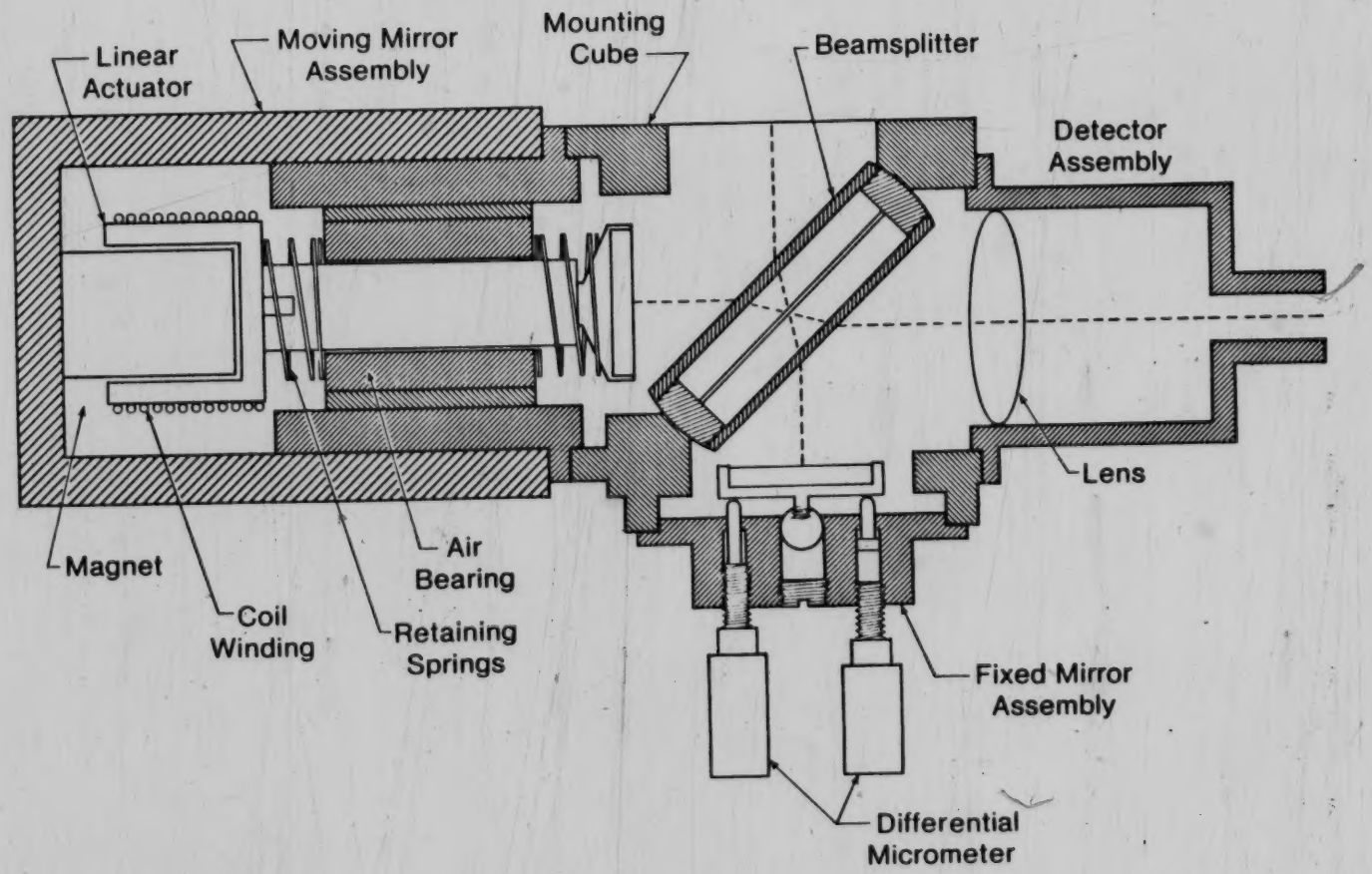

Figure 2. Schematic diagram of the Michelson interferometer.

interferogram processing programs have been well documented elsewhere [38,39] and will not be replicated in this thesis.

C. New Mirror Drive System

All modifications to the interferometer system were initiated following an improvement to the drive system for the moving mirror. The old drive system, a loudspeaker coil, has been replaced by a linear actuator (Kimco, Inc., San Marcos, California) also known as a linear moving coil motor. This drive is capable of delivering a peak force of eight pounds. However, with the new drive, it was not possible to signal average the interferograms properly. It was at first thought that the piston and spring assembly (Figure 2) originally designed for the old loudspeaker coil were not heavy enough to properly balance the heavier linear actuator. To this end, the aluminum piston was replaced by a brass piston, and heavier gauge springs were substituted for those previously in the interferometer. After several unsuccessful attempts to improve the drive, the optimum system appeared to be one with a very light aluminum piston and the heavier gauge springs. Although the performance of the interferometer improved with this system, the signal averaging capabilities were still not acceptable, leading to the modification of the drive electronics.

The basic mirror drive signal is a triangular waveform obtained from a standard function generator. For the old drive, the triangular waveform was amplified by a power amplifier (Model 6824A, Hewlett-Packard, New Jersey) to provide the current necessary to drive the loudspeaker coil. The effects of velocity changes of the moving mirror have been well documented [38,72] and in this system, the mirror velocity was stabilized using a phase-locked loop (PLL) feedback control system. A correction signal is generated by the PLL, based on the frequency difference of the input laser fringe frequency and an internal frequency reference. This correction is proportional in magnitude and similar in sign to the frequency and phase difference between the two signals. By applying the correction signal to the function generator, it is possible to increase or decrease the frequency of the triangular waveform to ensure stabilization of the moving mirror velocity.

With the new linear actuator, it appeared that the response of the moving mirror assembly to the frequency changes provided by the PLL was not rapid enough to enable stabilization of the mirror velocity. To this end, a new electronic circuit (Figure 3) was built which actually incorporates the feedback into the drive circuit. In essence, the operational amplifier (OA) and the pair of

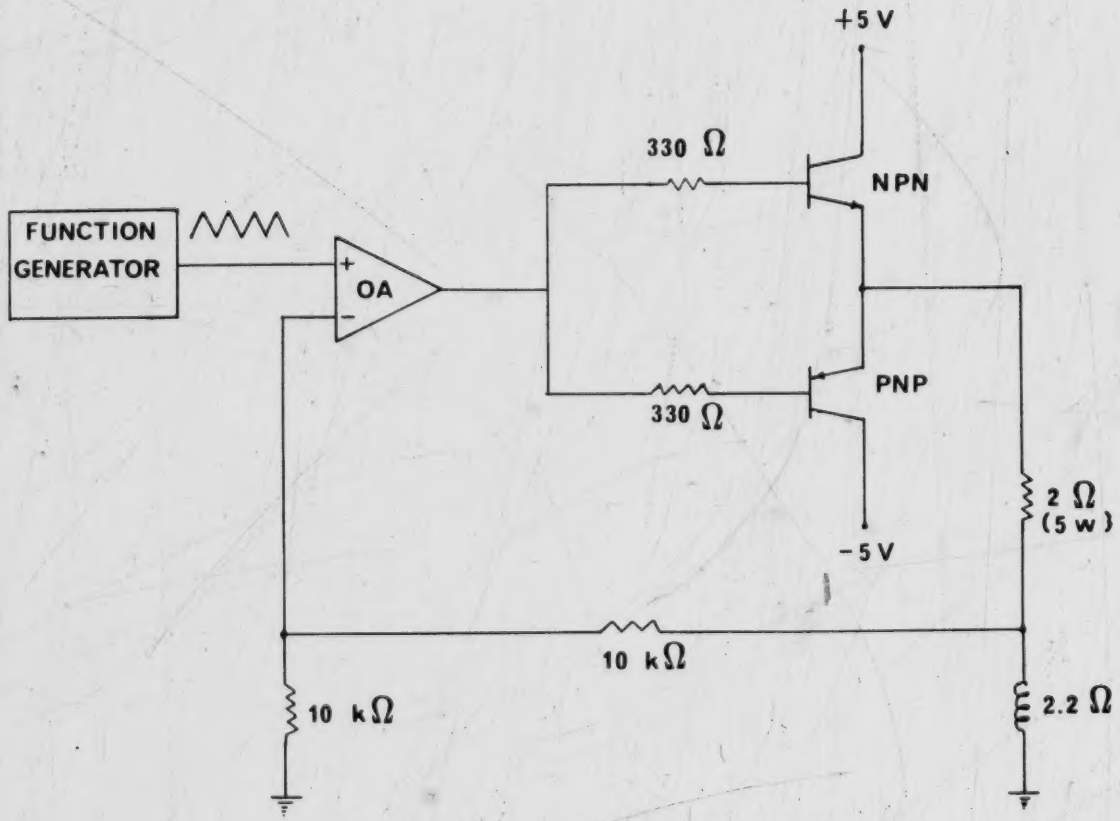

Figure 3. Electronic diagram for the moving mirror drive system.

transistors replace the power amplifier of the previous system. A simple voltage divider in the OA feedback circuit provides an overall gain of two for the signal driving the coil. The resistor in series with the coil has been matched with the static resistance of the linear actuator. This circuit provides excellent stabilization of the mirror velocity which translates into stabilization of the frequency of the laser clock. This stability is demonstrated in Figure 4. By triggering the oscilloscope on the white light central burst, the laser fringes from ten successive forward scans of the moving mirror were accumulated for each photograph. Figure 4a is the laser signal with the PLL and Figure 4b is the result using the circuit shown in Figure 3.

Signal averaging of interferograms using this drive circuit provides excellent results. As well, it is now possible to acquire data at a frequency of 5 kHz compared to the 2 kHz found to be optimum with the old drive. The data acquisition step can consequently be accomplished more rapidly.

One problem that arose with this circuit is that the input triangular waveform must be offset to provide a signal which is always negative. If the input signal becomes positive, the output from the OA starts to oscillate. This problem does not appear to affect the

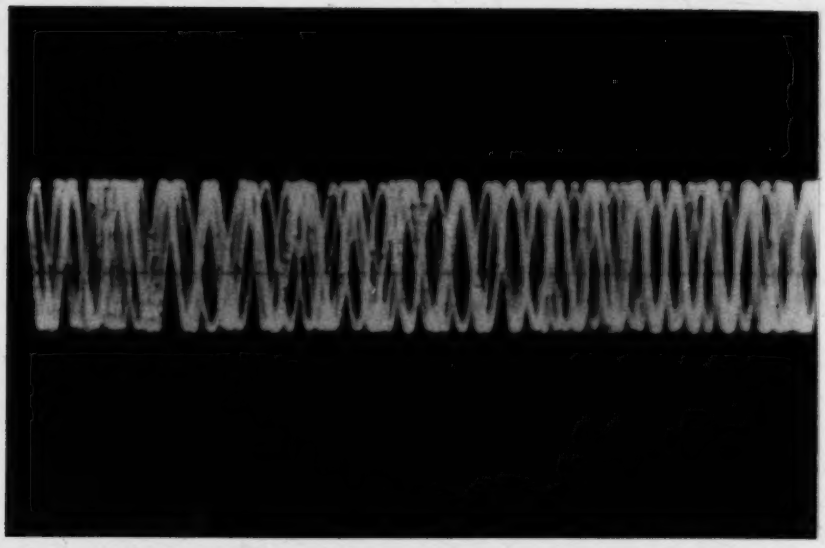

(a)

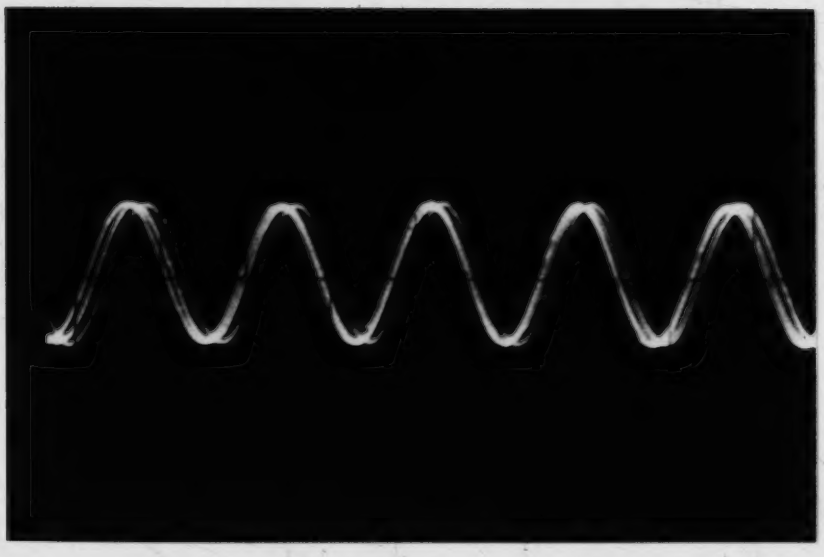

(b)

Figure 4. Laser analog signal under (a) PLL control (scope time base: 2 ms/division) and (b) new drive circuit control (scope time base: 0.5 ms/division).

stability of the drive. However, positioning of the white light in the center of the path travelled by the moving mirror must be accomplished by mechanically moving the entire assembly forward or backward to the appropriate position, increasing the difficulty of initial alignment.

It was thought that replacement of the OA and transistors with a power amplifier (PA11, Apex Microtechnology Corp., Tucson, AZ) would eliminate the oscillation problem. However, preliminary testing of the power amplifier chip revealed the same problem.

D. Microprocessor Generated Control Signals

In further modifications of the system, generation of the control signals for data acquisition is now accomplished by a 6502-based microprocessor, the AIM 65. Before discussing this system, a review of the timing sequence and method of data acquisition is helpful.

To enable signal averaging of interferograms, it is necessary to know precisely the location or timing of one point in the interferogram. In systems in which the source and the reference white light pass through different interferometers, it is possible to offset the white light interferometer relative to the source interferometer. This enables use of the white light central burst as a precise start flag. However, because a

single interferometer is used in our system, this technique is not practical. The sequence of events occurring with this interferometer is schematically depicted in the timing diagram shown in Figure 5. To acquire double-sided interferograms, an imprecise start flag, approximately 2400 laser fringes before the white light occurs, is generated. Once the white light central burst has occurred, exactly 2048 laser clock pulses are counted and then a precise stop flag is generated. Signal averaging is then accomplished by averaging the last point first.

Up until this time, a series of monostables and counters [38] have been breadboarded together in an ADD 8000, to generate the start and stop pulses for the PDP-11/10. A microprocessor-controlled system could increase the flexibility of the system as well as reduce the amount of troubleshooting necessary to keep the electronic system operating. The microprocessor available in the laboratory is a 6502 CPU based microprocessor, the AIM 65.

There are two basic approaches to this type of problem: 1) Simply use the microprocessor as a replacement for the control electronics; that is, the microprocessor would be used to generate the start and stop flags for the data acquisition stage or 2) take this approach one step further and employ the microprocessor

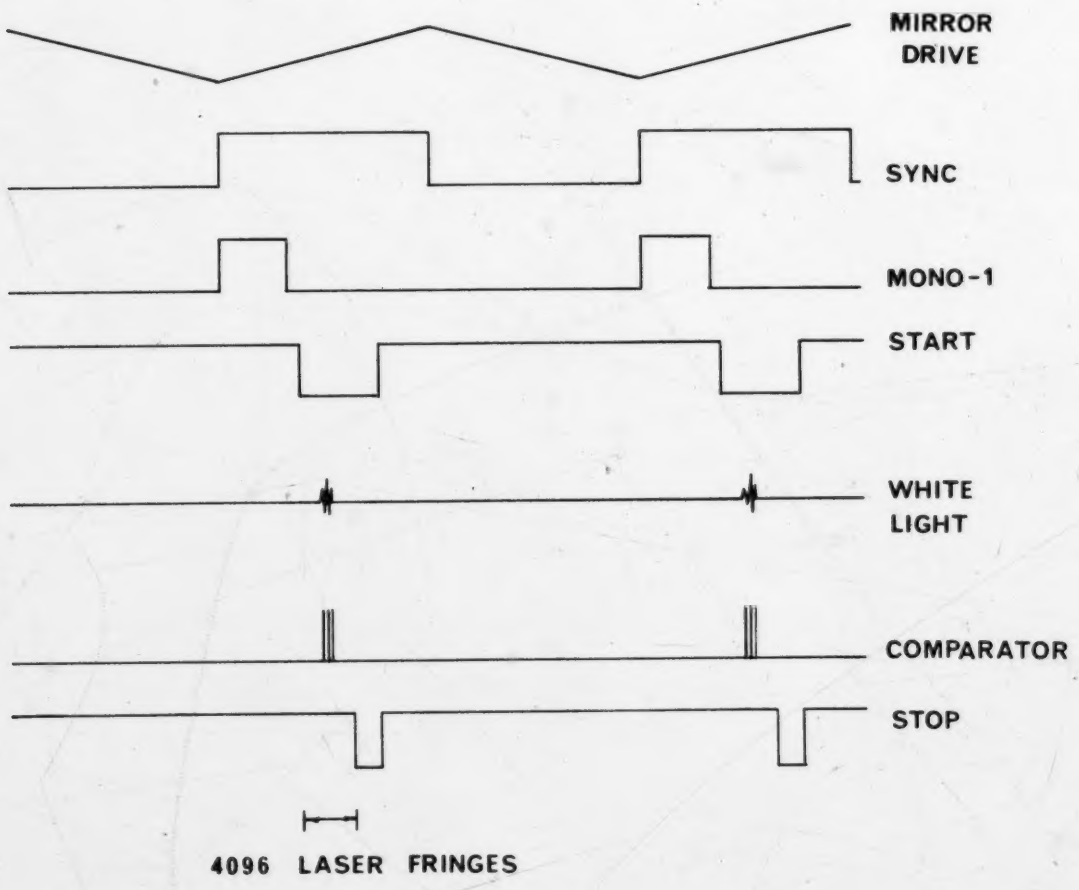

Figure 5. Schematic diagram of the control signals' timing sequence.

for the control of the moving mirror drive system. Both approaches [73] have been successfully used in this laboratory.

Because the external drive was quite stable, the first approach was taken with this system. In the following discussion, it will be helpful to consider the timing diagram (Figure 5) in addition to schematic diagrams of the microprocessor system (Figures 6 and 7). The basic role of the AIM 65 in this system is that of a counter. To provide the necessary timing sequence, three signals from the interferometer electronics are necessary (Figure 6). The counter initiator, supplied by the sync pulse from the function generator, has two purposes. The first is to ensure that data is taken only on the forward scan of the moving mirror and the second is to provide an initial imprecise starting point for the generation of the start and stop pulses for data acquisition with the PDP-11/10. The laser reference fringes provide the clock for both the microprocessor and the PDP-11/10. The third signal from the interferometer, the white light, has the role previously described.

In an application of this nature, the most important component of the microprocessor is the input/output (I/O) segment. In the AIM 65 [74], the entire I/O section is contained on one chip, the R6522 Versatile Interface

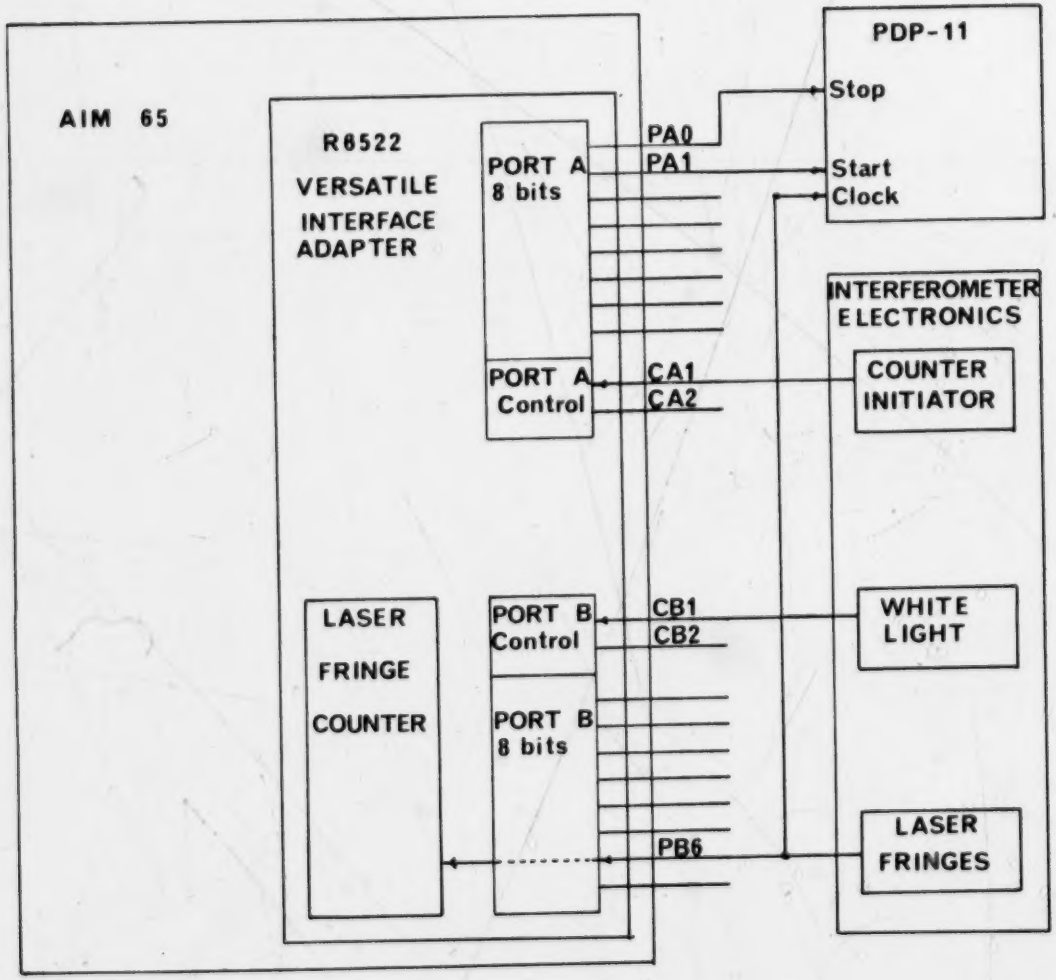

Figure 6. Schematic diagram of the AIM 65 control system.

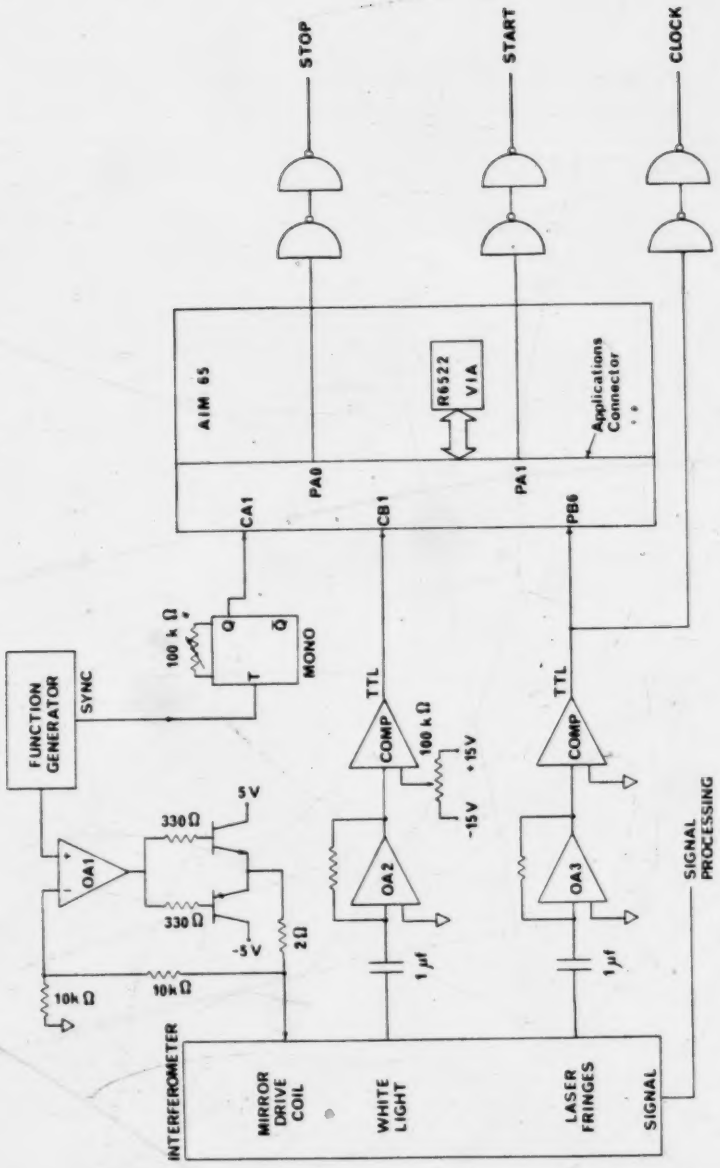

Figure 7. Interferometer electronics with the AIM 65 and the PDP-11/10 computer.

Adapter (VIA). A block diagram of this chip is illustrated in Figure 6. The VIA includes two 8-bit I/O ports (A and B in Figure 6) in which each pin can be selected as either an input or an output, two control lines (CA1, CA2, CB1, and CB2) for each port and two 16-bit timers. Each timer can be used to either generate or count pulses. In addition, of course, the VIA has access to both the data bus and the address and control buses of the AIM 65.

For the generation of the start and stop pulses for the PDP-11/10, it was necessary to use only one timer, timer 2. Both timers are down counters and the maximum count selectable, corresponding to 16 bits, is 65536 counts. Because the laser reference fringes are being used as the clock for both the AIM 65 and the PDP-11/10, timer 2 has been set so that it counts down on every negative-going edge of the laser pulses. The laser clock is brought into the microprocessor on one of the I/O lines of Port B, PB6 (Figure 6). Two control lines, one from each port (CA1 and CB1) have been used to inform the VIA of the start of the forward motion of the moving mirror (the sync pulse on CA1) and the occurrence of the white light (WL on CB1). Two lines on Port A, PA1 and PAØ, are used to generate the start and stop pulses for the PDP-11/10.

The actual timing sequence is illustrated in Figure 5. In a cold start sequence, one scan of the moving mirror is necessary to set the parameters for the AIM 65. Upon receiving the count initiator, the sync pulse, on CA1 the maximum count, 65536, is loaded into timer 2. Each time a clock pulse is received on PB6, the timer decreases the count by one. When the white light burst interrupts (CB1), the operation of the timer is stopped and the contents of the counter, for example, 55536, are stored in one of the internal memory locations of the AIM 65. The timer is then restarted with a maximum count of 2048. When the timer has counted 2048 laser fringes, that is, when the count becomes zero, the precise stop flag is generated on PAØ. The contents of the counter before the white light interrupt, in this example 55536, are then retrieved from their memory location. The number of laser fringes before the white light interrupt (since the counter is a down counter) can then be calculated to be 10000. To determine the position of the imprecise start flag, it is necessary to generate a delay count after the count initiator. This delay count is determined by subtracting 2300 from the number of laser fringes before the white light, 10000. On the next scan, and on every succeeding scan, the count initiator prompts the loading of the timer with the delay count, in this case 7700.

When the timer has counted down to zero, the imprecise start flag is sent to the PDP-11/10 on PA1. The same sequence of events is then followed as for the first scan: the timer counts clock pulses until the white light interrupt, counts exactly 2048 past it, generates the stop flag and then returns to wait for the sync pulse.

A flow chart and a complete listing of the machine language program used with the AIM 65 can be found in Appendix I.

The support electronics necessary to generate the control signals are now greatly simplified (Figure 7). A standard 44-pin J-connector was used to interface the interferometer electronics to the AIM 65 applications port. In Figure 7, only the pins actually used for connections are shown on this connector. Before going to the microprocessor, it was necessary to amplify the white light and the laser reference fringes and to convert both signals to TTL compatible square wave signals. It was found that the number of clock pulses between the start of the sync pulse and the white light interrupt was greater than the maximum count, 65536, for the timer. An additional time delay was provided by the monostable shown in Figure 7. All control signals were processed through double NAND gates to ensure TTL logic levels at the PDP-11/10.

Software control provides more flexibility than with the old hardware controlled system. With simple modifications to the software program, it should be possible to change the length of the interferogram to values other than 4096 points. By the interfacing of an 8253 timer/counter to the AIM, it would be possible, under software control, to adjust the clocking rate to some fraction, or multiple, of the base clocking rate provided by the laser reference. This would allow acquisition of interferograms of the same length but at different resolutions.

Although more flexible than a hardware controlled system, there is no provision for finding the white light or changing the pathlength that the moving mirror actually travels. These processes are accomplished separately from the AIM 65.

In this laboratory [73], a microprocessor-controlled system was developed for a separate but identical interferometer in which the moving mirror drive was incorporated into the AIM. To do this, two input/output (I/O) lines of the AIM were connected to a simple integrator circuit. With one line at logic "1" and the other at logic "0", the integrator circuit provides a ramp to drive the moving mirror forward. Reversing the logic at the two I/O lines also reverses the direction of the

moving mirror. The distance the mirror travels is easily controlled by changing the duration of the forward ramp - resetting the count for the timer. In this system, if the white light is not found, the count for the timer is increased under software control until it is found. Once the presence of the white light has been established, the movement of the mirror is centered around the position of the white light central burst, again under software control. This is a much more flexible and elegant system than the one currently in use with this system. However, any fluctuations in the voltage levels at the I/O lines will cause velocity fluctuations in the mirror movement. This could easily be rectified by placing digital-to-analog converters (DAC) at each input to the integrator. The DAC's would provide a more stable voltage for the integrator inputs and consequently a more stable velocity for the mirror. In addition, it has been shown that some form of feedback is necessary to ensure mirror velocity stabilization. It should be possible, under software control, to create a correction signal based on fluctuations of the laser clock frequency and hence change the input to the integrator to adjust the mirror velocity.

The optimum system would be one in which fixed mirror alignment is also under software control. No suitable method for accomplishing this has yet been designed in this laboratory.

E. Optical Modifications

1. Detector Assembly

In previous work, an off-axis parabolic mirror and folding mirror were utilized to collect light for the detector. However, this system was difficult to align and more importantly the diameter of the central fringe is limited to that provided by the focal length (16.8 cm) of the off-axis parabolic mirror. Changing this assembly to one involving a lens (Figure 2) to focus the light onto the detector facilitates alignment. As well, the diameter of the central fringe can then be tailored to the active area of the detector by adjusting the focal length of the lens in the detector assembly.

The radius of the first fringe (r) in the focal plane of the output of a Michelson interferometer is equal to $f(\lambda/d)^{1/2}$ where f is the focal length of the output, λ is the wavelength and d is the optical retardation. For maximum sensitivity, the first fringe should just fill the area of the detector window or the exit aperture. If the fringe area is larger than the detector then the signal intensity will be lowered. More importantly, if the fringe area is smaller than the detector aperture, contrast will be lost and the signal will be seriously degraded. At longer wavelengths, considering the above

equation, a shorter focal length lens would be beneficial to avoid overfilling the detector. For example, consider a focal length of 5.0 cm for a 1.0 μm wavelength. The optical retardation, for a 4096 point interferogram is 0.13 cm. The diameter of the central fringe can be calculated to be 0.28 cm, which is larger than the 0.1 × 0.1 cm PbS detector element used for this region. However, at 200 nm, with this same lens, the diameter of the fringe is much smaller, 0.12 cm. Use of a longer focal length lens, for example a 10 cm lens, yields a fringe diameter of 0.24 cm - allowing a much larger exit aperture in front of the photomultiplier tube used in this wavelength region. Utilization of this 10 cm lens in the near-IR would yield a fringe diameter that would overfill the PbS detector extensively and hence degrade the performance of the FTS system in the near-IR spectral region.

For the experiments presented in Chapter III, a five cm focal length lens was used while in Chapters V and VI, a ten cm focal length quartz lens was utilized.

2. Mirrors

Magnesium fluoride overcoated aluminum mirrors have replaced the old aluminum mirrors to enhance sensitivity in the ultraviolet spectral region. The new mirrors have a flatness of $\lambda/10$ and are 4.2 cm in diameter.

3. Beamsplitter Assembly

Previous measurements in the ultraviolet region of the spectrum were successful at wavelengths [39,72] longer than 240 nm. To enhance and extend response in the UV region, a beamsplitter specially coated for this spectral region has been obtained for the interferometer.

The beamsplitter consists of a Suprasil 1 substrate which has been coated with a 100 Å thick layer of aluminum (Acton Research Corp., Acton, Massachusetts) and a Suprasil 1 compensator plate. The efficiency of this beamsplitter is illustrated in Figure 8 and has its maximum efficiency in the 200 to 400 nm range.

In order to demonstrate the capabilities of this beamsplitter, the emission spectra of two hollow cathode lamps (HCL), cadmium and a multielement lamp, were measured in the ultraviolet region. The spectrum of the Cd HCL is shown in Figure 9. Three lines were observed, all with wavelengths shorter than 240 nm (Table 1). Wavelengths measured in this spectrum are in agreement with literature values [75].

The multielement HCL consisted of four elements, Cu, Zn, Pb and Sn. The spectrum of emission from this lamp is illustrated in Figure 10. Again, emission lines in the first half of this spectrum, with wavelengths shorter than 240 nm (or wavenumbers greater than 41650 cm^{-1}), have

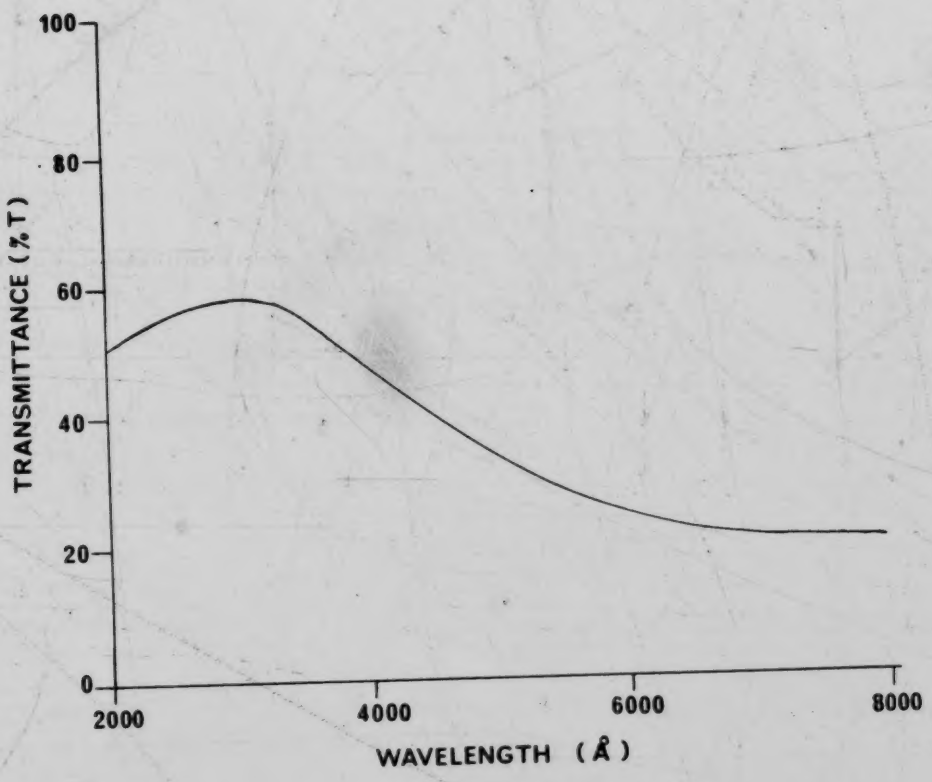

Figure 8. Efficiency of the ultraviolet beamsplitter, as measured by its transmission characteristics.

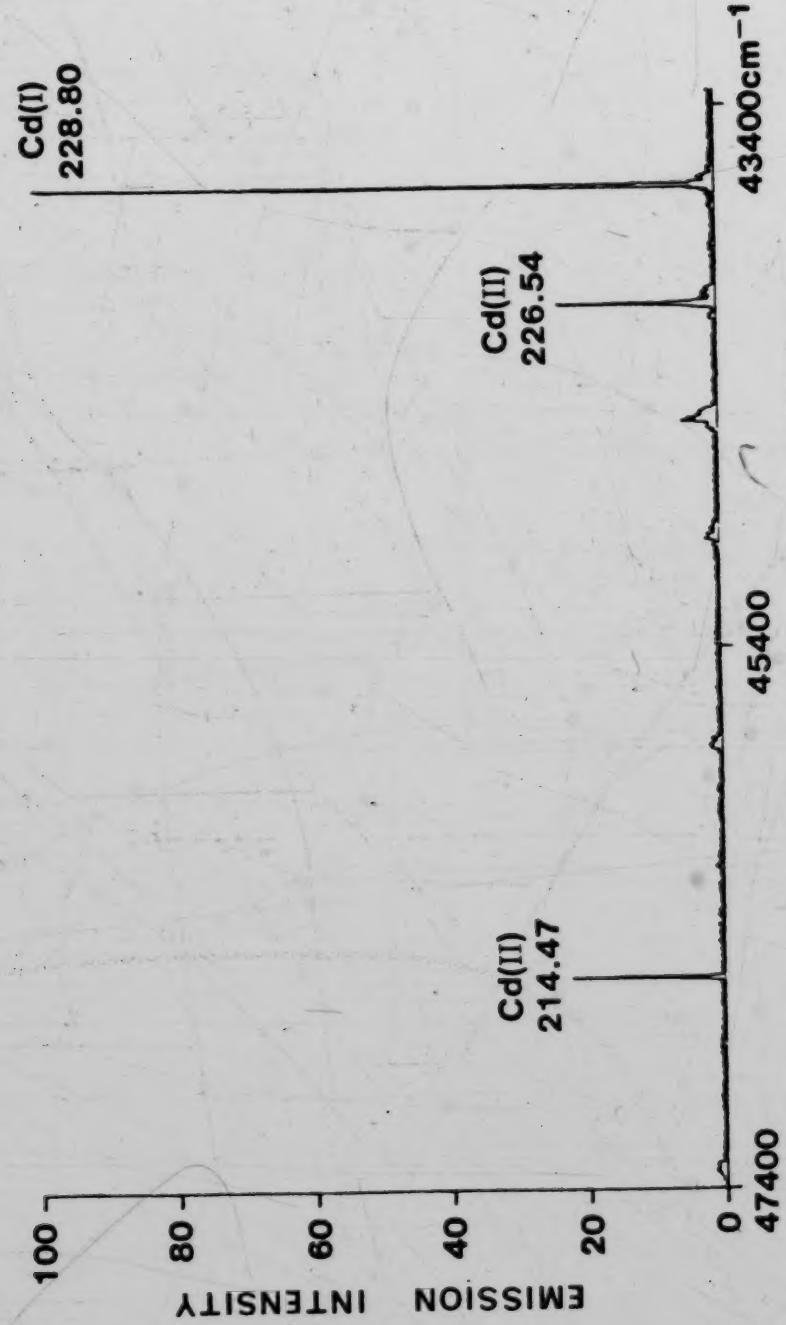

Figure 9. Emission spectrum of a cadmium hollow cathode lamp.

Table 1

Cd Hollow Cathode Lamp Emission Lines

Element	Observed		Literature[75]
	Wavenumber (cm^{-1})	Wavelength (nm)	Wavelength (nm)
CdII	46627.0	214.47	214.44
CdII	44149.7	226.54	226.50
CdI	43697.9	228.84	228.80

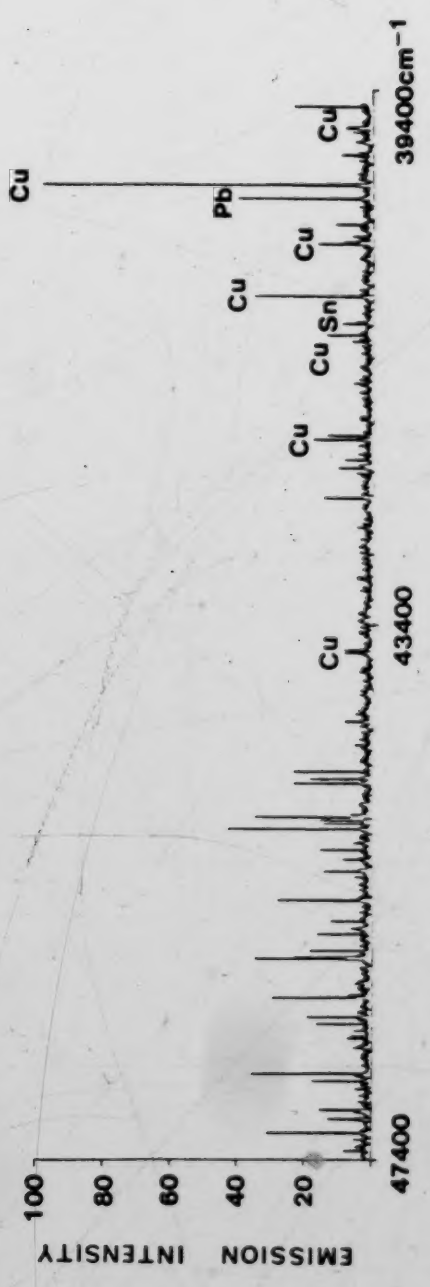

Figure 10. Emission spectrum of a multielement hollow cathode lamp containing the elements copper, lead, tin and zinc.

previously not been observed with the interferometer system. Figure 11 shows an expanded spectrum of this region. Literature and measured wavelengths are in agreement (Tables 2 and 3). The shortest wavelength observed in this spectrum is the ZnII line at 206.2 nm (49358.3 cm^{-1}). Observation of the ZnII 202.6 nm line is precluded by an aliasing overlap of the CuII line at 219.3 nm (45599.6 cm^{-1}). Further results, described in Chapters V and VI, show the usefulness of this beamsplitter at wavelengths as short as 180 nm.

F. Laser Reference Channel

The He-Ne reference laser (632.8 nm) used in the interferometer provides a very accurate wavelength reference thus allowing spectra to be measured with an accurate and precise predetermined wavelength axis. However, although there is good agreement between the measured and theoretical values, the discrepancy between them appears to be one sided. That is, the measured wavelengths are generally slightly higher than the literature values [75]. Several factors could possibly be involved in this discrepancy: 1) the wavelength used for the He-Ne line in the wavelength calculations might not be accurate enough, although this difference would be very small, or 2) the optical path length that the laser

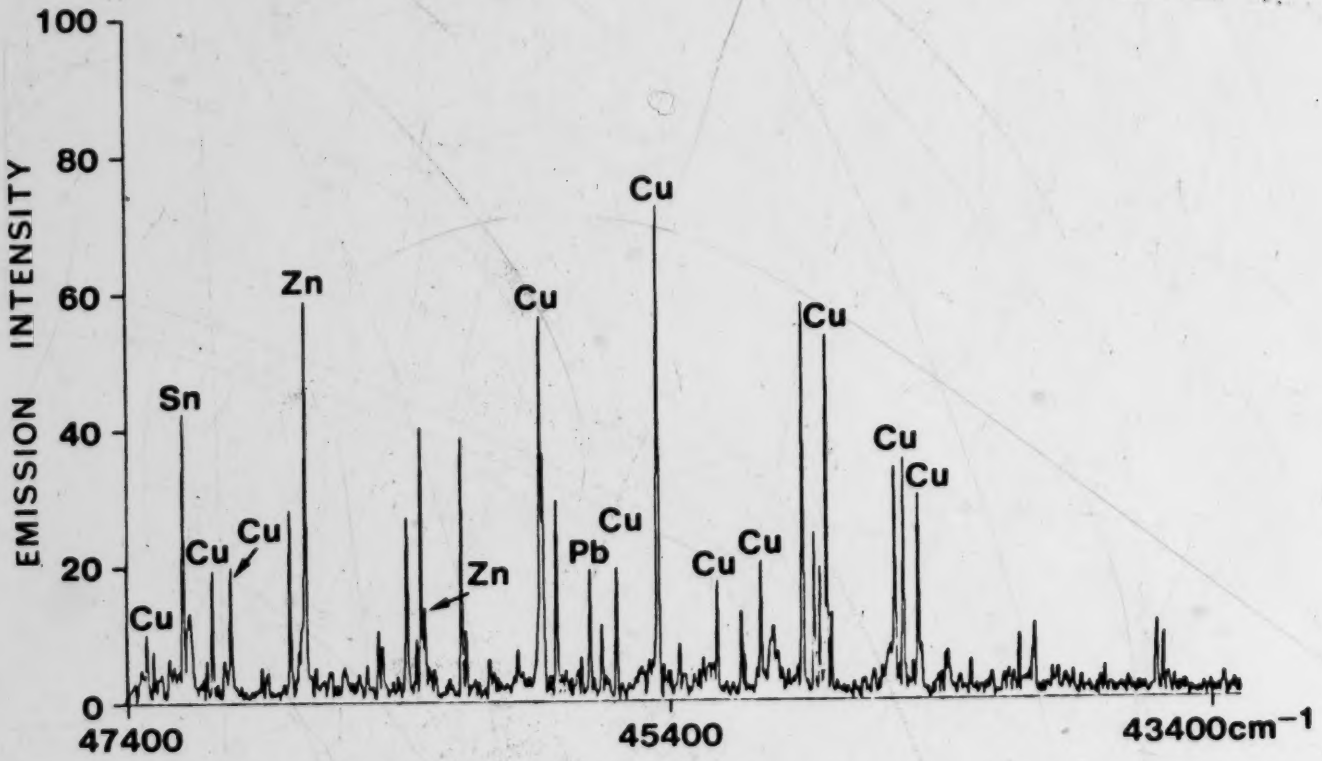

Figure 11. Expanded spectrum showing the wavelength region below 240 nm for the multielement hollow cathode lamp illustrated in Figure 10.

Table 2

Cu, Zn, Sn, Pb Hollow Cathode Lamp Emission Lines

(Above 240 nm)

Element	Observed		Literature[75]
	Wavenumber (cm^{-1})	Wavelength (nm)	Wavelength (nm)
CuI	35403.2	282.46	282.44
II	36989.0	270.35	270.32
II	37019.9	270.13	270.10
II	41239.7	242.49	242.45
I	40950.0	244.20	244.16
II	38484.3	259.85	259.88
I	40120.4	249.25	249.22
II	39292.9	254.50	254.48
SnI	41154.8	242.99	242.95
PbI	38800.3	257.73	257.79

Table 3

Cu, Zn, Sn, Pb Hollow Cathode Lamp Emission Lines

(Below 240 nm)

Element	Observed		Literature[75]
	Wavenumber (cm^{-1})	Wavelength (nm)	Wavelength (nm)
CuI	47338.8	211.24	211.21
II	47095.8	212.33	212.30
II	47028.3	212.64	212.60
II	45876.4	217.93	217.94
II	45608.2	219.26	219.23
I	45453.7	220.00	219.98
II	45235.8	221.06	221.03
II	45075.7	221.85	221.81
II	44834.4	223.04	223.01
I	44583.5	224.30	224.26
II	44496.7	224.74	224.70
ZnI	46752.3	213.89	213.86
II	48504.4	206.17	206.19
PbI	45704.7	218.80	218.76
SnI	47612.9	210.03	210.07

reference travels and that the source signal travels could be different.

In an experiment designed to check for optical path length differences within the interferometer itself, a He-Ne alignment laser was placed on the rails in front of the interferometer and used as the source signal. The signal, as detected by the silicon photodiode used at the output of the interferometer, was observed on an oscilloscope to be a cosine wave similar in frequency to that of the laser fringes. This is, of course, to be expected.

However, the question arises as to the shape of the interferogram acquired by the PDP-11/10. Theoretically, the modulated frequencies of the laser reference fringes used as the clock and the fringes of the laser source should be identical, since the wavelengths of the input signals should be identical. Consequently, the computer should acquire a dc level as the interferogram. The magnitude of the dc level will be dependent on the relative phase shifts of the reference and signal fringes.

Figure 12 shows the interferogram as it was acquired. Instead of the dc level expected, a sinusoidal waveform was obtained, indicating a slight difference in the apparent frequencies and hence the wavelengths of the reference and the source signals. If it is assumed that the wavelengths of the source and reference lasers are

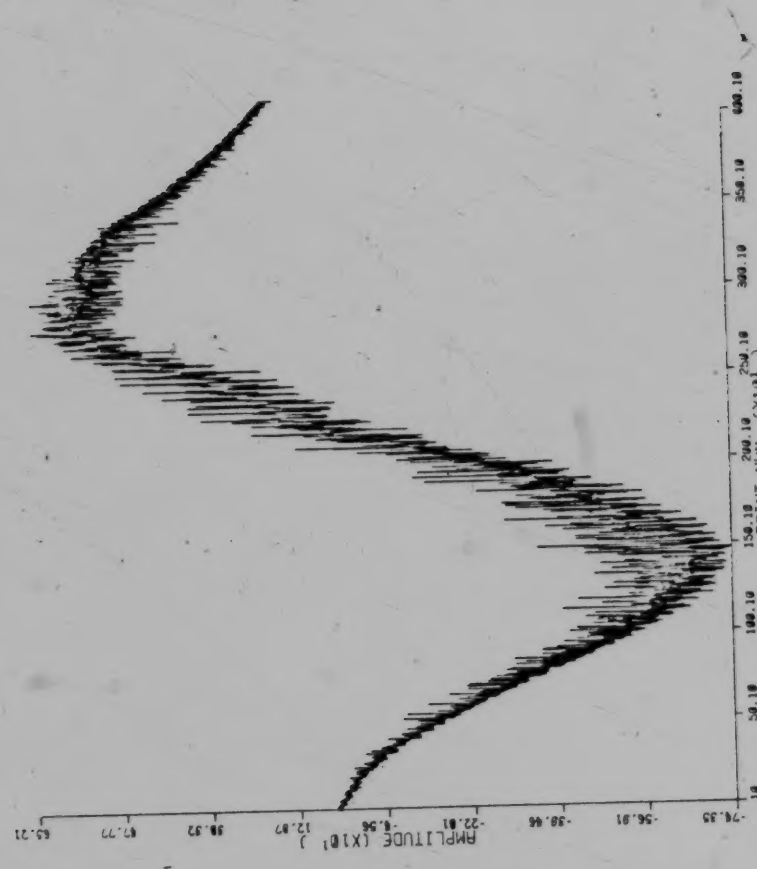

Figure 12. Digitized interferogram of a He-Ne laser source.

identical, the observed difference in frequency must be due to a different optical path length travelled within the interferometer for the source and reference signals. This could be caused by a slight tilt in one or more of the optical surfaces.

The sinusoidal waveform apparent in the acquired interferogram leads to an apparent frequency difference of 3.9 cm^{-1}. This can be observed in Figure 13, the first 100 cm^{-1} of the transformed spectrum. Theoretically, the spectrum should consist of a large spike at 0.0 cm^{-1}, rather than the spike observed here at 3.9 cm^{-1}.

This frequency shift will create an apparent wavelength shift which is dependent on the wavelength value. For a wavelength of 1.0 μm (10000 cm^{-1}) the wavelength error can be calculated as 0.004 μm, while at 200 nm (50000 cm^{-1}) the error would be 0.016 nm, which is similar in magnitude to the discrepancies, in the 0.02 nm range, noted in our measurements.

Although wavelength measurements appear to be one sided, it is difficult, with the laser data acquired, to determine whether the apparent wavelength shift is in a negative or positive direction. Consequently, no correction to the wavelengths reported in this thesis has been attempted.

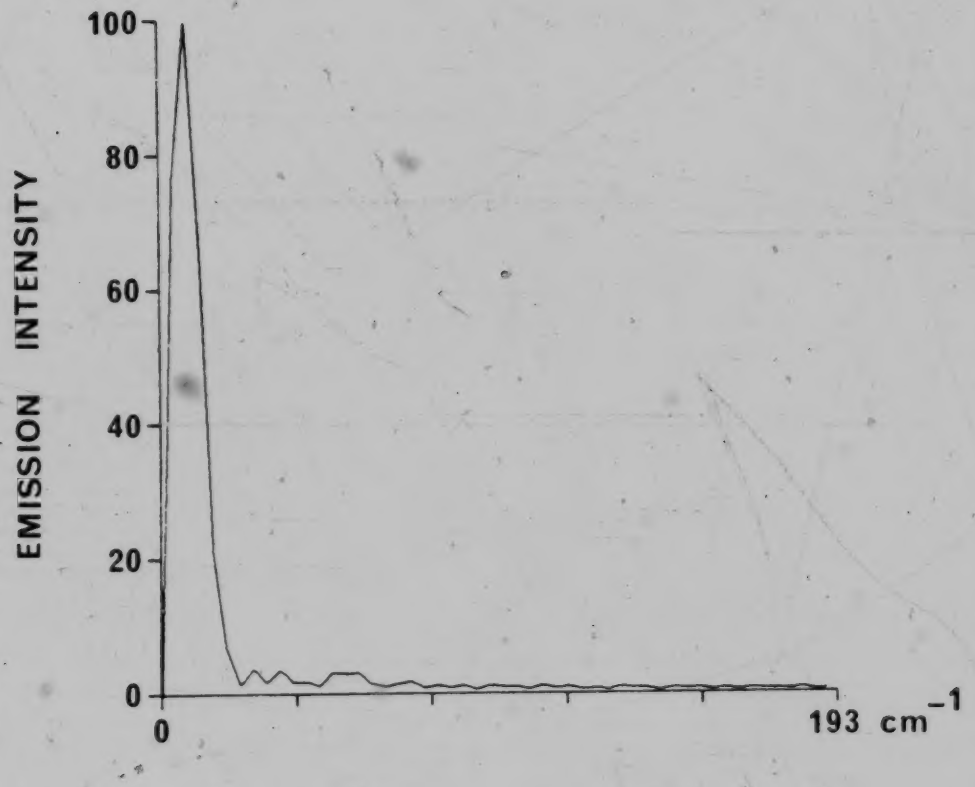

Figure 13. Partial spectrum obtained from the interferogram of the laser source illustrated in Figure 12.

CHAPTER III

AN INVESTIGATION OF ICP EMISSION IN THE NEAR- AND MID-INFRARED SPECTRAL REGIONS

A. Introduction

The inductively coupled plasma (ICP) is extensively used for the analysis of metals. It has, however seen limited use in the analysis of nonmetals, particularly for such elements as carbon, sulphur, oxygen and the halogens, thus excluding the analysis of many organic compounds using the ICP.

The main problem in the analysis of these elements lies in the measurement or detection step rather than in the excitation step accomplished by the ICP. The most sensitive atomic lines, the resonances lines, occur in the vacuum ultraviolet region (below 180 nm) for the majority of these elements. Detection of emission at these wavelengths requires the use of an inert gas-flushed or vacuum spectrometer. Although some nonresonance lines have been observed in the UV and visible regions, particularly for carbon and the halogens, their analytical usefulness has been limited [76,77]. It is for this

reason, that a study of emission in the near-IR region (0.7 to 3.0 μm), with particular emphasis on nonmetal emission, has been initiated in this research group.

Emission in the near-IR region originates mainly from atomic species, although as one approaches the 3.0 μm region, molecular emission becomes more important. The energy transitions involved in this region are nonresonance transitions; that is, emission is the result of a transition between two upper excited states. A resonance line, occurring at much shorter wavelengths and higher energy, is the result of a transition between an upper excited state and the ground state of the atom involved. In many excitation sources, upper excited states are not sufficiently populated to enable observation of nonresonance emission. However, the ICP is sufficiently energetic to populate these highly excited energy levels.

Initial interest in nonmetal emission from plasma sources was generated by attempts to introduce the microwave-induced plasma (MIP) and the ICP as detectors for gas and liquid chromatography. As early as 1965 [78], an argon MIP had been coupled to a gas chromatograph. Atomic emission spectra were obtained for elements such as phosphorus and carbon in the UV and visible regions of the spectrum. However, only diatomic molecular bands, for

example, the CCl fragment, were observed for halogen and sulphur-containing organic compounds.

Bache and Lisk [79,80] were successful, with the exception of fluorine, in obtaining atomic emission spectra for sulphur, phosphorus and halogen compounds. In their work, a helium MIP was utilized rather than the argon MIP used in the above study. For fluorine containing compounds, neither atomic nor molecular emission was observed. Sensitivity was found to be independent of the organic compound used, with detection limits in the nanogram range. Barnes et al. [81], in a very similar study, compared the argon and helium MIP's as gas chromatographic detectors, extending Bache and Lisk's work to include nitrogen and oxygen. Their conclusions were also similar, with atomic emission being observed for all elements in the helium MIP while in the argon MIP only diatomic molecular spectra were observed for nitrogen, oxygen and the halogens. However, in contrast to Bache and Lisk's work, Dagnall et al. [82] found that the emission intensity of some elements was dependent on the organic compound. In addition, the wavelength of maximum intensity for each element was also dependent on the compound containing the element in question.

In all research involving nonmetal emission from the MIP, only gaseous samples were analyzed and the spectral

region observed was restricted to either 250 to 700 nm with a monochromator-photomultiplier tube detection system or with a spectrograph, to the region 250 nm to 850 nm. No attempt was made to extend this research to emission at wavelengths longer than 850 nm.

The first studies involving nonmetal emission with the ICP as the excitation source can be considered as extensions of the research done with the MIP. Because the ICP has a higher temperature environment than either the argon or helium MIP, it was felt that the importance of molecular species would decrease. Denton and Windsor [76,77,83] did indeed verify this in their investigation of the ICP as a gas chromatographic detector. Although some molecular species were still observed, in particular C_2, CH, CN, CS, NH and OH, their intensities were weak and the proportion of molecular to atomic species in the ICP was markedly decreased over that of the MIP [77].

The goal of Windsor and Denton's research [83] was to determine the empirical formulas of organic compounds containing nitrogen, oxygen, sulphur, phosphorus, halogens, boron and, of course, carbon and hydrogen. They were, to a large extent, successful. For the wavelength region considered, between 190 and 650 nm, it was possible to analyze for these elements, with the exception of bromine, chlorine, fluorine, nitrogen and oxygen.

Empirical formulas were in good agreement with theoretical values. In a detailed study [83] of the carbon response of the MIP, the response was firstly found to be proportional to the carbon content of the compound being analyzed. Secondly, with the exception of pyridine and chlorine- and bromine-containing compounds, response was dependent only on the number of carbons in the compound and not on the functional groups contained in the compound. In their system, sample introduction was accomplished by either introducing the effluent from the gas chromatograph into the aerosol channel of the ICP [83] or by passing the nebulizer gas over the surface of a volatile organic liquid [77]. Detection limits were at the nanogram level, similar to those obtained with a helium MIP.

The emission lines in the ICP for several nonmetal elements have been well characterized in the spectral region 0.50 to 1.0 μm. Fry et al. [84-90], using a spectrographic detection system, examined the background emission spectrum of the ICP and emission lines of carbon, nitrogen, oxygen, sulphur and the halogens in this region. Analyte species were usually inorganic in nature; for example, such species as carbon dioxide and sulphur dioxide were introduced into the plasma for the study of carbon and sulphur emission. All samples were introduced

into the ICP as gases by either mixing the sample with the argon nebulizer gas or by using a gas sampling loop to inject the sample into the aerosol flow. Fry found that at forward power levels greater than 1.75 kW complete dissociation occurred in the ICP for all compounds studied. Tables of atomic nonresonance lines observed were presented as were partial Grotrian diagrams for the elements examined [84,86-90]. In contrast to the normal viewing zone in the ICP at 15 to 20 mm above the load coil for metal analysis, Fry found that the optimum viewing zone for nonmetal elements introduced as gases was actually between the turns of the load coil itself. Detection limits were found to be in the µg range for samples introduced through the gas sampling loop. Because it is difficult to measure emission within the load coil, detection limits were measured directly above the load coil with a red enhanced PMT-based detection system. Using lines in the region above 0.5 µm, detection limits were improved over those obtained by Denton [83]. Again, no attempt was made to consider emission at wavelengths longer than 1.0 µm.

More recently, Blades [91,92] has reported the use of a photodiode array-ICP spectrometer for the analysis of the sulphur content of tar sands petroleum products. He considered only a small spectral region around the sulphur

triplet at 0.922 μm. In his work, sulphur containing organic molecules were introduced into the ICP as liquids diluted with xylene. He obtained a detection limit for sulphur as thiophene of 122 ppm using the 0.9217 μm sulphur line. It was reported that the limiting factor in the analysis of sulphur would be the C_2 emission spectrum in this region. No attempt was made to determine the relative sensitivity of different sulphur containing molecules.

In this group [93,94], the above research has been extended to the emission of solution samples containing carbon, hydrogen, oxygen, sulphur, chlorine and bromine in both aqueous and organic solutions, in the wavelength region 0.7 μm to 3.0 μm. The purpose of this study was twofold:

1) to characterize ICP background emission in this region and
2) to attempt to find alternate analytically useful lines for the analysis of the above elements in the ICP.

To characterize emission of the ICP in this region, the Fourier transform spectrometer (FTS) with either a PbS or PbSe detector was chosen as the detection system. For this type of study, the FTS system has two main advantages over a grating-based detection system (see Chapter I):

1) wavelength assignments are greatly facilitated by the accurate and precise wavelength axis provided by the reference laser in the interferometer, and
2) in the FTS system [72], both background and analyte emission over the whole wavelength region of interest can be simultaneously measured.

B. The Experimental System

A commercially available 27.12 MHz radiofrequency inductively coupled plasma source was used (Plasma-Therm Inc., Kresson, N.J.). The source consists of a Model HFP-2500D 2.5 kW RF generator, a Model ADCS-3 automatic power control, a Model AMN-2500E automatic matching network and a Model PT-2500 plasma torch assembly. Plasma operating conditions and flow rates were as listed in Table 4. All samples were introduced as aerosols using a standard concentric glass nebulizer, with the exception of sulphur dioxide.

In some cases, it was necessary to use mixed gas plasmas. To accomplish this, a gas mixer (Model 605 flowtubes, Matheson, East Rutherford, N.J.) was used to mix argon with various other gases, mostly nitrogen and oxygen, prior to introducing the coolant gas into the plasma discharge. In all cases, both the auxiliary and nebulizer gases were totally argon. The mixed gas plasmas

Table 4

Plasma Running Conditions

Forward Power	1.5-2.0 kW
Reflected Power	<0.05 kW
Frequency	27.12 MHz
Coolant gas	a) Ar, 15 l/min
	b) Ar/30% N_2, 15 l/min
	c) Ar/10% O_2, 15 l/min
Auxiliary gas	Ar, 0.2 l/min
Nebulizer gas	a) aqueous aerosols: 0.5 l/min
	b) organic aerosols: 0.4 l/min
Viewing Zone	a) Ar, 18-20 mm above l.c.
	b) Ar/30% N_2, 5 mm above l.c.
	c) Ar/10% O_2, 5 mm above l.c.

were first initiated using pure argon, then crossed over to the applicable mixed gas conditions.

Sulphur dioxide was introduced into a 100% argon ICP as an approximately 0.1% solution with the nebulizer gas. The gas mixer was similar to that used with the coolant gas above except that the flowtubes had a smaller diameter (Model 603 flowtubes). Again, the plasma was initiated using 100% argon, the aerosol channel was formed using pure argon as the nebulizer gas and then SO_2 was introduced into the nebulizer gas.

The FTS system has been described in Chapter II. To cover the complete spectral region of interest (0.7 to 3.0 μm) it was necessary to use two different beamsplitters in the interferometer. With the PbS detector, a germanium coated quartz beamsplitter was in place, while with the PbSe detector a germanium coated salt beamsplitter was used. The optical system used for each beamsplitter is summarized in Table 5. The optical link between the ICP and the interferometer (see Figure 14) was accomplished by focussing a 1:1 image of the plasma onto a circular aperture with a 5.0 mm diameter using the first lens (Table 5). The second lens was placed at a distance of its focal length from the aperture, providing the collimated light necessary for the interferometer.

Table 5

Interferometer Opto-Electronic Components

WAVELENGTH	BEAMSPLITTER	LENS	DETECTOR
0.7-1.4 μm	Ge coated- Quartz substrate	1) 10 cm quartz 2) 10 cm quartz	PbS(uncooled) area = 1 mm^2
1.4-3.0 μm	Ge coated- NaCl substrate	1) 20 cm NaCl 2) 5 cm NaCl	PbSe(uncooled) area = 1 mm^2

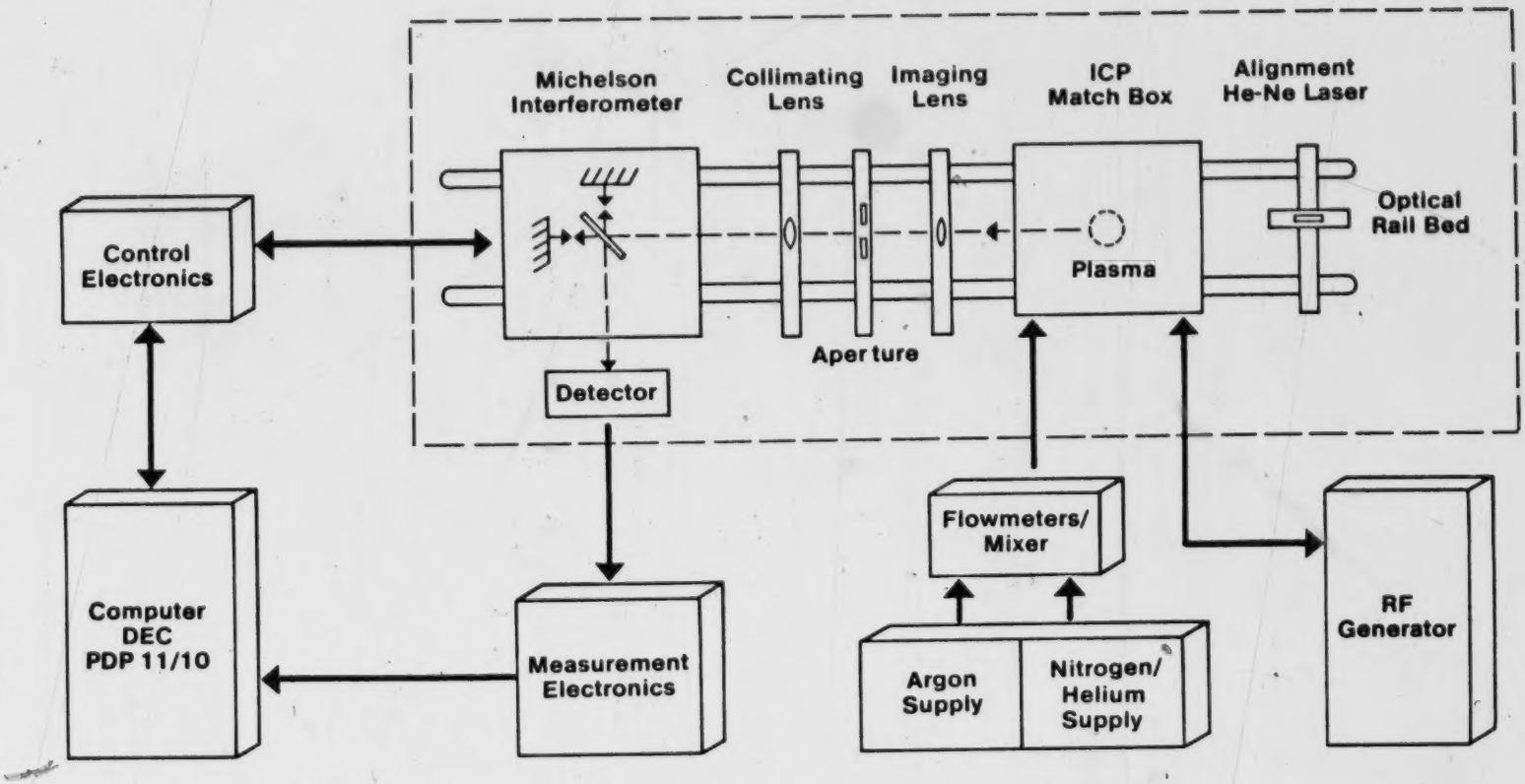

Figure 14. Block diagram of the ICP-Fourier transform spectrometer system.

Because the interferometer modulates all emission incident upon it, it was necessary to place a cold mirror (Melles Griot, Irvine, California) with a cutoff wavelength of 0.7 μm before the interferometer entrance. This mirror eliminated unwanted visible emission from the ICP. As well, to eliminate both radiation and noise pickup from outside the spectral region of interest, electronic filtering of the interferogram was performed using a variable electronic filter (Krohn-hite Model 3343, Avon, Massachusetts).

Depending upon the sample, either 32 or 128 interferograms were signal averaged. Gaussian apodization was performed on the averaged interferograms. All spectra were then calculated from 4096-point double sided interferograms, minimizing phase problems [72].

The lead sulphide and lead selenide detectors were used in a biased mode, with the bias voltage provided by a 62.5 V battery in series with a 1.0 MΩ resistor. Signal electronics were identical to that described in Chapter II.

C. Results and Discussion

1. Aliasing

An important aspect of the FTS system for measurements in the near-IR region is the phenomenon of

aliasing [67,72]. Aliasing, by definition, results from the incorrect sampling of a high frequency signal. This signal, instead of appearing at its correct frequency, will appear at a much lower frequency. In the interferometer the basic sampling interval using the He-Ne laser, is 0.6328 μm. Therefore, the shortest wavelength which can be sampled without aliasing is 1.26 μm (7901.4 cm^{-1}). Thus the 0 to 7901.4 cm^{-1} bandwidth can be covered without aliasing. Wavelengths shorter than 1.26 μm are folded or aliased into this bandwidth. Figure 15 illustrates this phenomenon for the near-IR region of the spectrum. An unaliased spectral region from 0.0 to 15802.8 cm^{-1} is depicted in Figure 15a. The spectral region covered in these measurements extends from the cold mirror cutoff at approximately 0.7 μm (13316 cm^{-1}) down to about 2.0 μm (5000 cm^{-1}) for PbS or 3.2 μm (3125 cm^{-1}) for PbSe. Under aliasing, the spectra will be similar to that depicted in Figure 15b. Although the two regions overlap, they do so in an accurately predictable fashion. One can either tolerate aliasing or increase the sampling frequency to twice the highest frequency of interest as previously discussed in Chapter I.

Spectra presented in this chapter appear as illustrated in Figure 15b. Spectral lines are either labelled with their correct wavelengths or, for more

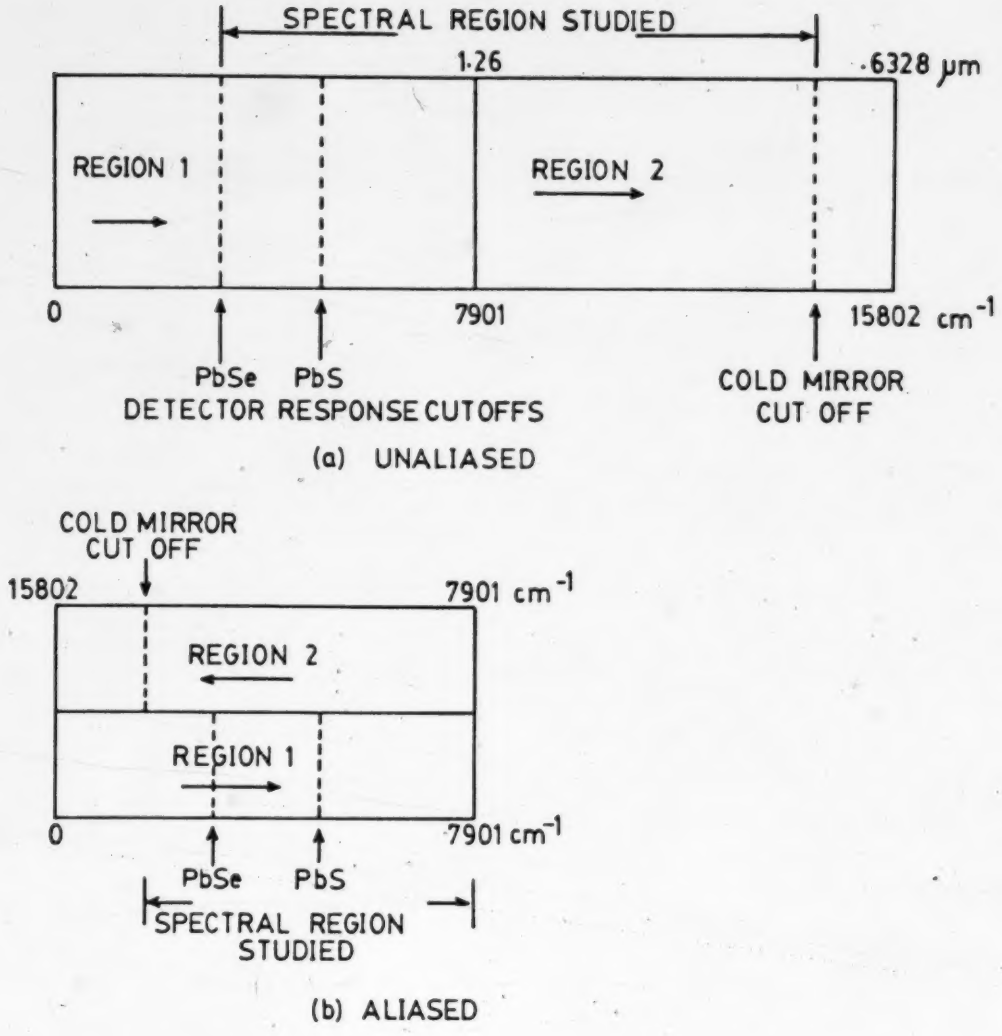

Figure 15. Schematic spectrum of the near infrared spectral region: (a) the unaliased spectrum and (b) the aliased spectrum.

complicated spectra by: 1; representing the spectral region 0.0 to 7901.4 cm^{-1} and 2; representing the spectral region 7901.4 cm^{-1} to 15802.8 cm^{-1}.

2. ICP Emission Spectra in the Near-IR

The background spectrum of the argon ICP is quite complex in both the spectral region covered by the PbS optical system (Figure 16) and the region covered by the PbSe optical system (Figure 17). Wavelengths for the major lines are tabulated in Table 6.[1] Literature wavelengths for all tables were taken from either Zaidel et al. [75] or Bashkin and Stoner [95]. All atomic lines observed were found to be the result of excited neutral argon atom emission. In addition to the atomic lines observed, a molecular or broad band signal was noted in Figure 17 with a wavelength of approximately 2.5 μm (4000 cm^{-1}). This band was most intense in the absence of the aerosol channel in the ICP and was attenuated by the introduction of water into the aerosol channel. It is, therefore, difficult to attribute this band to hydroxyl emission in the 3 μm (3333.3 cm^{-1}) region. As well, the band wavelength did not correspond to wavelengths of hydroxyl or water bands [96] in this region.

However, in an experiment designed to strongly reduce air entrainment in the ICP, a quartz extension tube was placed over the top of the regular torch. In this case,

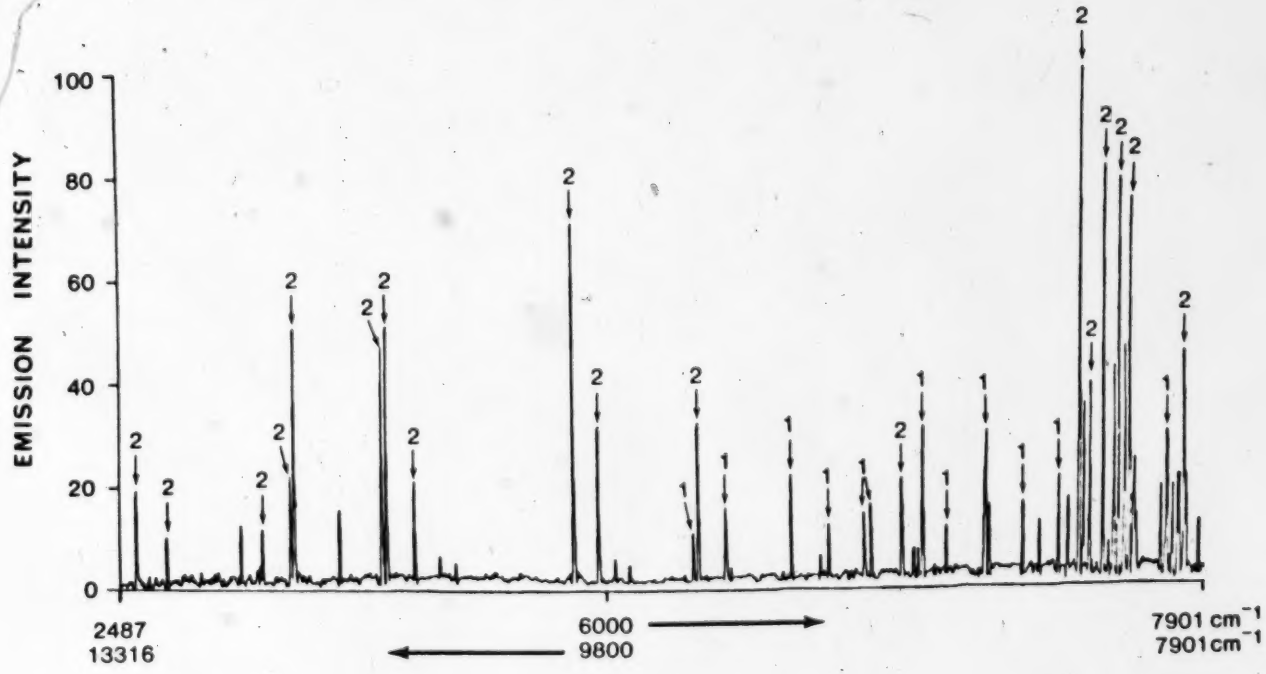

Figure 16. Spectrum of background emission from the argon ICP as measured by the PbS detector.

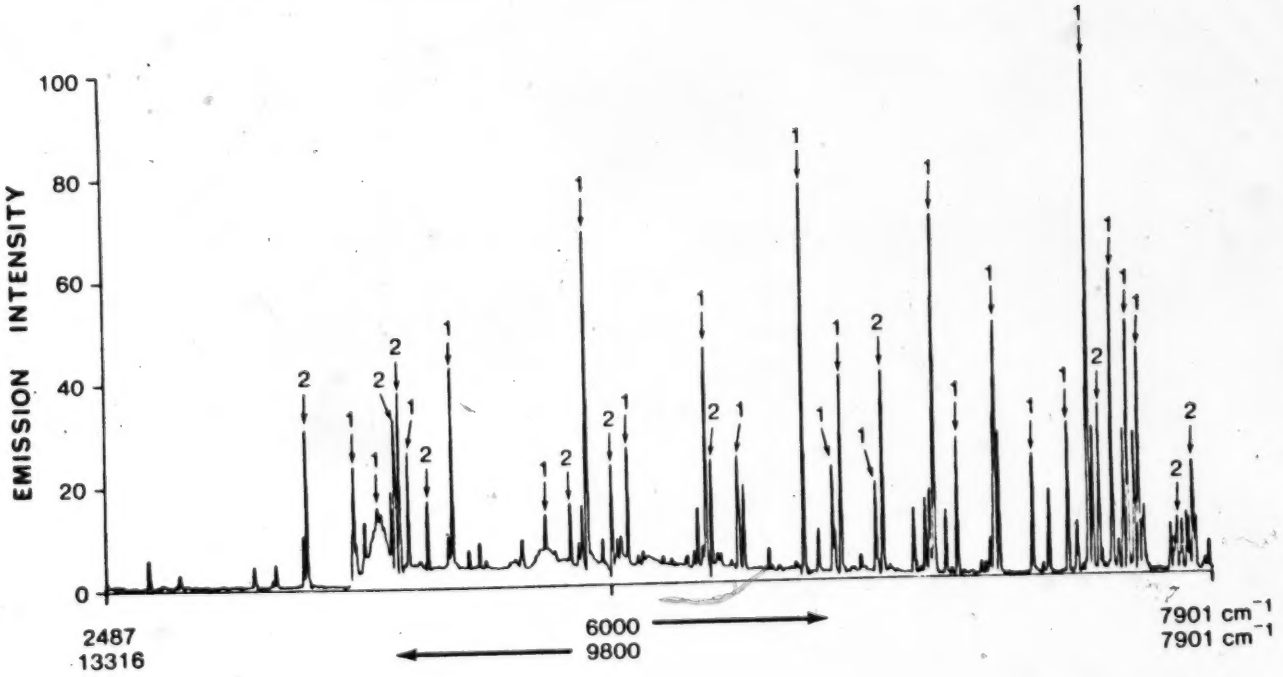

Figure 17. Spectrum of background emission from the argon ICP as measured by the PbSe detector.

Table 6

Major Argon Lines

Observed Lines		Literature[75,95]
Wavenumber (cm^{-1})	Wavelength (μm)	Wavelength (μm)
13086.0	0.7642	0.7636
12329.7	0.8110	0.8115
12312.3	0.8122	0.8119
11882.0	0.8416	0.8424
11858.9	0.8432	0.8443
11723.8	0.8530	0.8521
10952.0	0.9131	0.9123
10830.4	0.9233	0.9225
10344.2	0.9667	0.9667
8572.9	1.1665	1.1668
8515.0	1.1744	1.1738
8246.8	1.2136	1.2139
7999.8	1.2815	1.2803
7716.2	1.2959	1.2956
7533.0	1.3275	1.3273
7509.8	1.3316	1.3313
7478.9	1.3371	1.3367
7403.6	1.3507	1.3504
7341.1	1.3622	1.3628
7187.6	1.3913	1.3910
5900.5	1.6948	1.6940
5045.7	1.9819	1.9817
4194.8	2.3839	2.3845
3897.6	2.5657	2.5661
3859.1	2.5913	--
3830.1	2.6109	--
3716.3	2.6909	--

the plasma discharge expands to the length of the extension tube. The spectrum obtained (Figure 18) with the extended torch, was dominated by a similar broad band, but with a much higher intensity, also centered at approximately 2.5 μm (4000 cm^{-1}). It was felt that this band was due to radiation from the hot extension tube, and hence that the much weaker band apparent in the ICP spectral background was also due to radiation of the hot quartz torch.

As discussed earlier in Chapter I, the dynamic range of an interferometer based system can be limited by a small number of very intense lines or by a larger number of less intense lines. In this study, the argon ICP background limited the dynamic range to the extent that it was difficult to observe the weaker analyte emission lines of interest.

In work done previously in this laboratory [97] and in others [98,99] it was shown that the use of a mixed gas plasma reduces the intensity of the argon spectrum and gives detection limits comparable to, or better than, the conventional pure argon plasma. To take advantage of these features, several types of mixed gas plasmas in which varying proportions of either oxygen, nitrogen or helium were mixed with the argon coolant, were tried.

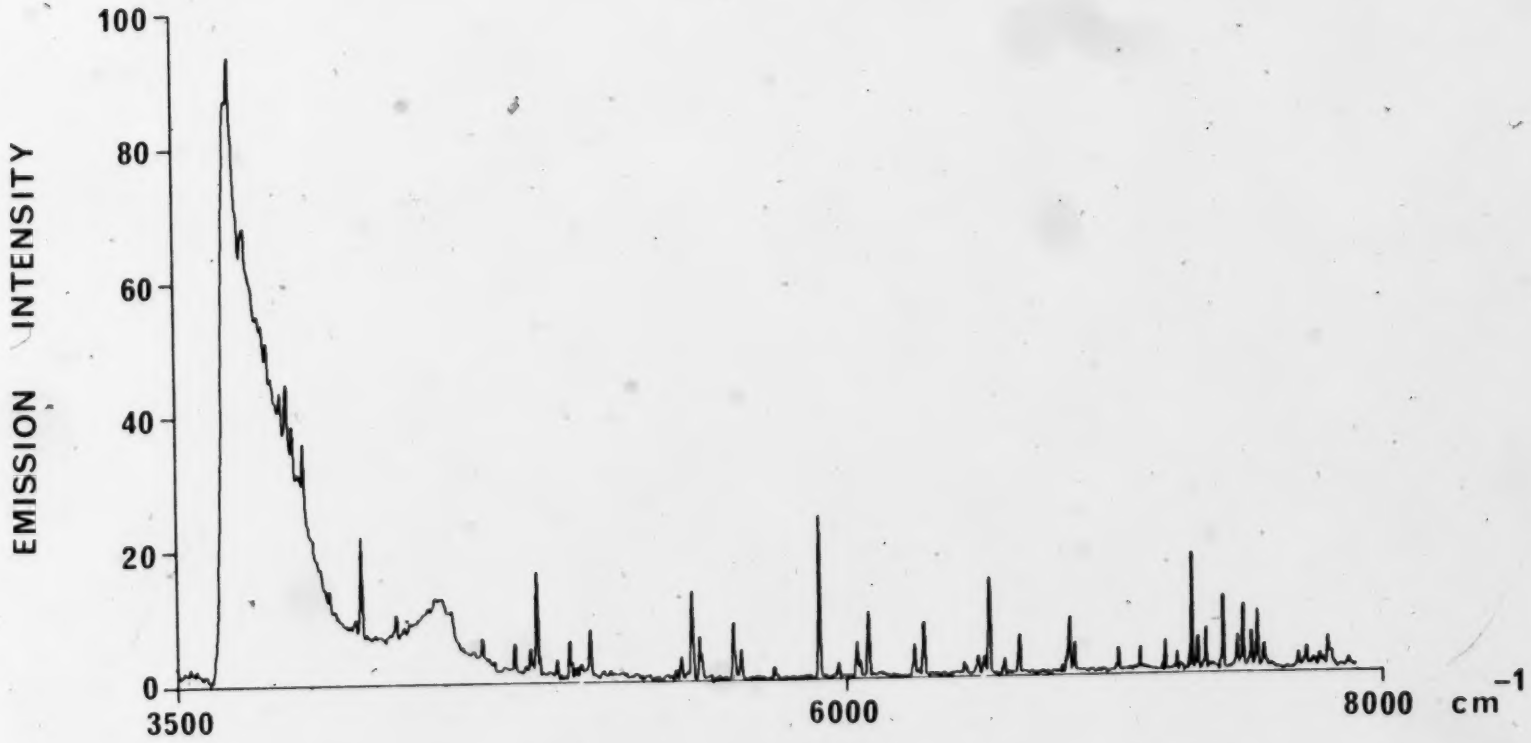

Figure 18. Emission spectrum of an ICP discharge using a tall torch.

Similar to the results reported by Choot [97,100], the introduction of helium into the argon coolant produced a much less stable discharge which was difficult to sustain. Only one helium line, at 0.955 μm (10471.2 cm^{-1}) was observed. However, the reduction in intensity of the argon background was minimal.

The addition of both oxygen and nitrogen into the coolant was more successful. In the 10% O_2/Ar cooled ICP (Figure 19), the intensity of the argon background was greatly diminished. However, the intensities of the major atomic oxygen lines (Table 7) were considerably more intense than the argon lines in the 100% argon cooled plasma. The most effective mixed gas plasma, illustrated in Figure 20, was a 30% N_2/Ar cooled ICP. The intensity scale of this spectrum is one-tenth of that illustrated in the argon spectrum shown in Figure 16. Although the background spectrum of the N_2/Ar plasma is slightly more complex than in the 100% argon plasma, the overall intensity of the background has been substantially reduced. It is clear from Figure 20 that the argon lines in the 1 μm (10000 cm^{-1}) region are much less intense than the additional nitrogen lines. As well, the intensity of the strongest line in the 30% N_2/Ar background spectrum is an order of magnitude weaker than that of the strongest line in the 100% argon background spectrum. All oxygen

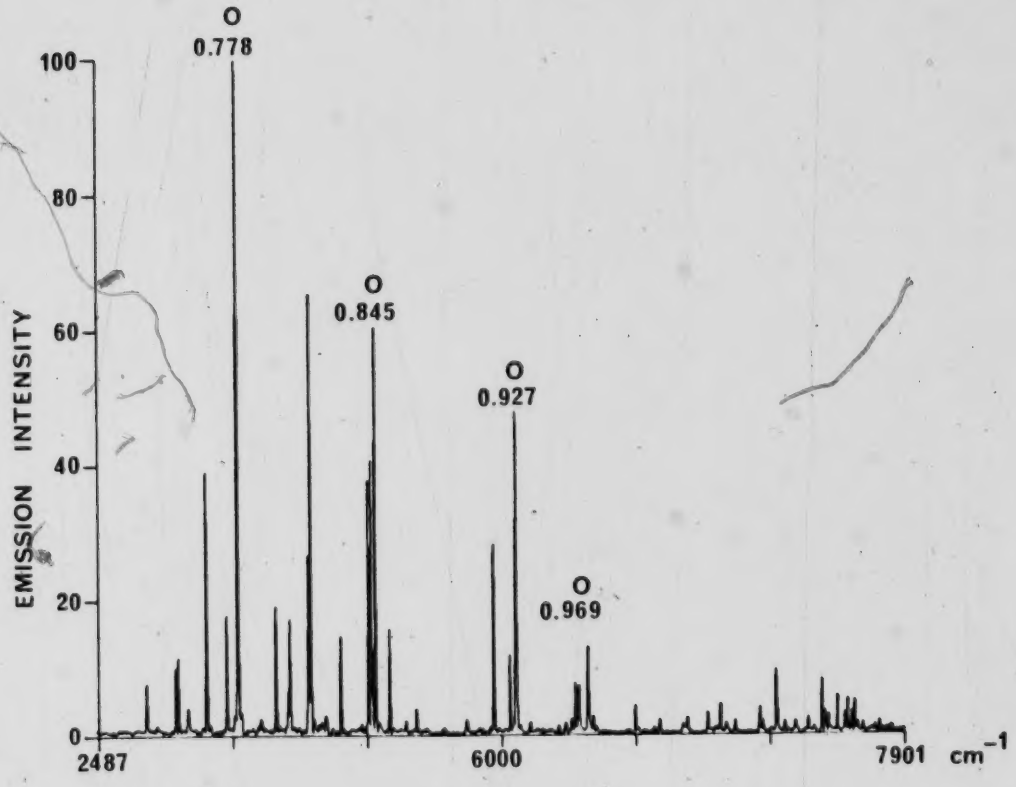

Figure 19. Spectrum of background emission from the 10% O_2/Ar ICP as measured by the PbS detector.

Table 7

Atomic Oxygen Emission Lines in the Near-IR Region

Observed Lines		Literature[95]
Wavenumber (cm^{-1})	Wavelength (μm)	Wavelength (μm)
12860.3	0.7776	0.7773
11833.8	0.8450	0.8447
10789.9	0.9268	0.9266
10321.0	0.9689	0.9686

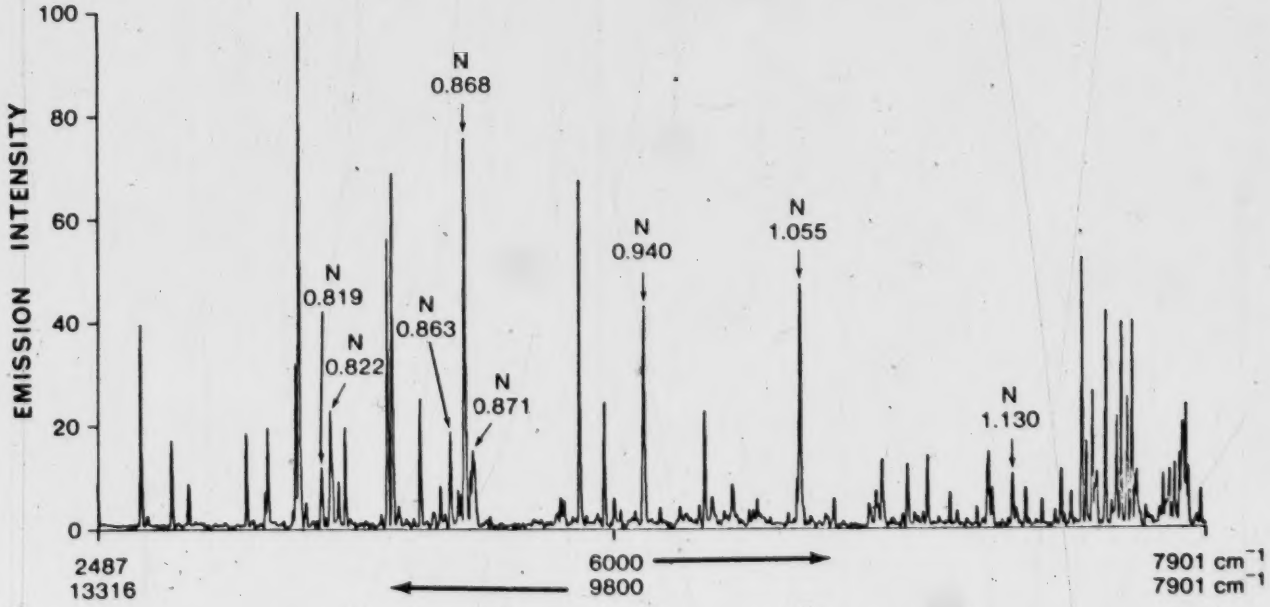

Figure 20. Spectrum of background emission from the 30% N_2/Ar ICP as measured by the PbS detector.

and nitrogen lines (Tables 7 and 8) were also the result of neutral atom emission.

One additional effect of introducing an alien gas into the coolant gas, is that the physical dimensions of the plasma become much smaller [100]. For this reason, instead of viewing in the normal viewing zone, 15 to 20 mm above the load coil, measurements were made in the region centered around 5 mm above the load coil (Table 5).

3. Spectra of Species Containing the Elements C, H, O and S

i) Sulphur Dioxide

The spectrum of sulphur dioxide, introduced into the 100% argon ICP as a 0.1% mixture with the nebulizer gas, is presented in Figure 21. For sulphur emission lines (Table 9) with wavelengths shorter than 1.0 μm, their relative order of intensity and their wavelengths were in good agreement with those reported by Fry [87]. However, due to dynamic range limitations, many of the weaker lines reported by Fry were not observed in this spectrum. The resolution of the interferometer, 8 cm^{-1}, is insufficient to completely resolve the sulphur triplet centered at 0.922 μm (10846.0 cm^{-1}). As well, this triplet is partially obscured by an interfering argon line at 0.9225 μm (10840.1 cm^{-1}). Several sulphur lines (Table 9), the most intense at 1.046 μm (9560.2 cm^{-1}), were observed in

Table 8

Major Nitrogen Lines

Observed Lines		Literature[95]
Wavenumber (cm^{-1})	Wavelength (μm)	Wavelength (μm)
12210.0	0.8188	0.8188
12167.6	0.8219	0.8216
11584.9	0.8632	0.8629
11515.4	0.8684	0.8683
11486.5	0.8706	0.8704
11474.9	0.8715	0.8719
10643.3	0.9396	0.9393
9483.6	1.0545	1.0539
8852.7	1.1296	1.1292

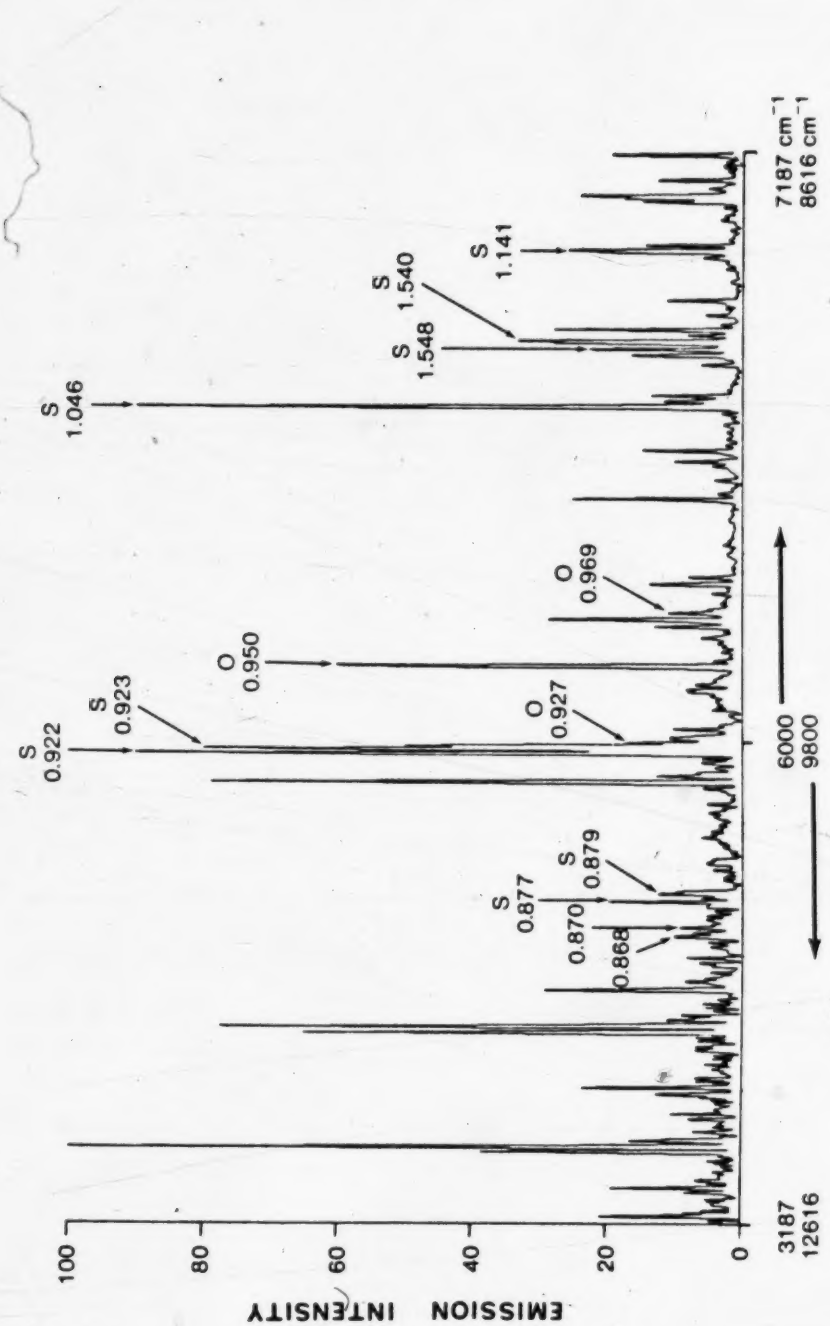

Figure 21. Emission spectrum of sulphur dioxide in the ICP.

Table 9

Major Sulphur Lines

Observed Lines		Literature[75,95]
Wavenumber (cm^{-1})	Wavelength (μm)	Wavelength (μm)
11515.4	0.8684	0.8680
11496.1	0.8699	0.8695
10849.7	0.9217	0.9215
10324.9	0.9699	0.9694
9558.9	1.0462	1.0462
8765.8	1.1408	1.1407
6492.8	1.5402	1.5407
6462.0	1.5475	1.5475

the region above 1.0 μm. These lines have not been reported in the ICP prior to this study. In the PbSe region between 1.6 and 3.0 μm, only argon and nitrogen lines were obseved.

Mermet [101] recorded sulphur emission lines in a 40 MHz plasma at relatively high powers, in the range of 6 kW. He identified singly ionized sulphur emission lines with an H_2S/Ar cooled discharge. With the lower frequency, lower powered plasma used in this study, no ion lines were observed.

ii) Xylene

The spectra of xylene in a 100% Ar cooled plasma in both the PbS and PbSe regions (Figures 22 and 23) exhibited only lines due to excited carbon neutral atom emission. Major lines are tabulated in Table 10. No hydrogen lines were observed. It should be possible to observe molecular fragment emission in these regions, for example, the C_2 bands reported by Blades [92]. However, there is no evidence for the presence of molecular species in either Figure 22 or 23. In fact, the spectrum of xylene was recorded at different viewing zones of the ICP, including the tailflame region. Although no molecular species were observed in the near-IR the blue color indicative of the presence of C_2 could be seen in the central aerosol channel and skirting the ICP. The blue

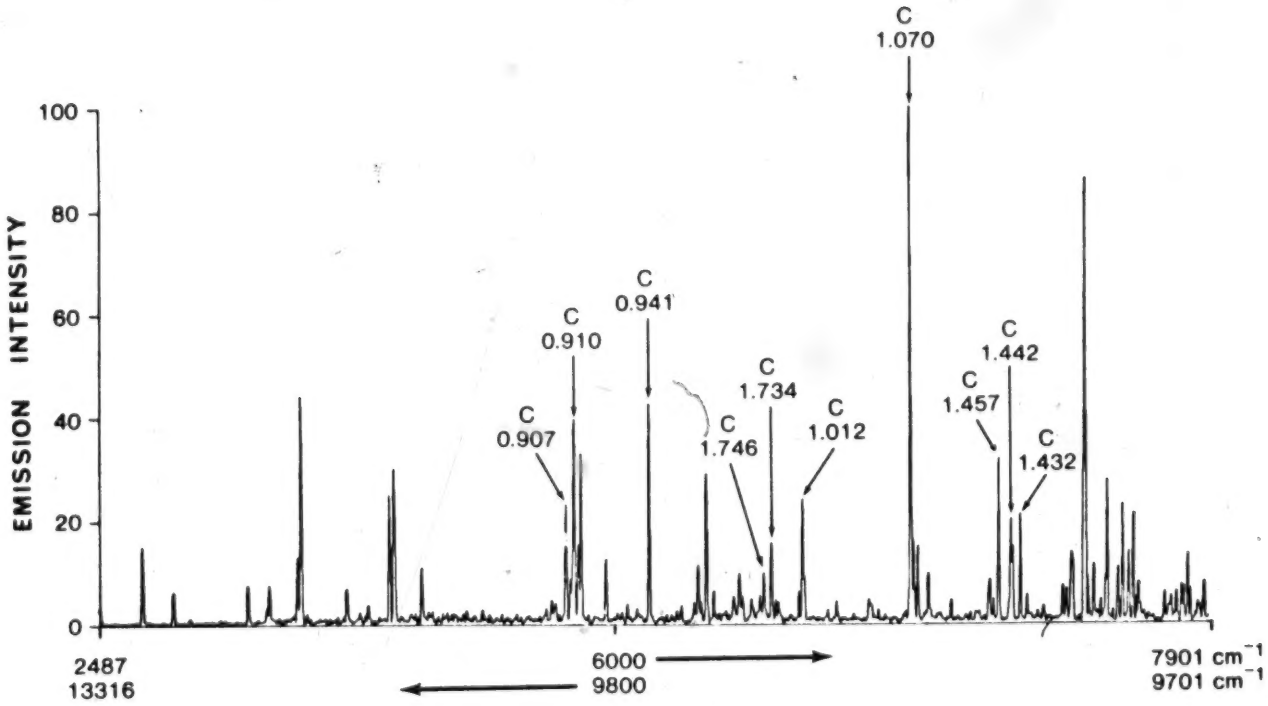

Figure 22. Emission spectrum of xylene in the ICP as measured by the PbS detector.

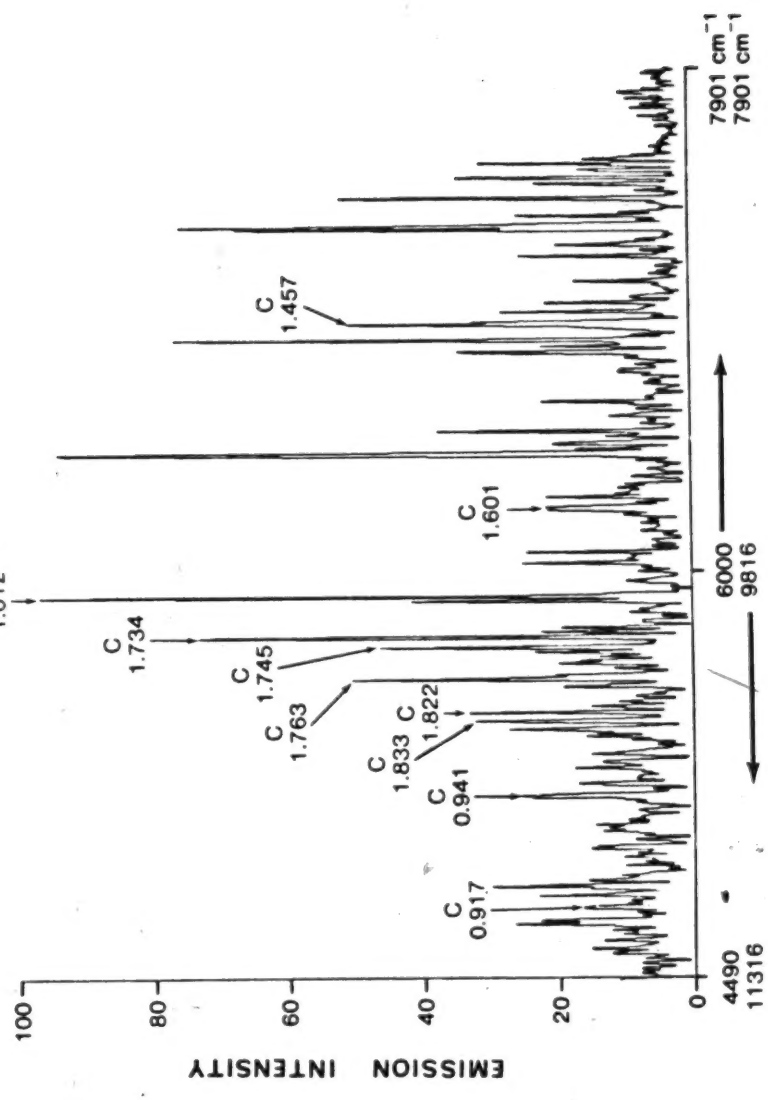

Figure 23. Emission spectrum of xylene in the ICP as measured by the PbSe detector.

Table 10

Major Carbon Lines

Observed Lines		Literature[75,95]
Wavenumber (cm^{-1})	Wavelength (μm)	Wavelength (μm)
11020.5	0.9074	0.9078
10989.0	0.9100	0.9104
10627.0	0.9410	0.9406
9879.5	1.0120	1.0124
9345.8	1.0700	1.0698
6934.8	1.4420	1.4420
6873.8	1.4548	1.4542
6253.9	1.5990	1.5987
6246.1	1.6010	1.6007
5766.7	1.7341	1.7338
5728.7	1.7456	1.7456
5669.9	1.7637	1.7637
5487.6	1.8223	1.8221
5455.5	1.8325	1.8321

color in the ICP can be attributed to C_2 emission in the 450 nm region. Emission in this spectral region was not measured in these experiments. It is possible that the intensity of these bands in the near-IR region were too weak to observe with the interferometer system.

In contrast to Fry's [84-90] results, the optimum viewing zone was not between the turns of the load coils, but rather was found to be in the normal viewing zone for metals, 15 to 20 mm above the load coil.

iii) Dimethylsulphoxide (DMSO)

The spectrum of 100% DMSO should be a composite of the SO_2 and xylene spectra. In a pure argon ICP, however, only the argon background spectrum was apparent. A 30% N_2/Ar ICP reduced the argon background to the extent that emission originating from DMSO could be observed (Figure 24). The more intense lines of sulphur and carbon as reported in the xylene and SO_2 spectra, were observed in the spectrum of DMSO. The weaker atomic lines, for example the sulphur lines around 0.870 μm (11494.3 cm^{-1}) in the SO_2 spectrum were not observed in the DMSO spectrum. Only one oxygen line at 0.950 μm (10526.3 cm^{-1}) was observed.

To obtain this spectrum, 100% DMSO was nebulized into the ICP. An unsuccessful attempt was made to observe sulphur emission in the near-IR region by aspirating a

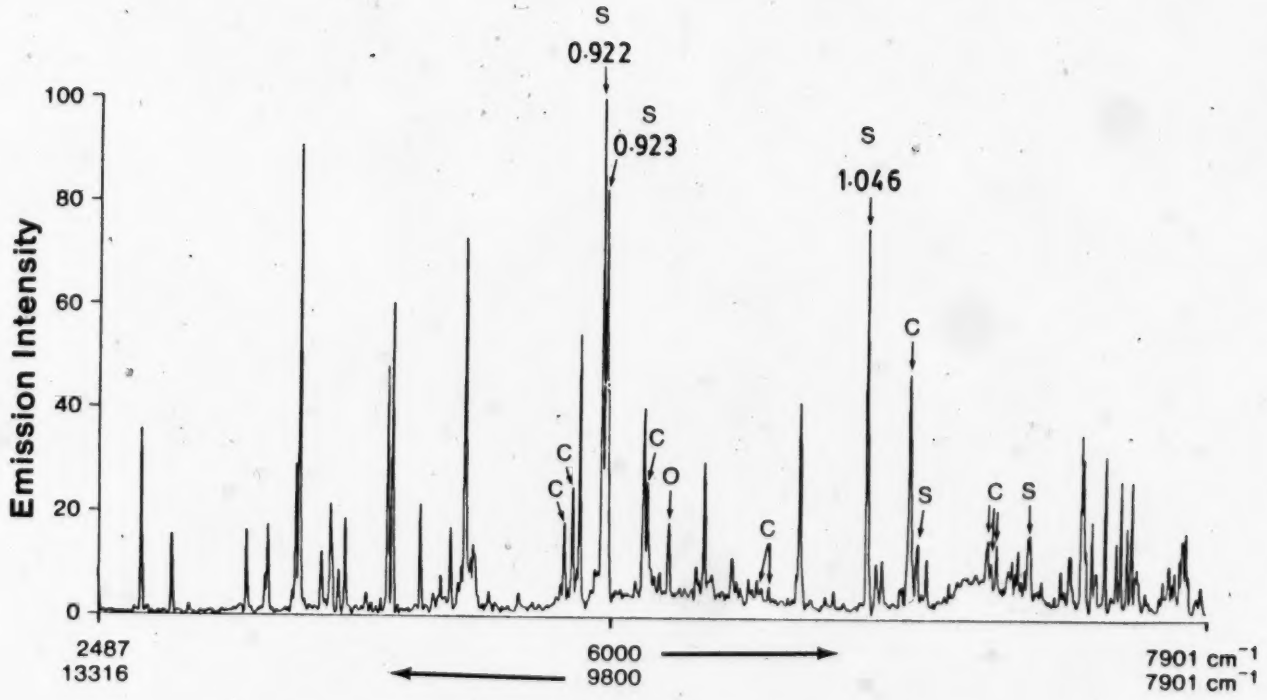

Figure 24. Emission spectrum of dimethylsulphoxide in the ICP.

1000 ppm aqueous thiourea solution into the ICP. Only background emission was observed. Part of this insensitivity can be attributed to the dynamic range problem imposed by the interferometer-based measurement system. However, it is evident that the sensitivity for these elements, carbon, oxygen and sulphur in the near-IR region cannot match that of the resonance lines in the vacuum ultraviolet region. Although it would appear that detection limits will prove inferior to those reported for the vacuum UV, there are several potentially useful analytical lines: for sulphur, the triplet centered at 0.922 μm (10846.0 cm^{-1}) and the 1.046 μm (9560.2 cm^{-1}) line; for oxygen, 0.950 μm (10526.3 cm^{-1}) and for carbon, 1.070 and 1.734 μm (9345.8 and 5767.0 cm^{-1}).

4. Halogen Containing Species

In the analysis of organic molecules, in addition to the major elements C, H, N, O and S, it is often important to be able to analyze for such elements as chlorine and bromine. Detection limits [89,90] in the ICP for these elements in the UV and visible region are poor and their resonance lines lie below 170 nm. The spectral emission of dichloromethane and dibromomethane have been characterized in the near-IR and will be presented below.

In a 100% argon discharge, the introduction of halogenated hydrocarbons into the plasma produced an

intense carbon continuum in this region, masking any atomic emission that was present. Addition of a small amount of oxygen into the argon coolant eliminated this interference. All spectra presented in this section were measured with an approximately 1% O_2/Ar cooled plasma.

i) Chlorinated Hydrocarbons

The spectrum of 100% dichloromethane in a 1% O_2/Ar ICP discharge is presented in Figure 25. This spectrum was obtained using the salt beamsplitter and the PbS detector. In contrast to the line emission spectra characteristic of sulphur and oxygen containing hydrocarbons, there are no apparent atomic lines, either of the analyte species or of the argon background. Instead, the dominant feature in this spectrum is a series of relatively evenly spaced lines in the region 2.584 to 2.294 μm (3869.9 to 4359.2 cm^{-1}). This type of structure (probably vibrational) is characteristic of a simple diatomic or triatomic species.

An expanded view of this structure is presented in Figure 26 with the wavelengths and relative intensities tabulated in Table 11. One complicating problem in attempting to identify this molecular fragment is that the emission due to hot quartz which was discussed earlier in this chapter occurs in the same region as this fragment. As well, several argon lines, in particular those at

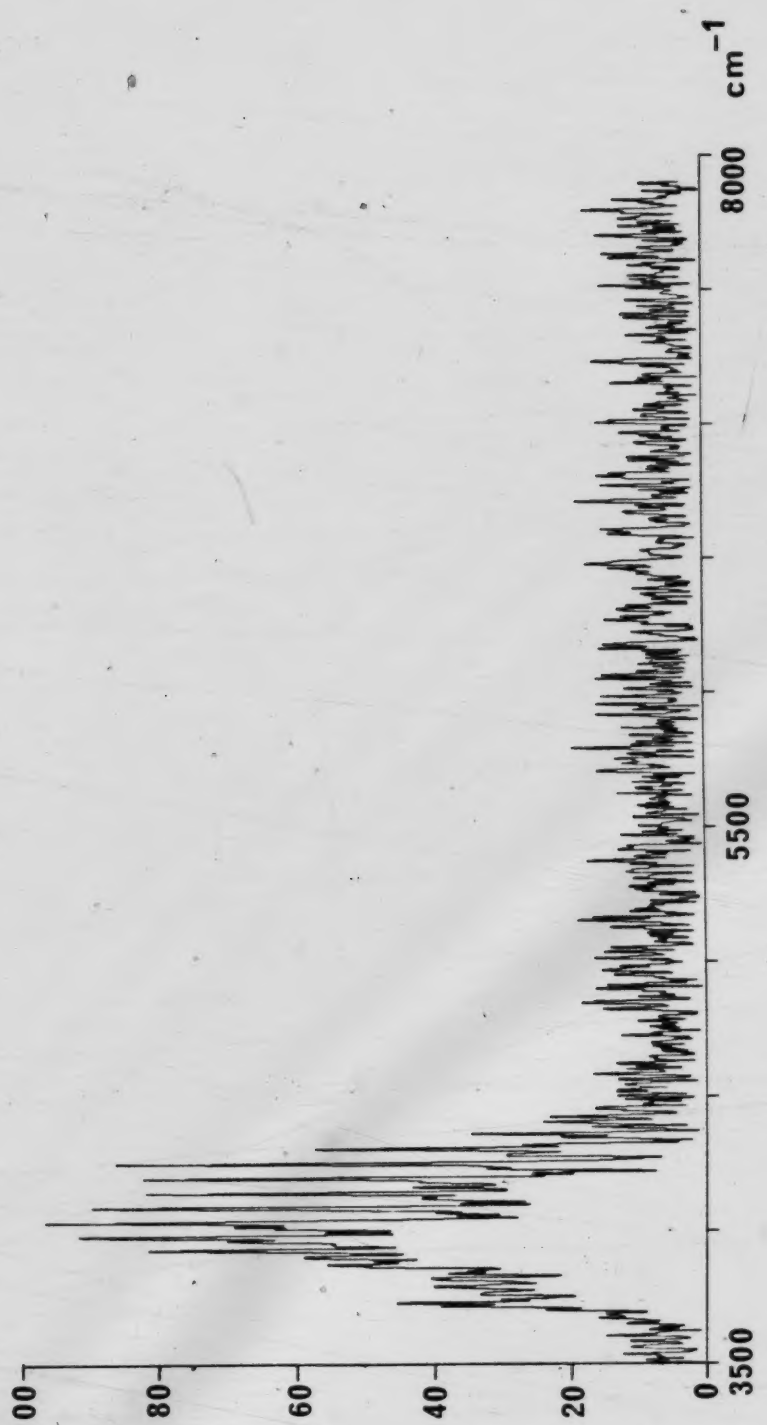

Figure 25. Emission spectrum of 100% dichloromethane in the ICP.

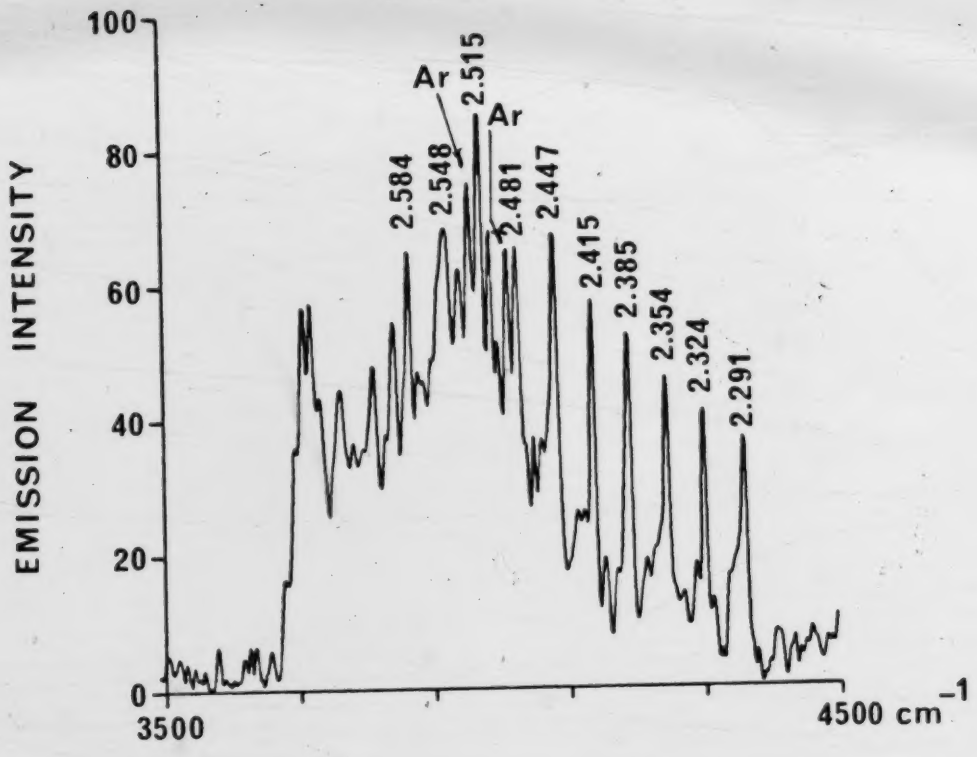

Figure 26. Expanded portion of the CH_2Cl_2 spectrum of Figure 25 showing the region between 3500 and 4500 cm^{-1}.

Table 11

Individual Peaks of C-Cl Fragment Band

Wavenumber (cm^{-1})	Wavelength (μm)	Relative Intensity
3870.6	2.584	19.1
3924.7	2.548	19.4
3976.8	2.515	55.8
4030.8	2.481	57.7
4086.7	2.447	67.6
4140.8	2.415	85.2
4192.9	2.385	100.0
4248.8	2.354	87.8
4302.8	2.324	75.9
4358.8	2.294	32.4

0.8613 μm and 0.8456 μm (11610.4 and 11825.9 cm^{-1}, Figure 26) are aliased into this region. Intensities of the lines in the molecular structure were measured by measuring the height of the line plus the background, measuring the height of the background and subtracting the two values to obtain the intensity of the peak (Table 11).

Consideration of the elements in dichloromethane leads to the possibility of several molecular fragments: CH or CH_2, CCl or CCl_2, or an ionized form of one of these fragments. It is difficult to believe that a CH or CH_2 fragment is responsible for this emission since there was no evidence for molecular species in either the xylene or the dimethylsulphoxide spectra presented earlier, leaving the possibility of a carbon-chlorine fragment.

To this end, various mixtures of dichloromethane in xylene were run in the ICP. As the concentration of dichloromethane decreased, so did the intensity of the emission in the 2.5 μm (4000 cm^{-1}) region in an approximately linear fashion. With this diminishing intensity, a number of other atomic lines, both for chlorine and carbon, became apparent (Table 12).

To completely eliminate the existence of emission from a C-H fragment, carbon tetrachloride was aspirated into the plasma (Figure 27). Although the intensities of the lines in the 2.5 μm (4000 cm^{-1}) region were much

Table 12

Major Atomic Chlorine Lines

Experimental		Literature[75]
Wavenumber (cm^{-1})	Wavelength (μm)	Wavelength (μm)
11170.0	0.8953	0.8948
11031.1	0.9065	0.9070
10955.3	0.9128	0.9121
10761.0	0.9293	0.9289
10641.3	0.9397	0.9394
10388.6	0.9626	0.9628
10124.2	0.9877	0.9876
9900.4	1.010	1.009
8962.7	1.116	1.113
6400.8	1.553	1.552
6355.9	1.573	1.573
6298.0	1.588	1.588
6263.2	1.597	1.597
4906.8	2.038	2.036
4484.3	2.230	2.229

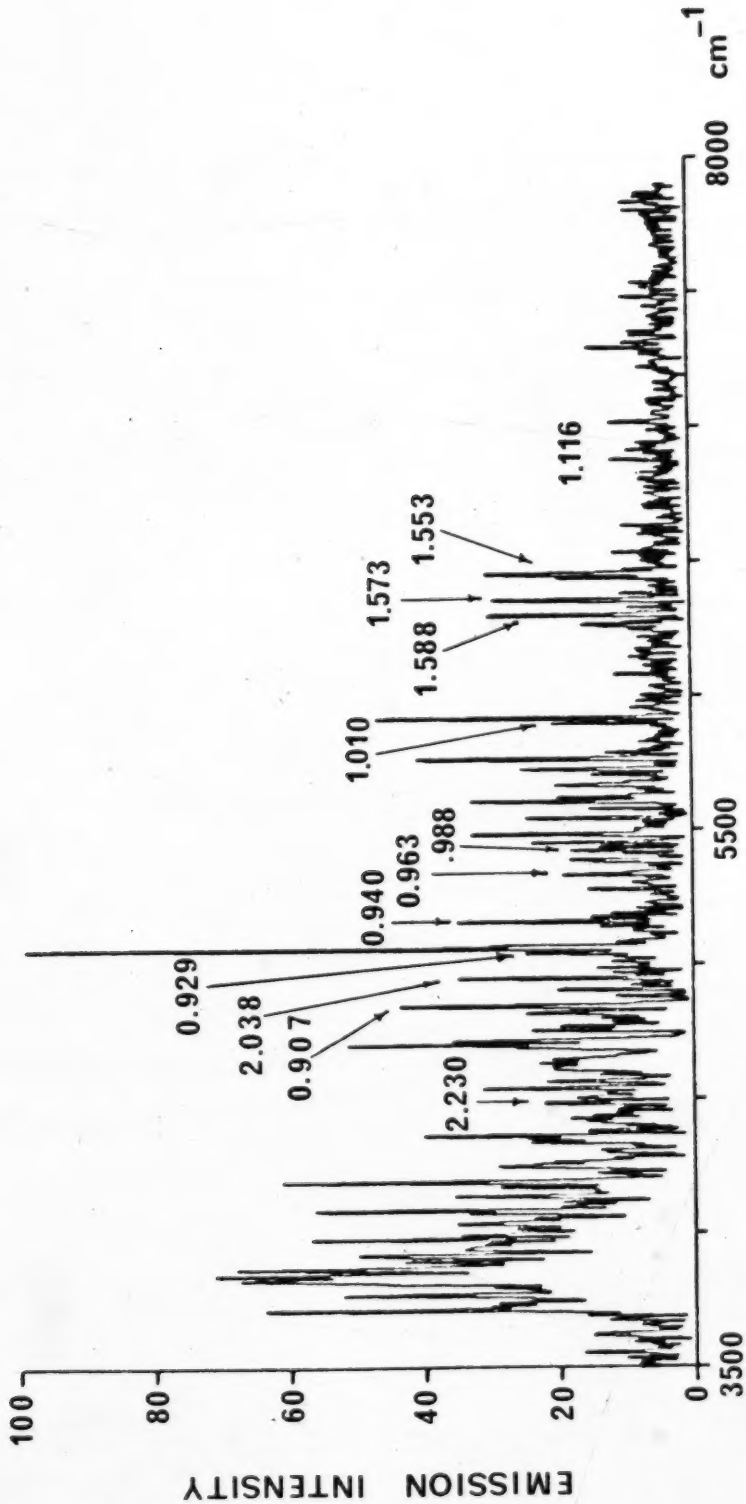

Figure 27. Emission spectrum of carbon tetrachloride in the ICP.

weaker, the molecular fragment emission was still apparent. As well, several further chlorine atomic lines became apparent (Table 12). In this instance, atomic emission appeared to be the dominant feature, with only a small proportion of a molecular species present. This is in direct contrast to the results obtained with dichloromethane. The presence of the molecular bands, albeit weak, in this spectrum lends support to the existence of a molecular fragment containing carbon and chlorine.

The spectra of the C-Cl and $C-Cl_2$ radicals generated in shock tube experiments, have been well characterized in the literature for the ultraviolet [102-104] and mid- to far-infrared [105] regions of the spectrum. The most prominent band, involving the ground state of the CCl radical occurs in the ultraviolet region between 270 and 290 nm. There have been no reports of either emission or absorption spectra for such radicals in the near-IR region.

In an attempt to fully ascertain the identity of the molecular fragment observed, the spectrum of dichloromethane was measured in both the UV and visible regions using the Al-coated quartz beamsplitter described in Chapter II and a photomultiplier tube as the detector. Only the atomic carbon lines at 193.1 and 247.9

nm were observed. Failure to observe any molecular fragment emission in these regions eliminates the possibility of positively identifying the molecular fragment and the transitions involved in the emission observed in the 2.5 μm (4000 cm^{-1}) region. Because the ICP is energetic enough to allow the population of various highly excited energy states, it is very difficult to ascertain which energy levels are involved in the transition without some knowledge of the ground state level of the molecule.

In the absence of a positive identification, a CCl or CCl_2 fragment can be inferred by considering the force constants of the C-Cl bonds in various chloromethanes [106]. Table 13 presents the C-Cl bond lengths and force constants for CH_2Cl_2, $CHCl_3$ and CCl_4 as determined by Shimanouchi and Suzuki [106]. It can be seen that the force constant decreases with increasing chlorine substitution and hence the tendency for the molecule to completely dissociate will increase. This is in agreement with the relative intensities of the fragment emission in the dichloromethane and carbon tetrachloride spectra. Chloroform, then, should have fragment emission intensities intermediate between these two cases. This was verified by aspirating chloroform into the ICP. The relative intensities were found to be approximately 4:2:1

Table 13

Bond Lengths and Force Constants for Several Chloromethanes

	Bond Length C-Cl (Å)	Force Constants C-Cl
CH_2Cl_2	1.772	1.950
$CHCl_3$	1.767	1.918
CCl_4	-	1.810

for the compounds CH_2Cl_2:$CHCl_3$:CCl_4. Further weight is given to the argument of the existence of the CCl radical by its observation in an argon MIP [81], at 278.8 nm.

In addition to the above chlorinated hydrocarbons, the spectrum of a 20000 ppm NaCl solution was obtained under the same conditions. Only atomic chlorine lines were observed.

Of the atomic chlorine lines observed (Table 12), the lines at 0.9397 μm and 0.9877 μm (10641.7 and 10124.5 cm^{-1}) were also reported by Fry [89]. Lines at wavelengths longer than 1.0 μm have previously not been reported for the ICP. All lines were due to excited neutral atom emission.

It is difficult to assess the utility of these chlorine lines for analysis. In the absence of any molecular fragments, that is, for inorganic salts similar to NaCl, analysis in the ICP for chlorine content should be straightforward. However, the existence of molecular fragments when chlorinated hydrocarbons are introduced into the ICP would make analysis of the chlorine content of organics difficult.

ii) Dibromomethane

The spectrum of dibromomethane again exhibited only atomic bromine lines (Figure 28). There was no evidence for the existence of a C-Br fragment similar to the CCl

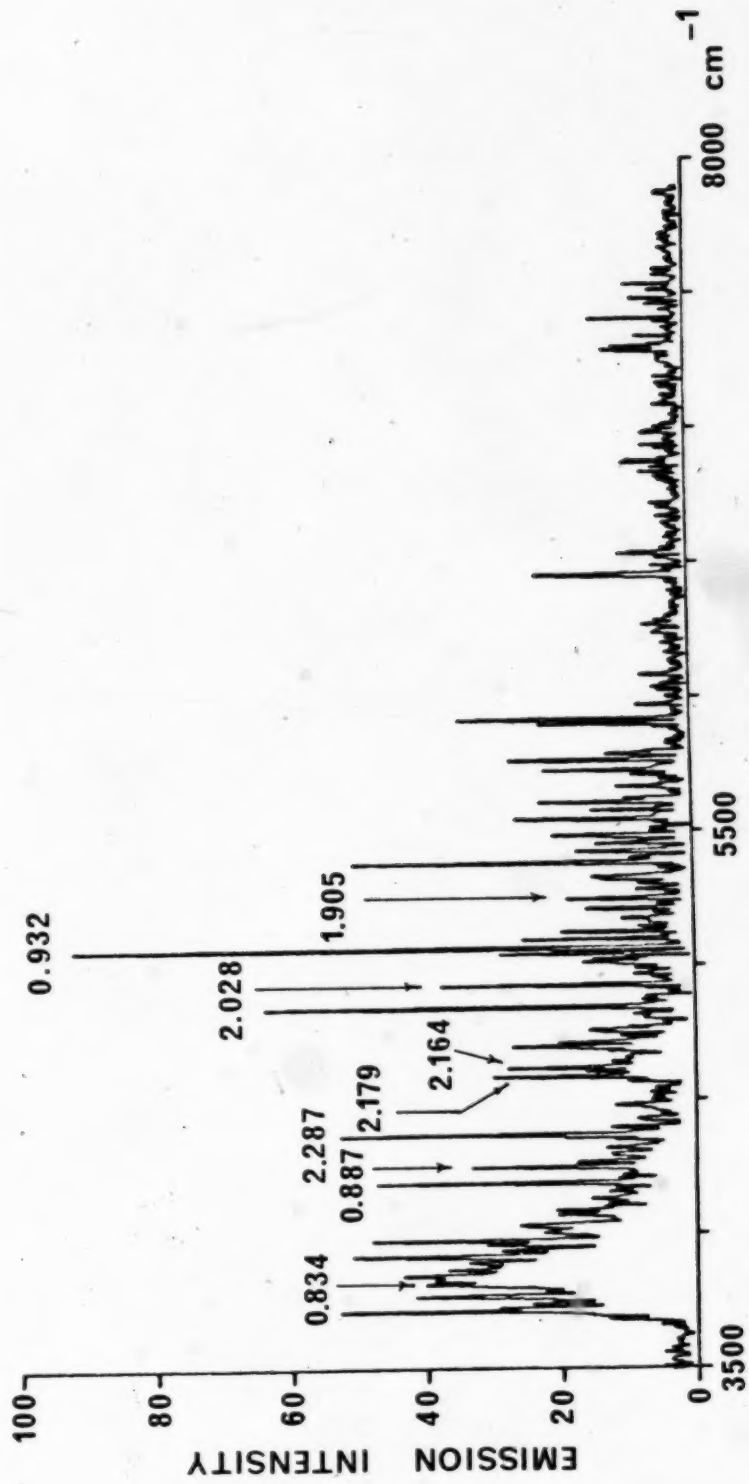

Figure 28. Emission spectrum of dibromomethane in the ICP.

fragment observed in the chloromethanes. Atomic emission lines (Table 14) were observed up to 2.287 μm (4372.5 cm^{-1}). Lines below 1.0 μm were also reported by Fry [89] and those at wavelengths longer than 1.0 μm have previously been unreported in the ICP.

5. Metals

It was thought that the near-IR region might prove useful for the analysis of heavy metals, for example, those of the lanthanide series. In this light, 10000 ppm solutions of several metals, including praesydinium, europium, cesium, and cerium were aspirated into the plasma. With the exception of several weak europium lines (Figure 29 and Table 15) only the background argon spectrum was observed. It was felt that the europium lines were too weak to be analytically useful.

6. Mid-Infrared Region

One of our initial interests was an investigation into molecular species in the ICP. It was thought that it might be possible to gain a better understanding of processes occurring in the ICP by such a study.

To this end, a series of measurements using the germanium-coated salt beamsplitter and a TGS detector were initiated. However, only noise peaks with frequencies of approximately 200 and 400 Hz were observed. These peaks

Table 14

Major Atomic Bromine Lines

Experimental		Literature[75]
Wavenumber (cm^{-1})	Wavelength (μm)	Wavelength (μm)
11986.1	0.8343	0.8344
11687.7	0.8556	0.8558
11532.7	0.8671	0.8669
11193.2	0.8934	0.8932
10735.4	0.9315	0.9320
5249.3	1.905	1.905
4931.0	2.028	2.028
4621.1	2.164	2.163
4589.3	2.179	2.179
4372.5	2.287	2.287

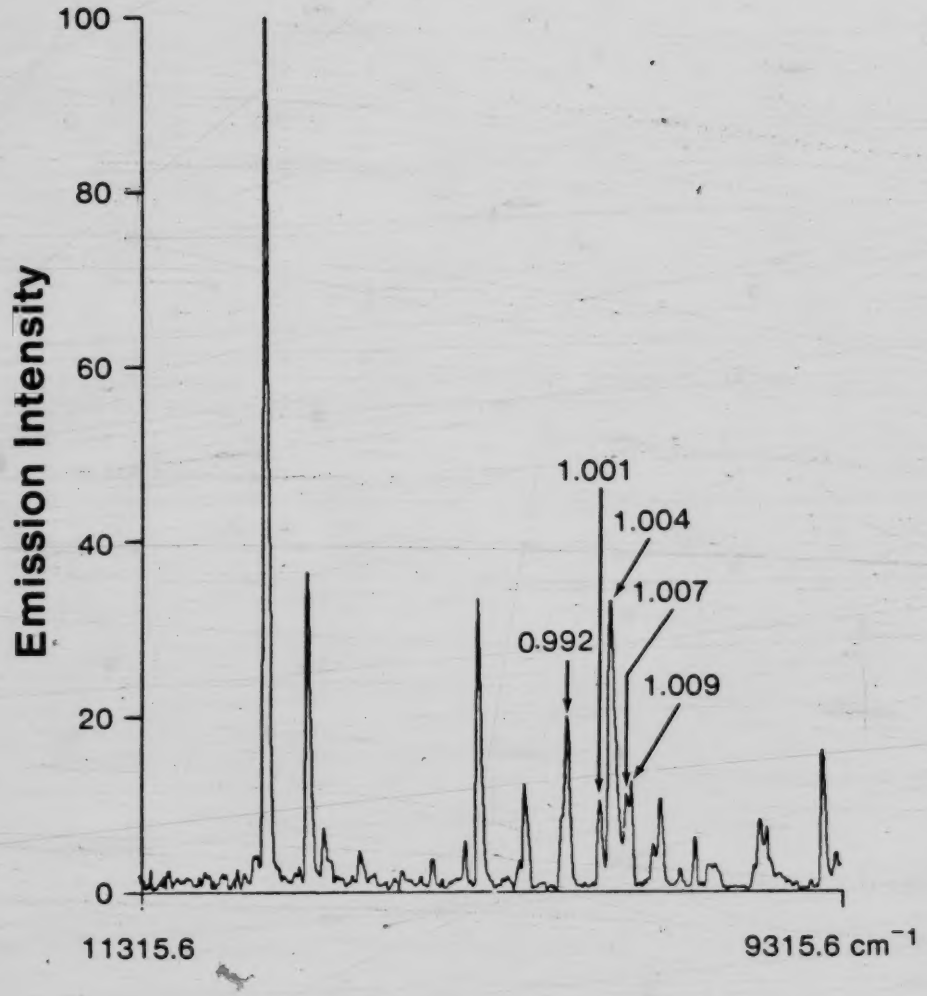

Figure 29. Emission spectrum of a 10000 ppm Europium solution in the ICP.

Table 15

Major Europium Lines

Wavenumber (cm^{-1})	Wavelength (μm)
10085.6	0.9915
9985.1	1.0015
9964.1	1.0036
9948.6	1.0052
9906.2	1.0095

are similar in structure and frequency to those observed by Belchamber [107,108] in a study of the noise characteristics of the ICP. The presence of these noise peaks was attributed to the plasma actually rotating in a counterclockwise direction.

To eliminate these noise peaks from our spectra it would be necessary to speed the mirror drive up and hence increase the modulation frequencies of analyte species of interest to a frequency region far removed from the noise peaks. Not only would it then be more difficult to obtain reproducible drive speeds with our system, but it would not be possible to acquire data rapidly enough with the current data acquisition system.

Any further study of the mid-infrared region was consequently abandoned.

D. Conclusions

One major problem in using an FTS system in the near-IR region is the dynamic range limitations imposed by the complex ICP background in this region. However, the FTS system proved invaluable in terms of its inherent wavelength accuracy and its ability to simultaneously measure the entire spectral region of interest. It would have been considerably more tedious and time-consuming to obtain the same information with other types of measurement systems.

A previously unexplored region of the spectrum between 1.0 and 3.0 μm has been shown to have potential for the analysis of nonmetals, including oxygen, sulphur, chlorine and bromine: elements which have classically been difficult to analyze in the ICP. Wavelengths of elemental lines have been tabulated and the wavelengths obtained in these measurements agree with the literature values.

As well, in contrast to work reported by Fry [12-18], the optimum viewing zone for these elements in the ICP was found to be in the normal viewing zone for metals, facilitating the simultaneous measurement of both metals and nonmetals. However, the analytical usefulness of the near-IR region for the analysis of metals appears to be limited.

Fry [84-90], in his reports, stated that molecular dissociation was complete for the gaseous small molecules studied. In this work, the presence of a molecular fragment of the chloromethanes could cause considerable difficulties in attempts to analyze for the chlorine content of organic molecules. More work would be necessary to determine the proportion of the fragment to the total organic content before any atomic chlorine analysis could be attempted. Along the same lines, the spectra of dichloromethane, discussed earlier in this

chapter, xylene and DMSO were recorded in the UV region of the spectrum. For all three compounds only the two carbon lines at 193.1 and 247.9 nm were observed. However, the relative intensities of the two lines were markedly different: the ratio C (193.1):C (247.9) was found to be 0.22 for dichloromethane, 0.45 for xylene and 1.49 for DMSO. In other words, for organic molecules, the intensity of these lines is species dependent as well as concentration dependent.

The most potentially useful analytical lines for these nonmetal elements are tabulated in Table 16. The interferometer, because of dynamic range limitations in the near-IR, is obviously not the best choice for the determination of small quantities of these elements.

In the next chapter, the analysis of sulphur using lines in the near-IR will be presented in order to demonstrate the analytical usefulness of this region.

Table 16

Potentially Useful Analytical Lines

	Wavelength (μm)
Sulphur	0.922
	0.923
	1.046
Carbon	1.070
	1.734
Oxygen	0.950
Chlorine	0.907
	1.553
Bromine	0.932
	2.287

CHAPTER IV

SULPHUR ANALYSIS IN THE NEAR-IR REGION

A. Introduction

Interest in the environmental impact of the combustion of petroleum-based products has escalated rapidly in the last ten years. The sulphur content of these products is of especial importance. Sulphur, either elemental or as sulphur containing organic molecules, during the combustion process is oxidized to species such as sulphur dioxide and sulphur trioxide. This leads, of course, to the well-known acid rain problem.

The sulphur problem is especially important in the tar sands and petroleum industries in Alberta. The oil and gas reserves in this province have one of the highest sulphur contents of any known reserves. For example, the sulphur [109,110] content in the oil sands deposits in Alberta varies between four and six percent elemental sulphur.

There is, consequently, an ongoing interest in methods for analysis of the sulphur content of these samples. Classically, sulphur has been a difficult

element to analytically determine. The most common procedure [111] is an acid bomb digestion to form sulphate ion, followed by either a $BaSO_4$ precipitation or a Ba^{2+} titration with the endpoint being determined by measuring the turbidity of the solution. Both of these methods are quite time and labour intensive.

As mentioned in Chapter III, the ICP has not commonly been utilized for the analysis of sulphur. In fact, in an applications note [112] on the analysis of coal and coal fly ash by ICP, one instrument manufacturer states: "the determination of that element is not possible with Plasma technology at this time."

To determine the analytical usefulness of the sulphur emission lines found in the near-IR region, detection limits with the ICP as the excitation source and a monochromator-based detection system have been determined. Two wavelengths, 0.922 μm and 1.046 μm, have been utilized. Several detectors which respond in the near-IR were coupled to the monochromator. Although the PbSe detector, as presented in the last chapter, responds in this region, it was felt that little would be gained by using it since it is a factor of ten less sensitive than the PbS detector in the 1 μm region. Detection limits for sulphur obtained using the silicon photodiode, silicon photodiode array (PDA) and PbS detectors will be presented and compared in this chapter.

B. Experimental

The ICP system and conditions used were identical to those described in Chapter III.

For determination of detection limits, the plasma was imaged onto the entrance slit of a 0.35 meter monochromator (GCA-McPherson, Acton, Massachusetts) with a single spherical quartz lens (focal length = 10 cm, diameter = 5 cm) at a magnification of unity. The entrance slit was set to 50 µm.

With the PbS and Si photodiode detectors, the monochromator was equipped with a 600 line/mm grating (blaze angle of 1 µm) to allow observation of the spectral region beyond 1 µm. For proper operation of the PbS detector, it was necessary to modulate the incident radiation. The light imaged onto the monochromator was modulated at a frequency of 900 Hz using a variable speed chopper. The signal from the detector was processed through a lock-in amplifier (Model HR-8, Princeton Applied Research, Princeton, N.J.) and then output to a chart recorder.

The silicon photodiode was used in a photoconductive mode. The signal from the detector was amplified by a current-to-voltage amplifier (Keithley Model 427, Cleveland, Ohio) and then output to a chart recorder.

The photodiode array spectrometer has been previously described in the literature [25]. In this spectrometer, a 1200 line/mm grating with a blaze angle of 0.250 µm was used and consequently it was not possible to measure emission at wavelengths longer than 1.0 µm. Detection limits with this system were based on a signal integration period of 10 s and 32 replicate measurements.

C. Results and Discussion

In the FTS spectrum of DMSO, the sulphur triplet centered at 0.922 µm is partially obscured by an interfering argon line at 0.9225 µm. In order to clearly observe this triplet, the spectrum of DMSO in the ICP was measured using the PDA spectrometer. A small spectral region centered around the sulphur triplet is shown in Figure 30.

The three peaks of the sulphur triplet are clearly discernable. With pure DMSO being nebulized as shown in Figure 30, the central peak of the triplet appeared as a shoulder on the interfering argon line. However, at lower concentrations of DMSO, the interference was more severe.

In terms of analytical usefulness, then, the first peak of the sulphur triplet, at 0.9217 µm and the sulphur line at 1.046 µm appeared to be the best choices for determination of analytical working curves and detection limits.

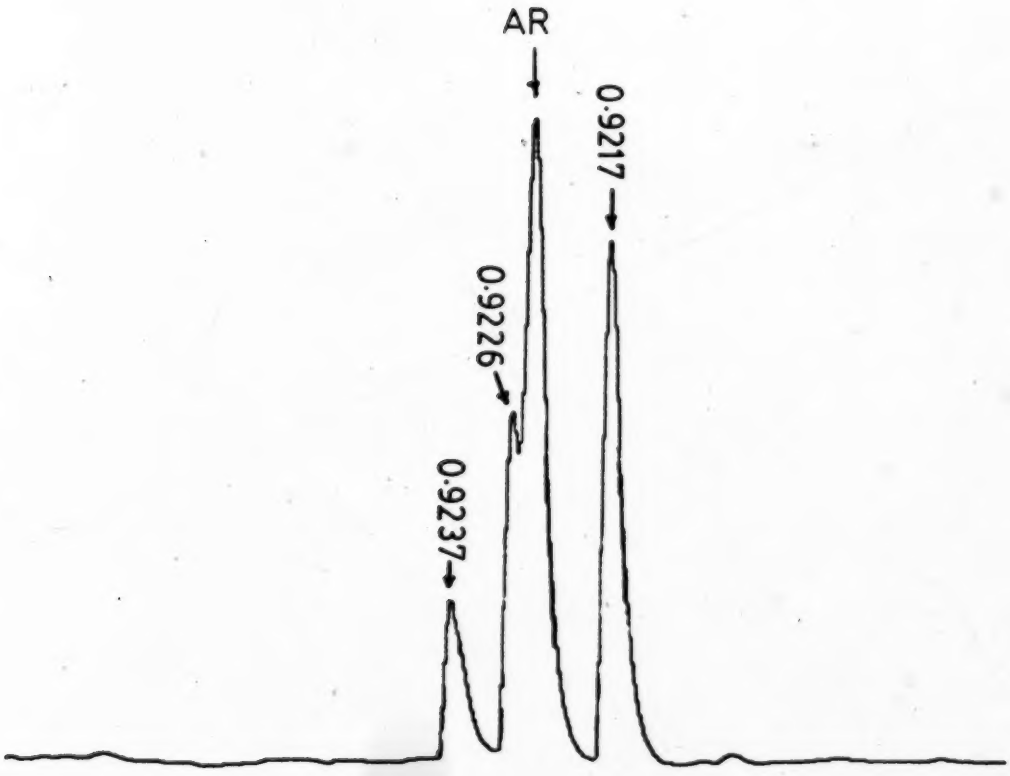

Figure 30. Spectrum of the sulphur triplet as measured by the PDA spectrometer.

Although the N_2/Ar mixed gas plasma was found to be most effective in reducing the intensity of the background spectrum with the FTS system, use of an O_2/Ar mixed gas ICP yielded the most sensitive analytical results. As well, the addition of oxygen to the coolant prevented carbon build-up on the torch. A 10% O_2/Ar mixture as coolant was used for all calibration curves and detection limit measurements.

Analytical calibration curves were measured using aqueous solutions of DMSO in the concentration range of 500 to 100000 ppm sulphur. The PDA spectrometer is suitable only for measurements at wavelengths shorter than 1.0 µm. Consequently, measurements were restricted to the 0.9217 µm sulphur line for this system. Measurements were made at both 0.9217 and 1.046 µm with both the Si photodiode and the PbS detectors.

A typical calibration curve, as measured at the 0.9217 µm sulphur line by the Si photodiode, is presented in Figure 31. The slope of this log-log plot was 0.993. Good linearity was obtained with all three detectors at both wavelengths, with slopes ranging between 0.94 for the PbS detector at 0.9217 µm and 0.99 for the Si photodiode at the same wavelength.

Detection limits were defined as the concentration necessary to give a signal intensity of twice the standard

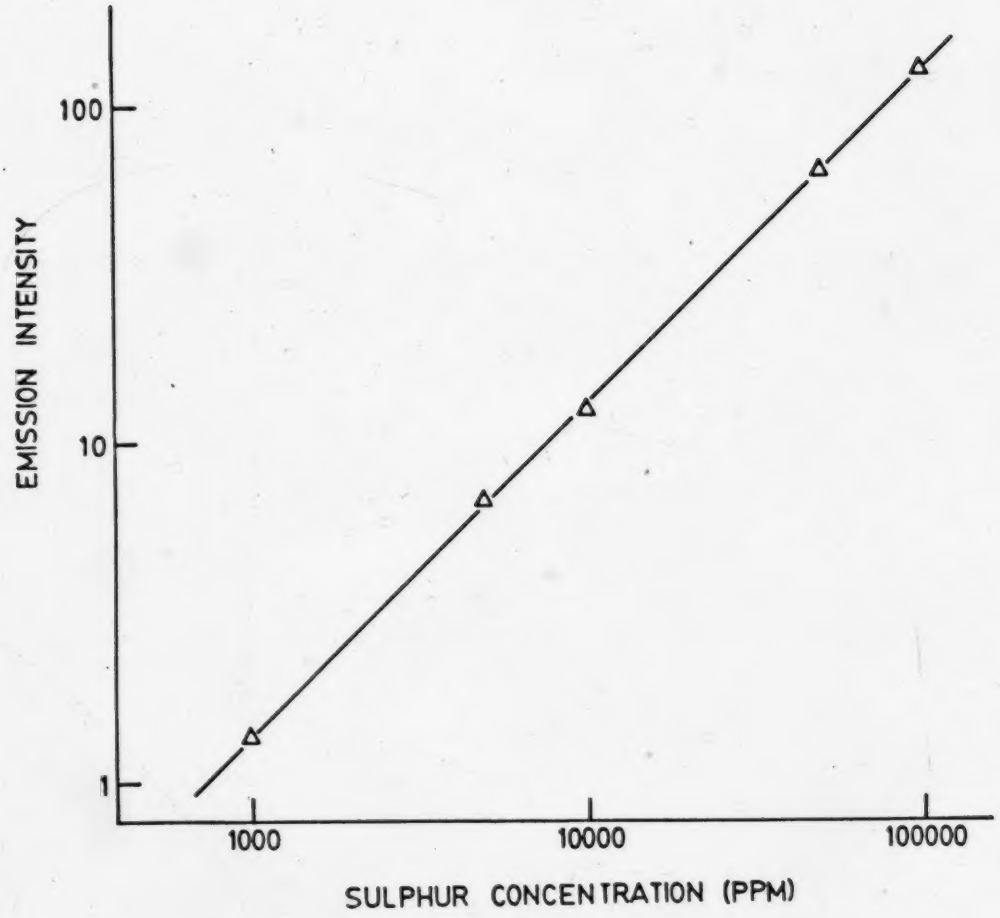

Figure 31. Calibration curve for sulphur as dimethylsulphoxide with the silicon photodiode as the detector.

deviation of the background. The background, with distilled water being aspirated into the ICP, was measured at four second intervals for a period of sixty seconds, followed by averaging of these measurements to obtain one result. Thirty-two replicates were measured and the standard deviation of the background was then calculated. An average signal intensity for a 10000 ppm sulphur solution was measured in the same manner.

Detection limits varied between 20 ppm for the silicon photodiode and 420 ppm for the PbS detector (Table 17). Although there was little evidence for the presence of undissociated sulphur containing fragments in the spectra presented in Chapter III, a calibration curve and detection limit was also determined for aqueous solutions of thiourea in the same concentration range as the DMSO solutions. No significant difference between DMSO and thiourea was noted. Measurements were made using the sulphur line at 0.9217 μm and the silicon photodiode detector.

In the determination of the detection limit of sulphur in the ICP as thiophene, Blades et al. [92] reported a detection limit of 122 ppm with a PDA spectrometer as the measurement system. Results obtained with the PDA spectrometer in this study were slightly higher but still comparable to those obtained by Blades

Table 17

Sulphur Detection Limits (ppm-S)

	Wavelength	
Detector	0.9217 µm	1.046 µm
Si photodiode	19 (DMSO) 22 (Thiourea)	45 (DMSO)
Si PDA	182 (DMSO)	--
PbS	404 (DMSO)	420 (DMSO)

[20]. As well, he reported that the C_2 bands in the 0.920 µm region would limit the detection of sulphur at lower concentrations. With the addition of a small amount of oxygen into the argon coolant, as in this study, the C_2 band emission disappears and hence can no longer be a limiting factor.

The silicon photodiode was found to yield the best detection limits at both wavelengths. Although the difference was small, detection limits for the 1.046 µm line were consistently poorer than for the 0.9217 µm line.

In a comparison of the three detectors, significant differences were noted in the noise limiting features of the uncooled PbS detector and the other two detection systems. For both the silicon photodiode and the photodiode array, at concentrations significantly greater than the detection limits, the system appeared to be source flicker limited [59]; that is, the standard deviation of the signal increased directly as the analyte concentration increased. However, in the case of the PbS detector, the standard deviation of the signal was virtually independent of concentration, in other words, the system appeared to be detector-noise limited. This factor was thought to play an important role in the poorer detection limits obtained with the PbS detector.

D. Conclusions

The detection limits reported in this paper are considerably inferior to those obtained using the sulphur resonance line at 180.73 nm in the ICP. Detection limits with this line have been reported in the literature as low as 24 ppb [113] and in this laboratory, using the ARL 34000 ICP system, the detection limit was found to be 18 ppb. The sulphur emission lines in the near-IR, at present, provide detection limits which are, at best, three orders of magnitude poorer. Of the detectors examined in this study, the Si photodiode-monochromator system was most effective, providing detection limits in the 20 ppm range. Although detection limits obtained with the PbS detector were significantly poorer, improvement should be realized by using a cooled PbS detection system. As well, a higher resolution monochromator would allow separation of the central peak of the sulphur triplet at 0.922 μm from the interfering argon line. Use of this peak should also help to improve sensitivity for sulphur detection limits.

Although the detection limits obtained were poor, it is often necessary to analyze for sulphur in samples containing relatively high sulphur concentrations. As mentioned previously, fossil fuels are in this category. Most fossil fuels [109,110] have sulphur concentrations

ranging between one and five percent. In fact, it is difficult to obtain sulphur standards for oil analysis at concentrations below one percent (10000 ppm). At these levels, the detection limits obtained in the near-IR are adequate for the analysis of sulphur.

It is to be expected that the analysis of other nonmetal elements, in particular carbon, oxygen, chlorine and bromine, in the near-IR region would yield detection limits in the same range, approximately 100 to 500 ppm, as those obtained for sulphur. Again, for trace analysis, these detection limits would not be acceptable. However, in applications involving concentrations greater than approximately 0.1%, analysis of ICP emission in the near-IR region should provide a viable alternative for the determination of these elements.

The major advantage of using nonresonance lines in the near-IR over the resonance lines found in the vacuum UV region is that a vacuum instrument is not required, allowing simpler, less expensive instrumentation and facilitating upkeep and maintenance of the instrument.

Along this line, several ICP instrument manufacturers have, in addition to a direct reader, incorporated a scanning monochromator - the n+1 channel - into their instruments. For nonvacuum instruments and/or instruments without, for example, an existing sulphur channel it would

be possible to set this n+1 channel to the sulphur line at 0.922 μm facilitating sulphur analysis, or analysis of other nonmetals, simultaneously with that of other elements of interest.

CHAPTER V

FTS IN THE ULTRAVIOLET AND VISIBLE SPECTRAL REGIONS

A. Introduction

The ability of the FTS measurement system to qualitatively characterize emission from the ICP has been aptly demonstrated in Chapter III for both background and analyte emission in the near-IR spectral region.

However, most of the analytical lines currently utilized for the analysis of metals in the ICP have wavelengths in the ultraviolet and visible regions of the spectrum. To be an effective measurement system for the ICP, the interferometer must be able to provide both qualitative and quantitative information in the ultraviolet and visible spectral regions. Preliminary experiments utilizing hollow cathode lamps as emission sources (Chapter II) have demonstrated the qualitative spectral response of the interferometer at wavelengths as short as the ZnII 206.2 nm emission line.

In this chapter, the emission spectra of a sixteen element multielement solution aspirated into the ICP as measured by the FTS measurement system in both the

ultraviolet and visible spectral regions will be presented. To ascertain the quantitative capabilities of the interferometer in these regions, detection limits for each element in the multielement solution were determined and are discussed in this chapter.

As discussed in Chapter I, there are a number of possible limitations due to dynamic range and noise problems in an FTS system in regions other than the infrared spectral region. To illustrate the existence and magnitude of these limitations, detection limits and background standard deviations for zinc emission in the presence of varying concentrations of magnesium are presented in this chapter.

B. Experimentation

The ICP parameters and conditions were identical to those described in Chapter III for a 100% argon ICP. The spatial viewing zone in the ICP was centered at 17 mm above the load coil, being the optimum viewing zone for most metals, and was kept constant for all measurements.

The FTS measurement system has also previously been described (Chapter II). The ultraviolet beamsplitter described in that chapter was in place in the interferometer. To cover the entire spectral region of interest, it was necessary to measure the emission

spectrum of the ICP using two separate detectors, both photomultiplier tubes. For the wavelength region 180 to 290 nm, the solar blind PMT (R166, Hammatatsu) was applicable and for the spectral region 250 to 650 nm the 1P28 PMT was utilized. Although the 1P28 PMT responds in the spectral region below 250 nm, its sensitivity is markedly reduced over that of the solar blind PMT in the same spectral region.

The optical coupling between the ICP and the interferometer was accomplished in a slightly different manner than that described in Chapter III. An iris diaphragm has been placed before the interferometer entrance to limit the diameter of the incident collimated light. It was then only necessary to ensure collimation by placing a 30 cm focal length quartz lens at its focal length from the plasma. The optimum diameter of the iris diaphragm aperture was empirically found to be approximately one cm. This value is similar to the diameter of the incident collimated beam produced by the optical coupling system described in Chapter III.

Detection limits were again defined as the signal necessary to obtain an intensity equal to twice the standard deviation of the background. To determine the signal intensity, a sixteen element multielement solution, each element at the 10 ppm concentration level, was

aspirated into the ICP. Six replicate measurements were made, with each replicate consisting of thirty-two consecutive interferograms signal-averaged together. The standard deviation of the background was determined by measuring emission from a plasma into which distilled water had been aspirated. Again, each spectrum was determined from a 32 scan signal-averaged interferogram. Only one replicate was necessary. The standard deviation was calculated from the intensities of thirty-two consecutive points in the spectrum. These points were arbitrarily chosen in a region of the spectrum determined to be free from atomic argon background emission.

Signal intensities for the zinc analytical working curves were determined by the same method as those determined for detection limits. For determination of the detection limits for zinc in the presence of magnesium, each solution contained zinc at 100 ppm and magnesium at either 0, 100 or 500 ppm.

Single element stock solutions, at either the 5000 or 1000 ppm concentration levels, were made from reagent grade metals dissolved in 5% nitric acid, or were already available in the laboratory. All other solutions were prepared by using the appropriate stock solutions and diluting to the desired concentration levels using deionized distilled water (Milli-Q Water Purification System, Millipore Corporation, Bedford, Massachusetts).

C. Results and Discussion

1. Multielement Spectra

A sixteen element multielement solution, consisting of those elements most commonly analyzed in the ICP, was aspirated into the ICP. This solution was composed of the elements aluminum, barium, boron, cadmium, calcium, copper, iron, magnesium, manganese, nickel, lead, silicon, vanadium, zinc and two of the alkali metals, sodium and potassium. All elements were present at the 10 ppm concentration level. The spectra for the solar blind and for the visible (1P28) regions are illustrated in Figures 32 and 33. All analyte emission lines are identified in these spectra by both element and wavelength. Wavelengths are listed in nanometers. Both the literature wavelengths and experimental wavelengths are tabulated in Table 18 for the solar blind spectrum and Table 19 for the 1P28 spectrum. All literature wavelengths were obtained from Zaidel [75]. As in the results obtained in the near-IR spectral region, experimental and literature wavelengths were in agreement.

As a consequence of a radiative recombination process [114,115], a continuum emission from the ICP is produced. This continuum results in a sloping baseline when a dispersive-based measurement system is utilized.

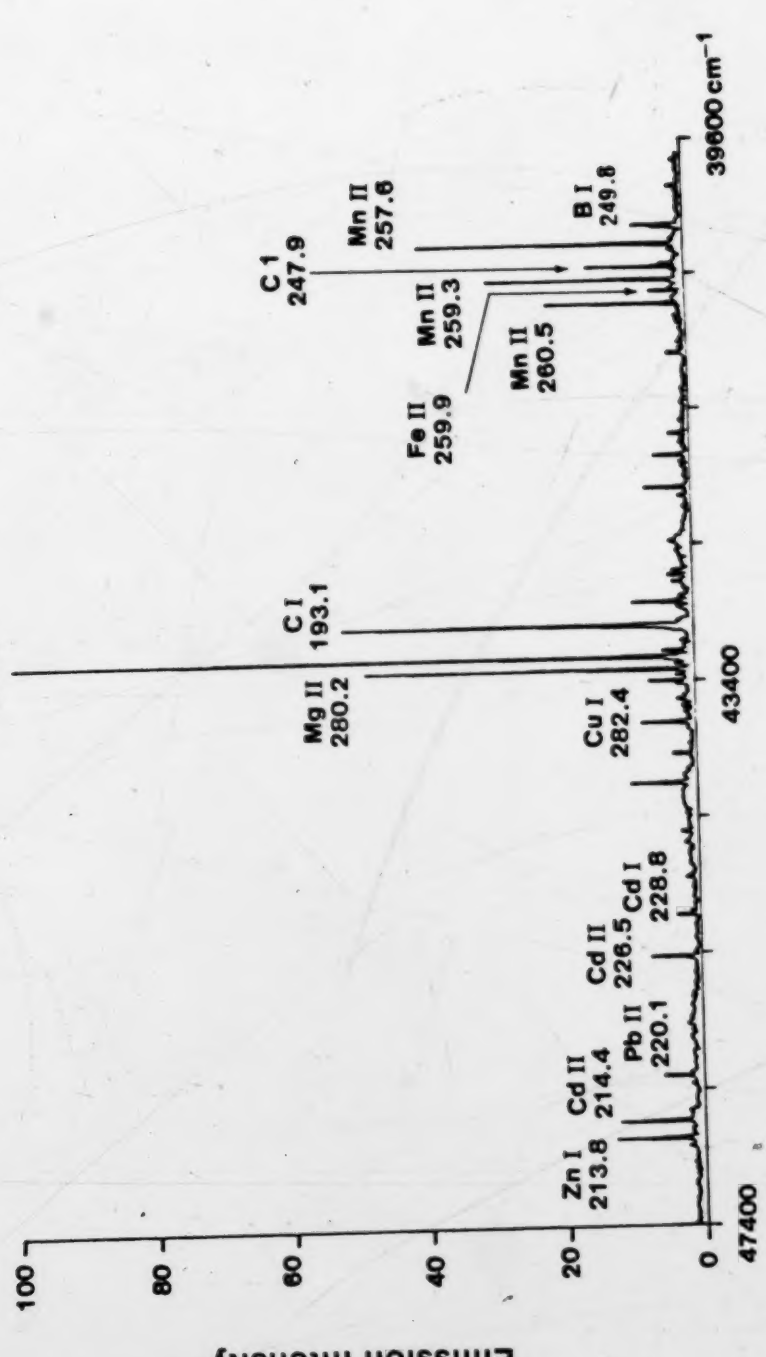

Figure 32. Emission spectrum of the multielement solution as measured by the solar blind PMT.

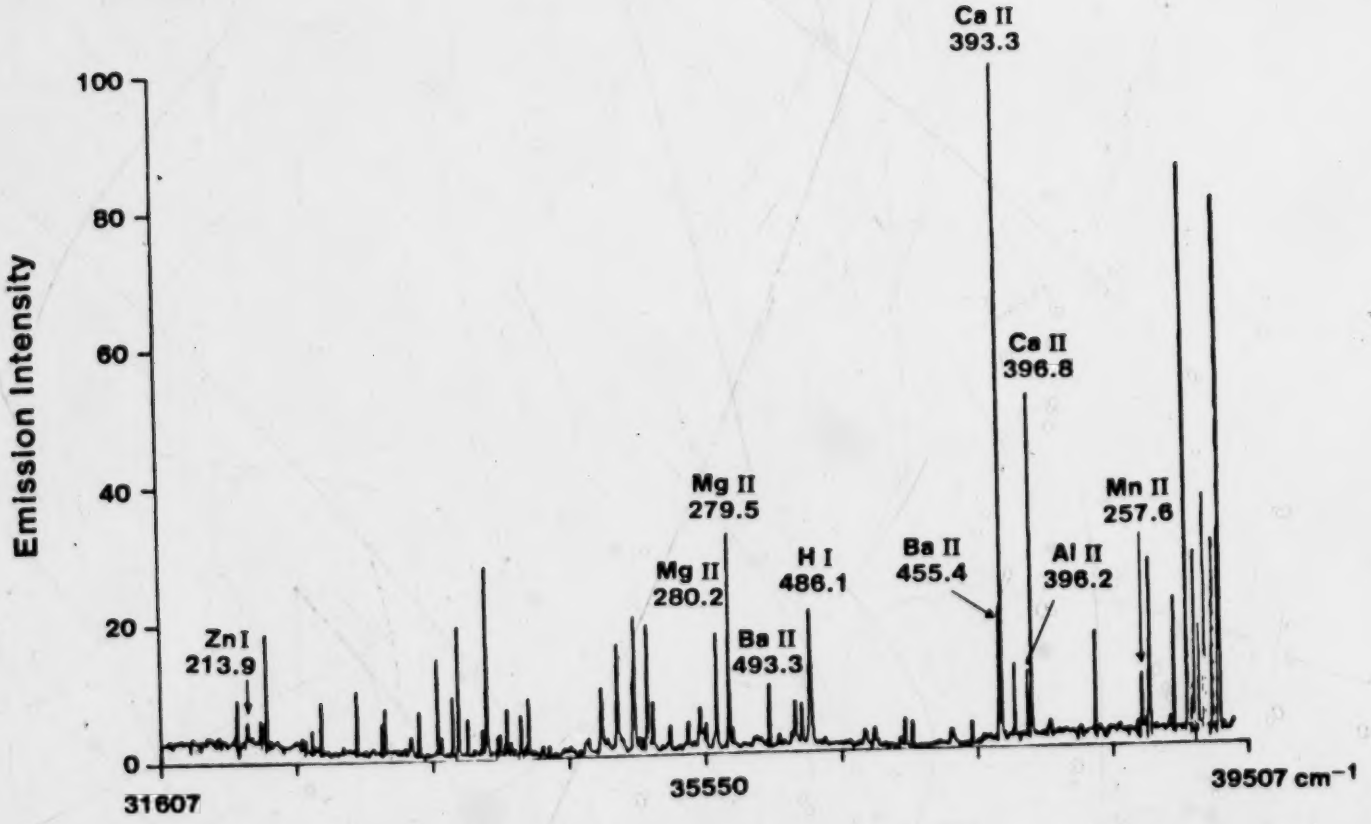

Figure 33. Emission spectrum of the multielement solution as measured by the 1P28 PMT.

Table 18

Emission Lines Observed in Multielement Spectrum with Solar Blind PMT

Element	Observed		Literature[75]
	Wavenumber (cm^{-1})	Wavelength (nm)	Wavelength (nm)
ZnI	46753.0	213.89	213.86
CdII	46627.0	214.47	214.44
CdII	44149.7	226.54	226.50
CdI	43697.9	228.84	228.80
PbII	45378.2	220.37	220.35
CuI	35403.2	282.46	282.44
MgII	35688.4	280.27	280.27
MgII	35779.2	279.49	279.55
CI	40345.4	247.86	247.86
CI	51794.7	193.07	193.09
MnII	38821.4	257.59	257.61
MnII	38559.4	259.34	259.37
MnII	38384.8	260.52	260.57
FeII	38476.3	259.90	259.94
BI	40040.0	249.75	249.77
BI	40054.5	249.66	249.68

Table 19

Emission Lines in Multielement Spectra with 1P28 PMT

Element	Observed		Literature[75]
	Wavenumber (cm^{-1})	Wavelength (nm)	Wavelength (nm)
ZnI	46753.0	213.89	213.86
MgII	35688.4	280.27	280.27
MgII	35779.2	279.49	279.55
BaII	20271.6	493.34	493.41
BaII	21963.8	455.37	455.40
HI	20572.7	486.08	486.13
CaII	25425.3	393.31	393.37
CaII	25201.5	396.80	396.85
AlI	25244.9	396.12	396.15
MnII	38821.4	257.59	257.61

The continuum becomes apparent around 250 nm and increases in magnitude at longer wavelengths, extending into the visible spectral region. This sloping baseline is not observed with the FTS measurement system. A continuum type emission would have an interferogram resembling that of a white light and, in fact, the interferogram of ICP emission observed on an oscilloscope does have a white light component in addition to the component which is characteristic of atomic emission. However, after the interferogram has been acquired by the computer, this white light component is rarely observed. The explanation for this is that the width of this component is much narrower than the sampling interval of the clock and hence is missed in the data acquisition process.

Spectral response, in terms of the wavelengths observed in these spectra, appears to be excellent in the ultraviolet spectral region. In the spectrum measured with the solar blind PMT (Figure 32) two carbon lines at 247.9 nm and at 193.1 nm, were observed. Although carbon was not one of the elements in the multielement solution, several standard solutions available in the laboratory were derived from the respective metal carbonate. In addition, as carbon dioxide, carbon is a common impurity in argon tanks. The sensitivity of the FTS measurement system at wavelengths as short as 193 nm does not appear

to be seriously degraded in comparison to the sensitivity at longer wavelengths. The possibility of observing resonance lines for such elements as sulphur (180.7 nm) and phosphorus (178.3 nm) is clearly evident. A purged optical path would be necessary to observe emission at wavelengths shorter than approximately 190 nm, due to atmospheric absorption at these wavelengths. Purging is not easily accomplished with this system and consequently was not attempted. However, in the measurement system described in Chapter VI, purging of the optical path with argon was more easily attained and indeed, the sulphur resonance line at 180.7 nm has been observed (see Chapter VI).

The spectrum measured with the 1P28 PMT, shown in Figure 33, is considerably more complex than that measured with the solar blind PMT. This increase in complexity can be attributed to the more complex argon background spectrum in the visible spectral region. All spectral lines in Figure 33 that are not identified are due to the argon background spectrum in this region. Most of these wavelengths occur in the wavelength region 450 nm to 800 nm. Aspiration of any aqueous solution into the ICP yields the hydrogen emission line observed in this spectrum at 486.1 nm.

Although the spectral response of the interferometer appears to be excellent, a qualitative examination of these spectra reveals several points. A sixteen element solution was aspirated into the ICP. Of these sixteen elements, only eleven elements were observed in either the solar blind or visible spectra. Of the remaining five elements, only potassium (766 nm) was outside the spectral viewing region. The major emission lines for sodium (598.8 nm) and vanadium (310 nm) were not observed in the visible spectrum. For vanadium, argon lines at longer wavelengths provide spectral line overlaps due to aliasing. Although the optimum viewing zone for the alkali metals is higher, approximately 20 mm above the load coil, some indication of sodium emission should be present. Both nickel (226 nm) and silicon (288 nm) were conspicious in their absence from the solar blind spectrum (Figure 32). In addition to the absence of any emission lines for the above elements, several prominent emission lines for other elements present in the ICP are absent. Consider the element zinc observed in the solar blind spectrum at 213.8 nm. Based on information obtained using a monochromator-based measurement system (and Figure 34), two other emission lines of zinc at 206.1 and 202.6 nm should be observed. These peaks are not evident in the multielement spectrum even though no spectral line

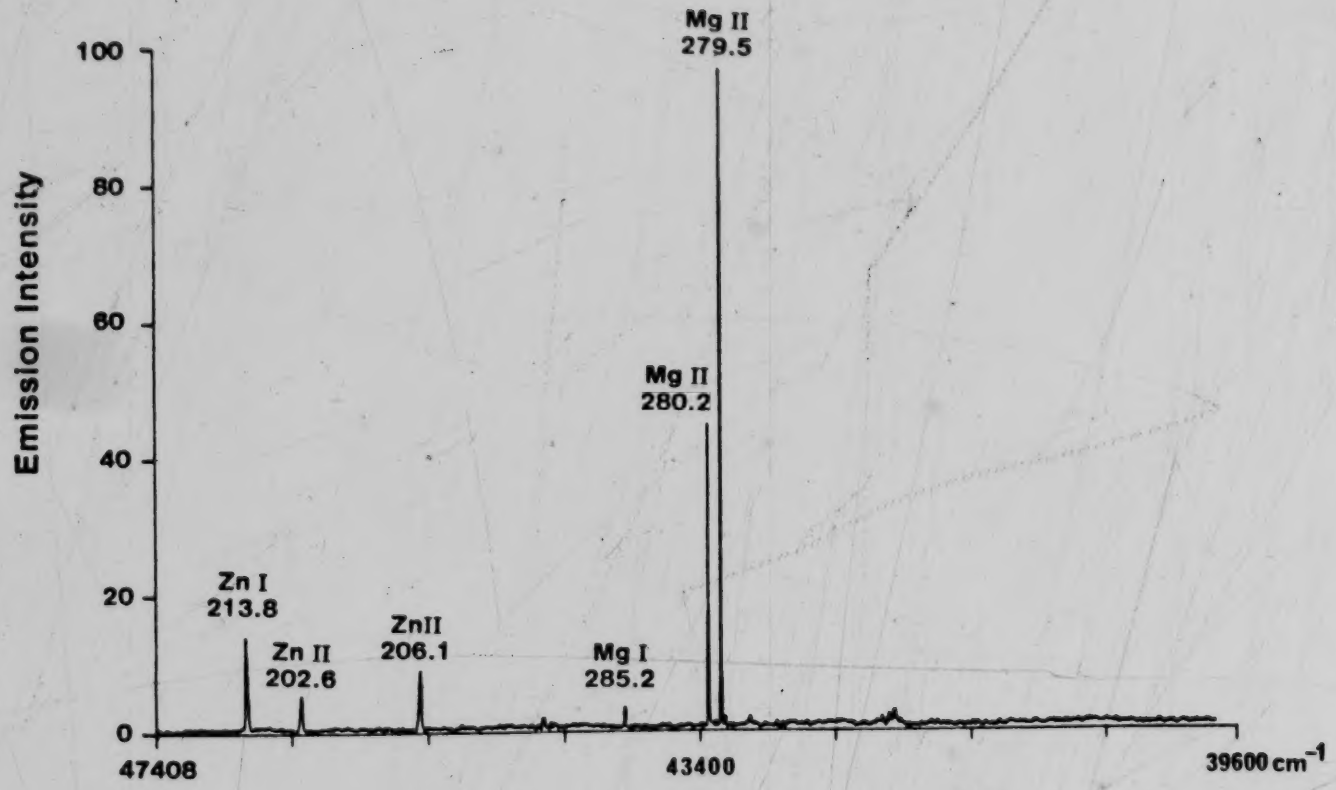

Figure 34. Emission spectrum of a 100 ppm zinc and magnesium solution.

interferences are observed in this region. A second example is the manganese triplet at 257.6, 259.3 and 260.5 nm, clearly evident in the solar blind spectrum, but in the visible spectrum only the most intense line of the triplet, at 257.6 nm, is weakly apparent. The lack of some expected spectral features can be attributed to, in some cases, spectral line interferences but mostly to dynamic range limitations or the multiplex disadvantage explained in Chapter I and illustrated as well in Chapter III. In the near-IR region, dynamic range limitations were mainly imposed by the complex background spectrum. This is not the case in the ultraviolet and visible regions. Rather, the presence of intense emission lines for elements of interest in the spectrum impose limitations on the observation of other elements in the same spectral region. For example, magnesium emission is the dominant feature in the solar blind spectrum while in the visible region, calcium plays the same role. To examine the quantitative effect of these limitations a less complex system, zinc in the presence of magnesium will be considered.

2. Analytical Determination of Zinc in the Presence of Magnesium

In Figure 34, the emission spectrum of a 100 ppm zinc and 100 ppm magnesium solution is shown. As is expected, three zinc lines were observed in this spectrum. Experimental wavelengths were found to be in agreement with the literature wavelengths (Table 20). A spectral feature not readily apparent in the multielement spectra is the difference in line width between the zinc lines in the 210 nm region, and the magnesium lines in the 280 nm spectral region. The difference in line width can be attributed to chromatic aberrations in the collimation lens. This means that the focal length of the lens, necessary for collimation, is dependent on the wavelength. Ideally, of course, it would be independent of the wavelength. Chromatic aberrations become more important at the shorter wavelengths as illustrated here. It was found to be impossible to collimate the incident radiation from the plasma at both 210 and 280 nm. In most cases, collimation was empirically optimized for the shorter wavelengths in the spectral region of interest.

Analytical working curves, on a log-log plot, for zinc using the 213.8 nm emission line in the presence of varying concentrations of magnesium are presented in

Table 20

Emission Lines Observed in Zn and Mg Spectrum

Element	Observed		Literature[75]
	Wavenumber (cm^{-1})	Wavelength (nm)	Wavelength (nm)
ZnI	46753.0	213.89	213.86
ZnII	48503.7	206.17	206.19
ZnII	49380.3	202.51	292.55
MgI	35069.1	285.15	285.21
MgII	35688.4	280.27	280.27
MgII	35779.2	279.49	279.55

Figure 35. Good linearity was obtained for all three curves, with slopes ranging between 0.999 and 0.997. It can be seen from Figure 35 that sensitivity for the analysis of zinc decreases as the magnesium concentration increases. The detection limits for zinc (Table 21) also illustrate this point. The background matrix for the determination of the zinc detection limits was assumed to be one in which zinc was absent, but magnesium was present at the identical concentration used for the analytical working curve. Standard deviations of this background were then calculated, using a portion of the spectrum well removed from the magnesium emission lines. The detection limits measured for zinc, shown in Table 21, demonstrate a dependence on the magnesium concentration. If the detection limits are calculated using distilled water as the background, they would be somewhat improved - for the 100 ppm Mg case, 1.9 ppm and for the 500 ppm Mg solutions, 11.2 ppm. However, the deterioration of the zinc detection limits with increasing magnesium concentrations is still evident.

These different detection limits, obtained using different background matrices, lend credence to the argument of a multiplex disadvantage in the ultraviolet and visible regions of the spectrum. Because the zinc emission lines are contained in a spectral region clearly

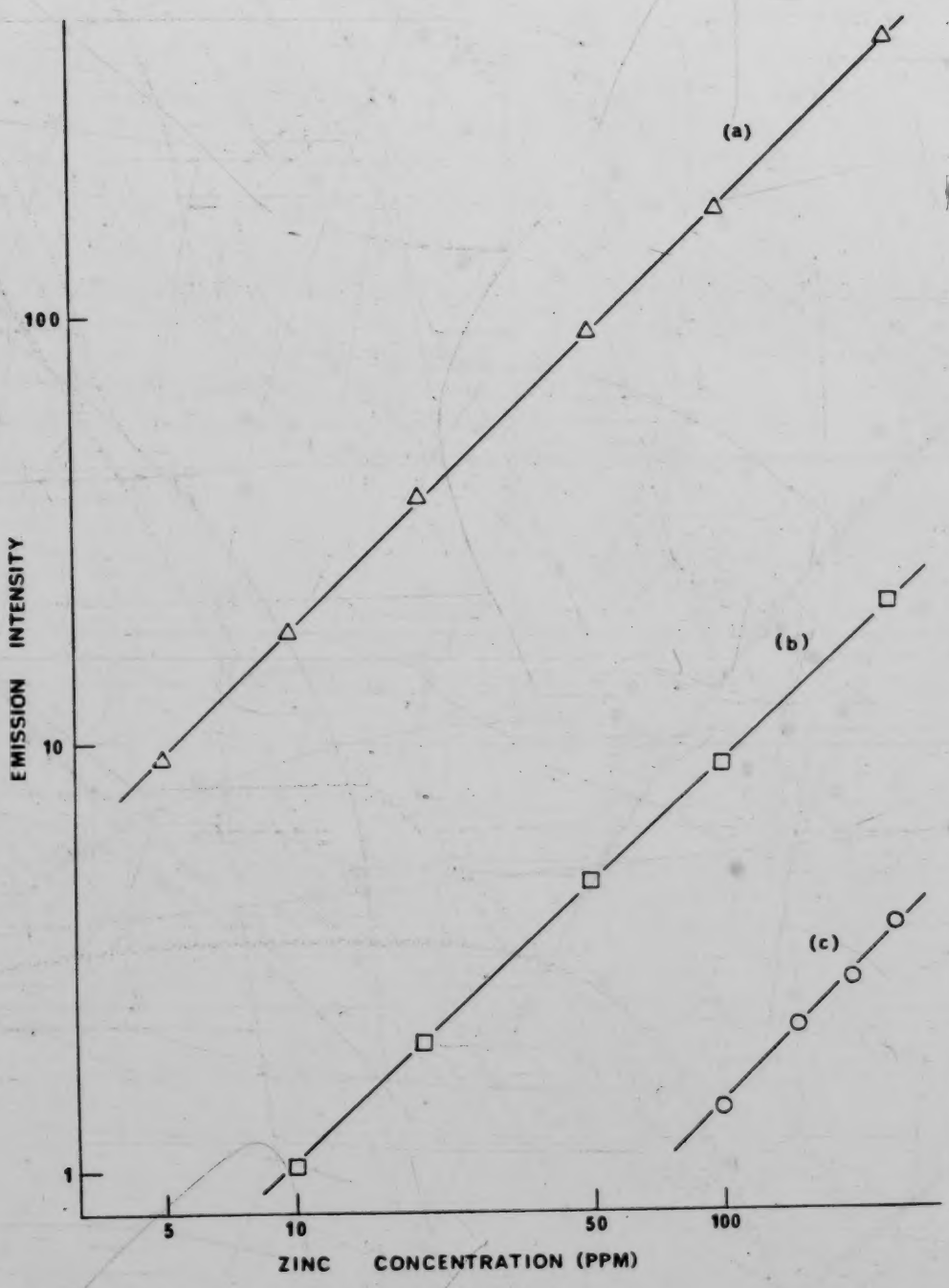

Figure 35. Calibration curves for zinc at 213.8 nm in the presence of varying magnesium concentrations: (a) 0 ppm Mg, (b) 100 ppm Mg and (c) 500 ppm Mg.

Table 21

Detection Limits for Zinc at 213.8 nm

in the Presence of Magnesium

Mg conc. (ppm)	Slope	Corr. Coeff.	Detection Limit (ppm)
0	0.986	0.9997	0.57
100	1.080	0.99997	2.3
500	1.060	0.991	25.3

separated from that containing magnesium emission lines (Figure 34), this detection limit difference would indicate that noise in the FTS system does distribute at least partially over the entire spectrum rather than being localized on the peaks as in a dispersive measurement system. The initial results obtained with the zinc calibration curves prompted an investigation into the standard deviation of different points in the baseline of these spectra. This type of investigation should provide evidence for either simply a dynamic range limitation, a multiplex disadvantage or a combination of the two factors.

3. The Effect of Magnesium Concentration on the Standard Deviation of the Background Spectrum

Three solutions were aspirated into the ICP, each containing 100 ppm zinc. Magnesium concentrations were 0 ppm, 100 ppm and 500 ppm, respectively. Each spectrum, when transformed, contains 4096 points of spectral information. Six points in each spectrum were chosen somewhat arbitrarily for this noise study. Two points were chosen, one at each end of the spectrum, that represent positions well removed from either the magnesium or the zinc emission lines. An additional two points were taken, one on each side of the two magnesium lines at

279.5 and 280.2 nm. The positions of these points were far enough removed from the two lines to ensure that no artifacts of the measurement system, for example side lobes, would be accidentally included in the standard deviation determinations. Points close to the strong magnesium lines were chosen in order to ascertain if the baseline noise has a frequency dependent component. The last two points were taken on either side of the zinc 213.8 nm emission line.

For each magnesium concentration, ten replicates of 32 signal-averaged interferograms were recorded. Standard deviations were determined on 32 points, centered around each chosen position for the six points in each spectrum. The ten results for each position were then averaged to give the final average standard deviations. To ascertain if there was a significant difference between this method of calculation, taking consecutive points in the same spectrum to determine the standard deviation, or of the alternate method, taking the same point in the ten spectra and calculating the standard deviation of that point, the statistical F-test was applied. With nine degrees of freedom and a confidence level of 95%, no statistical difference was found between the two standard deviations.

The standard deviations of the baseline for each magnesium concentration are illustrated in Table 22. Several interesting trends can be noted in the noise structure of the baseline. Firstly, there appears to be a frequency independent noise structure which is dependent on the concentration of magnesium. The standard deviation of the background increases markedly as the magnesium concentration increases. An attempt was made to fit a mathematical equation to express the relationship between the noise in the background, as measured by the standard deviation, and the magnesium concentration. However, the three different concentrations were not sufficient for these purposes. It is clear from Figure 36, a plot of the standard deviation of the point 116 as a function of magnesium concentration, that the relationship is nonlinear. Similar graphs were obtained for the remaining five points.

A second trend evident in Table 22 is the apparent localization of noise around the actual emission lines. This effect is much larger for the stronger magnesium lines than for the weaker zinc emission lines. Again, the magnitude of this increase in noise around the magnesium emission lines is dependent on the concentration, or the emission intensity of the magnesium present in the solution. No attempt has been made to quantify this

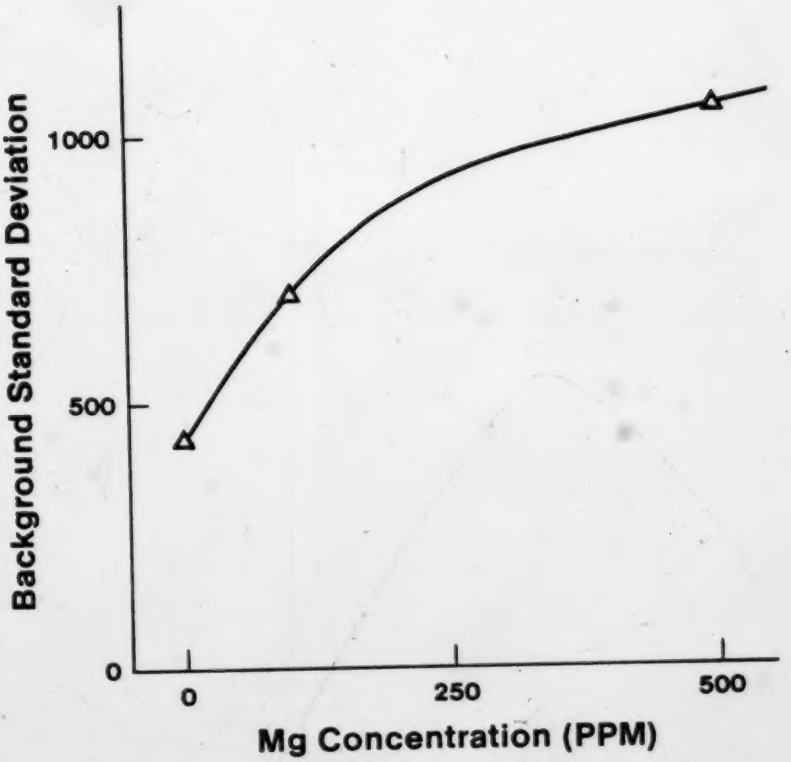

Figure 36. Standard deviations of the baseline point 116 as a function of magnesium concentration.

Table 22

Standard Deviations of the Background as a Function of Magnesium Concentration

POINT NUMBER	STANDARD DEVIATION		
	500 ppm Mg	100 ppm Mg	0 ppm Mg
116	1042	701	452
321	1142	585	446
416	1153	653	501
2080	1494	836	357
2184	2364	970	392
3516	1172	693	399

relationship. In the absence of magnesium (Table 22), there is no increase in noise in the spectral region around the position of the two magnesium lines, as would be expected.

It would appear, then, that there is both a frequency independent and a frequency dependent noise structure in line emission spectra measured by FTS. The magnitudes of both types of noise are dependent on the concentrations or emission intensities of the analyte species in the ICP. As discussed in chapter I, noise in FTS is expected to be distributed evenly over the entire spectrum. It is not entirely unexpected, however, that a frequency dependent noise component exists. In the ICP, the dominant noise features are shot noise and source flicker noise. Both these noise types are dependent on the intensity of an emission signal and hence should also be dependent on the frequency of that signal, creating the frequency dependent noise structure evident in this study. It would appear that the difficulty in observing weak signals in the presence of one or more strong signals with FTS is not simply due to dynamic range limitations but can also be attributed to a noise disadvantage in the ultraviolet and visible regions of the spectrum.

It is difficult, from these preliminary noise experiments, to determine exactly the effect of strong

emission lines on weaker emission lines and to ascertain completely the magnitude of these effects for multicomponent spectra. In this laboratory, fundamental noise characteristics [66] of the interferometer-based measurement system for emission from the ICP are currently under investigation. For this thesis, it is sufficient to ascertain that strong emission lines do have an effect on the magnitude of the noise in other areas of the same spectrum.

4. Detection Limits of the Multielement Solution

Although several limitations of the FTS measurement systems have been illustrated in this chapter, the FTS system is still unmatched in its qualitative spectral characteristics. Its excellent UV response demonstrated in this thesis should still allow good quantitative capabilities in the ultraviolet and visible regions. For this reason, detection limits were determined for the sixteen elements in the multielement solution. The detection limits obtained with the visible PMT (1P28) and with the solar blind PMT (R166) are listed in Table 23. All detection limits were calculated using a distilled water background, as described in the Experimentation section of this chapter. It was not possible to determine detection limits for potassium, its emission lines being outside the spectral response of the PMT, and for the

Table 23

Detection Limits Measured for the Multielement Solution

Element	Wavelength (nm)	Detection Limits (ppb)		% RSD
		1P28	R166	
Al		--		
B	249.7		62	5.3
Ba	455.4	77		4.9
Ca	393.3	16		5.2
Cd	226.4		48	4.3
Cu		--		
Fe		--		
Mg	279.1	58	5	3.9
Mn	257.6	145	17	5.8
Na		--		
Ni			--	
Pb	220.7		130	6.2
Si		--		
V		--		
Zn	213.8		37	5.4

elements aluminum, vanadium, nickel, sodium, iron and copper since their lines were too weak to be observed in the multielement spectra. For those elements, magnesium and manganese, apparent in both the visible and solar blind spectra, significantly improved detection limits were obtained with the solar blind PMT. This is due, in part, to the improved response of the solar blind PMT in that spectral region, but also to the fewer and less intense lines present in the solar blind spectrum than in the visible spectrum. In the solar blind spectrum, magnesium and manganese provide the strongest emission, thus limiting the dynamic range. In the visible spectrum, calcium and the argon background spectrum play this role.

The detection limits shown in Table 23, are relatively poor in comparison to state-of-the-art detection limits. For comparison purposes, detection limits obtained with the Applied Research Laboratories (ARL) 34000S commercial system available in this laboratory are tabulated in Table 24. These detection limits were obtained using the same multielement solution used for this study. In most cases, the detection limits measured with the FTS system are at least one, and often more, orders of magnitude poorer than those obtained with the direct reader system. In the few cases, for example magnesium, in which the discrepancy is not as great, a

Table 24

Detection Limits Measured with a

Commercial ICP Instrument

Element	Detection Limit (ppb)	% RSD
Al	55	0.42
B	3	0.25
Ba	0.6	0.24
Ca	8	0.28
Cd	2	0.32
Cu	3	0.22
Fe	2	0.26
K	89	0.14
Mg	26	0.13
Mn	0.7	0.27
Na	14	0.53
Ni	14	0.30
Pb	37	0.39
Si	23	0.20
V	3	0.25
Zn	4	0.33

less intense emission line was used for the analysis of that element in the direct reader commercial instrument.

Another figure of merit for quantitative analysis is the relative standard deviation of the analytical signal intensity. For the 10 ppm multielement solution, the relative standard deviations for each element have been included in Table 23 for the FTS measurement system and in Table 24 for the commercial ICP instrument. Relative standard deviations determined by FTS were also poorer, in the five percent range, in comparison to those obtained with the commercial instrument, in the 0.25 to 0.50 percent range.

D. Conclusions

The FTS measurement system has excellent qualitative simultaneous multielement measurement capabilities. The spectral response of the interferometer has been shown in this chapter for wavelengths as short as 193 nm and up to the maximum response of the PMT, 650 nm. It should be possible to extend the spectral response of the FTS measurement system to longer wavelengths by changing the detector to, for example, a silicon photodiode. At the shorter wavelengths, purging of the optical path should allow measurement of wavelengths as short as 180 nm.

The advantages of FTS as a measurement system, discussed in Chapter I, have been demonstrated in this chapter and in Chapter III. The ability to measure simultaneously over a wide wavelength region both background and analyte spectrochemical information is unparalleled by any other spectrochemical measurement system. This ability should facilitate background correction and allows alternate line selection when a spectral line interference occurs. In addition, the accurate wavelength axis inherent in the interferometer facilitates precise and accurate wavelength identification.

Quantitatively, the FTS measurement system has room for improvement. Detection limits are several orders of magnitude poorer than those obtained with a commercial ICP instrument. These detection limits represent the best possible situation for the current FTS system - that is, the background standard deviation was calculated using a distilled water background. In a dispersive-based measurement system, the assumption that for ICP emission, the standard deviation of the background will decrease linearly as the signal decreases is approximately valid. However, it was shown in this chapter that the standard deviation of the background is dependent on all the elements contributing to the measured emission, not just

on the element of analytical interest. The use of a distilled water background as a measure of the standard deviation is, in the FTS measurement system, an unrealistic assumption. It could be considered valid only when, as the detection limit for one element is approached, the concentration of all other elements in the sample decreased proportionally. A more realistic approach to calculating the detection limits might be to measure the standard deviation of the baseline of the multielement spectra themselves, in spectral regions devoid of spectral emission lines. This method would degrade the detection limits further by an estimated one-half to one order of magnitude.

In order to improve the quantitative performance of the interferometer, some modifications are necessary. A novel measurement system, a windowed slew-scan Fourier transform spectrometer, will be described in Chapter VI. This instrument improves the quantitative capabilities of the FTS system while keeping most of the current advantages of the FTS measurement system.

CHAPTER VI

WINDOWED SLEW-SCAN FOURIER TRANSFORM SPECTROMETRY

A. Bandpass Limiting in the Interferometer

To improve the quantitative performance of the FTS system in the ultraviolet and visible spectral regions, two criteria must be met. The first criterion is that the dynamic range limitations imposed by strong emission signals must be reduced to allow the simultaneous observation of other weaker signals. The second, and more important criterion, is that the noise imposed on one spectral line by other emission lines in the same spectral region must be eliminated, or at least strongly reduced. In order to accomplish this, additional filtering, either optical or electronic, must be employed.

Electronic filtering is already utilized in the FTS system developed in this laboratory to eliminate aliasing into the spectral region of noise at frequencies outside the spectral region. Further electronic filtering, to limit both noise and signal information to a smaller spectral window, could be employed. However, all incident radiation from the ICP would still be collected at the

detector in the interferometer. A more practical approach might be to limit the optical bandpass into the interferometer itself.

1. Optical Bandpass Limiting

To limit the optical bandpass into the interferometer, several different approaches could be envisioned. The first approach is one in which the spectral region of interest would be scanned in a series of smaller consecutive spectral windows; that is, in a sequential mode. This approach would decrease, but not totally eliminate, the simultaneous measurement capabilities inherent in the interferometer.

i) Sequential Optical Bandpass Limiting

To limit the spectral bandpass into the interferometer, optical interference filters could be used. For each spectral window of interest, a different interference filter would be necessary. This approach is practical if one is interested in a small number of spectral windows. The different interference filters could be mounted onto a filter wheel and the spectral window of interest could then be selected by rotating the appropriate filter in front of the interferometer entrance. In order to keep the ability to measure the entire ultraviolet and visible regions of the spectrum by

FTS, a large number of interference filters would be needed. A filter wheel approach would rapidly become unwieldy and unmanageable. The flexibility of the FTS measurement system thus becomes greatly reduced.

An alternative approach is the introduction of a low to medium resolution monochromator with wide entrance and exit slits. This allows a narrow spectral bandpass into the interferometer. Scanning is again accomplished in a sequential fashion. The instrument developed in this laboratory is based on this concept. Before discussing this instrument, several other methods of bandpass limiting will be briefly presented.

ii) Simultaneous Optical Bandpass Limiting

It would be advantageous to design a method to limit the optical bandpass at the detector while keeping the simultaneous multielement measurement capabilities of the interferometer. To accomplish this, it would be necessary to place the bandpass limiting device between the interferometer and the detector. Consider a direct reader type instrument. Placing an interferometer such that the interference fringes from the interferometer are focussed onto the entrance slit of the direct reader would result in a series of interference fringes, with a narrow optical bandpass, at the exit slits of the direct reader. At each detector, a narrow bandpass interferogram would be

recorded. The width of the optical bandpass would depend on the width of the exit slits. Spectral information can then be obtained by Fourier transforming these interferograms. Simultaneous multielement analysis could be easily attained with this instrument and both background and analyte spectral information would be available.

iii) Random Access Optical Bandpass Limiting

In a more futuristic design, an instrument could be imagined in which the desired spectral windows could be "dialed in" and then simultaneous analysis performed on these windows. For example, if quantitative information for zinc and nickel is desired, it would be only necessary to dial in the two elements. The appropriate optical windows would then be automatically selected, the interferogram recorded and the results for zinc and nickel displayed. To date, a method to randomly access any wavelength has not been developed.

B. The Monochromator as an Optical Bandpass Limiting Device

As mentioned previously, an instrument has been developed in this laboratory to improve the quantitative performance of the FTS measurement system. In this

instrument, a medium resolution monochromator with wide entrance and exit slits has been placed before the interferometer to limit the optical bandpass into the interferometer. The wide slits will provide a narrow optical window at the exit slit of the monochromator. Scanning between spectral windows is accomplished by simply rotating the grating. This instrument, termed a windowed slew-scan Fourier transform spectrometer (WSS-FTS), should provide a partial, if not complete, solution to the quantitative limitations of the interferometer in the UV and visible spectral regions.

In the conventional configuration of the slew-scanning monochromator, with entrance and exit slits in the 50 to 100 μm range, no advantage is realized with this instrument. Narrow slits are required to avoid degrading the resolution capabilities of the monochromator. But high resolution is not required in the monochromator part of WSS-FTS. In the interferometer, resolution is determined ultimately by the optical path difference or by the distance the moving mirror has travelled. In other words, resolution is provided by the interferometer, not the scanning monochromator.

To attain the goal of simultaneous multielement analysis then, it is necessary to alter the width of the entrance and exit slits to their maximum value, in this

case, 2 mm. The spectral bandpass at the exit slit will be dependent on the focal length of the monochromator, on the number of lines in the grating and on the width of the slits. Because it is desirable to have a reasonably wide bandpass at the exit slit, at least in the order of several nanometers, if not larger, a low to medium resolution monochromator is more than adequate for this application. In this laboratory, the monochromator used for this purpose has a 0.35 m focal length and is equipped with a 1200 line/mm grating blazed at 250 nm. With an entrance and exit slit of width 2 mm, the spectral bandpass is approximately 4 nm. To obtain a larger or smaller spectral bandpass, the grating in the monochromator can be easily changed. For example, a 600 line/mm grating will provide a bandpass of approximately 8 nm, while a 2400 line/mm grating yields a spectral window of 2 nm. Both of these gratings are available in this laboratory.

Simultaneous multielement analysis is possible for elements with emission lines of similar wavelengths; that is, wavelengths which differ by less than 4 nm. One example would be the simultaneous analysis of zinc, cadmium and lead using their emission lines at 213.8, 214.9 and 217.0 nm. Of course, all spectrochemical information, both background and analyte, will be simultaneously measured with WSS-FTS.

The role of the monochromator is to simply limit the optical bandpass into the interferometer. Both resolution and wavelength accuracy are provided by the interferometer. Consequently, the resolution of WSS-FTS is identical to that in the conventional FTS measurement system.

The inherent wavelength accuracy available in the interferometer eliminates the wavelength alignment problem of the conventional slew-scanning monochromator. The spectral line of interest need only be contained in the 4 nm spectral window. Exact positioning of that wavelength at the exit slit is not essential since all wavelengths within the spectral window are easily identified using the accurate wavelength axis of the interferometer.

A schematic diagram of the WSS-FTS is illustrated in Figure 37. In this system, the slew-scanning monochromator simply replaces the limiting aperture described in Chapter III. A 1:1 image of the plasma has been focussed onto the entrance slit of the monochromator using a 15 cm focal length quartz lens. A second quartz lens, of focal length 10 cm, was placed after the monochromator to provide the collimated light necessary for the interferometer. All optical components have been aligned so that the spatial viewing zone in the ICP is centered at 17 mm above the load coil.

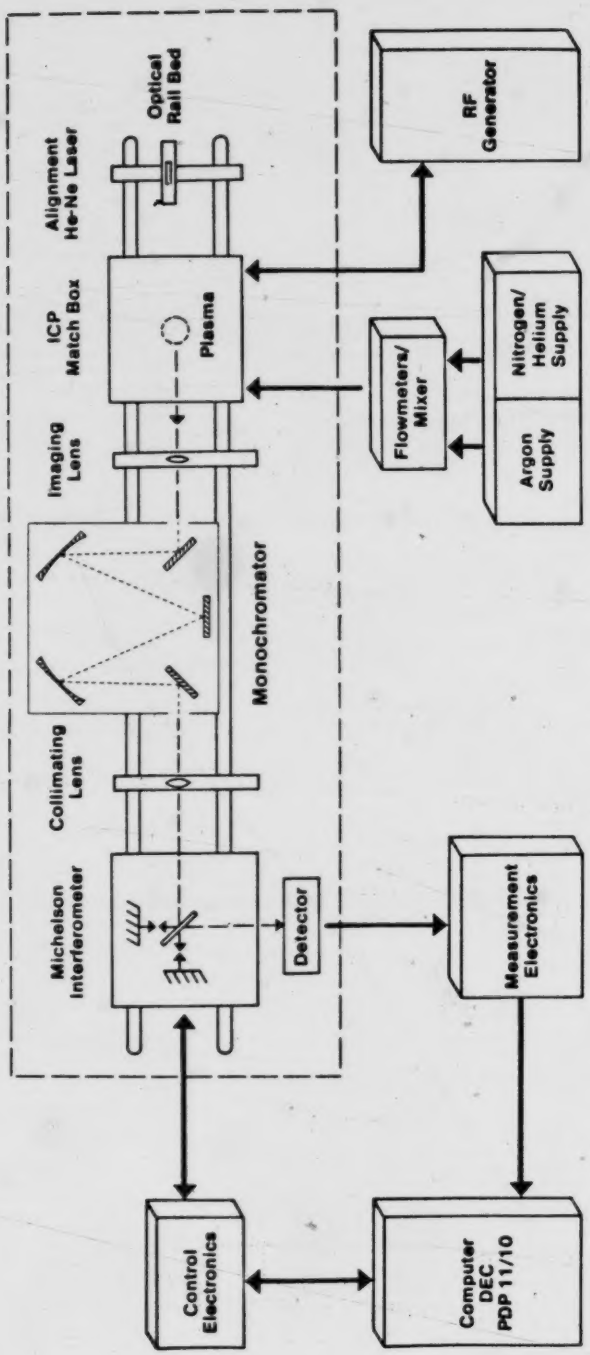

Figure 37. Block diagram of the ICP-windowed slew-scan Fourier transform spectrometer measurement system.

One of the classic advantages of FTS in comparison to a scanning monochromator is the throughput advantage. This advantage exists when the throughput in the FTS system is limited by the entrance optics to the interferometer and for narrow slits in the monochromator. It might be thought, then, that introduction of the monochromator into the FTS measurement system would reduce the throughput of the system.

The throughput is not necessarily limited by the entrance optics. However, this assumption will be made for the purposes of the following discussion. The throughput [56], E, is defined as:

$$E = \Omega_c A_s \tag{1}$$

where Ω_c is the solid angle subtended by the collimating lens at the centre of the source (see Figure 38) and A_s is the area of the incident source radiation beam. The solid angle, Ω_c, can be determined from the equation

$$A = \Omega_c f_c^2 \tag{2}$$

where A is the area of the collimating lens in m^2 and f_c is the focal length in m of that lens as shown in Figure 38.

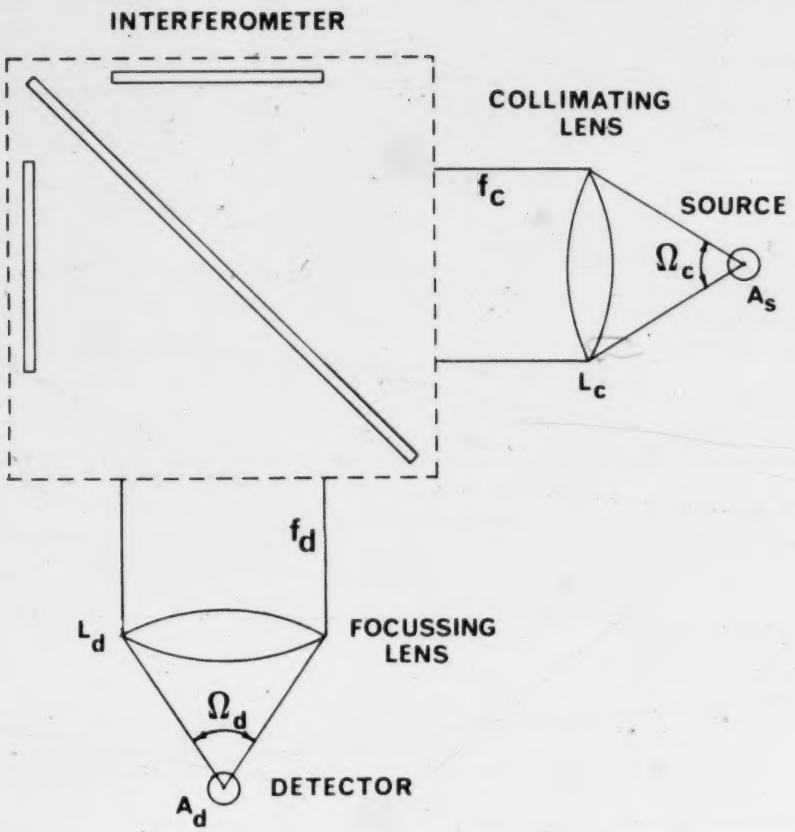

Figure 38. Throughput parameters in the interferometer.

For both FTS and WSS-FTS, the same collimating lens was employed. Consequently, the solid angle will be identical for the two systems. With a lens diameter of 0.05 m and a focal length of 0.1 m, the solid angle, Ω_c, can be calculated as 0.206 sr, which corresponds to approximately 8.3°.

The difference in throughput of the two measurement systems is therefore dependent on the difference in the area of the source beam before the collimating lens. In the interferometer system, without the monochromator, the area of the source beam is limited by the intermediate circular aperture (Chapter III) which has a diameter of 5 mm. The source area, A_s, is then calculated to be 1.96×10^{-5} m^2 and E_{FTS}, the throughput, is determined to be 4.04×10^{-6} $m^2 \cdot sr$.

For WSS-FTS, the aperture for the source radiation is the entrance slit of the monochromator, which is rectangular in shape. The area of the entrance slit, with a height of 0.1 m and width of 0.02 m, is calculated to be 2.00×10^{-5} m^2 yielding a throughput, $E_{WSS-FTS}$, of 4.12×10^{-6} $m^2 \cdot sr$. The ratio of the throughput, E_{FTS}, for the interferometer system is:

$$\frac{E_{FTS}}{E_{WSS-FTS}} = 0.99 \qquad (3)$$

The theoretical throughputs of the two meaurement systems are virtually identical. However, this argument assumes that all optical components in the measurement system are perfect. In reality, there is always some loss of light at each optical component. In FTS, the only optical components before the interferometer are the imaging and collimating lens. However, in WSS-FTS, the monochromator, in a Czerny-Turner configuration, has five optical surfaces: the grating, two off-axis parabolic mirrors and two plane mirrors. With this configuration, the effective throughput has to be reduced due to reflection and transmission losses at each optical surface.

The above argument also assumes that the throughput is limited by the entrance optics of the interferometer. More often, the throughput is limited by the detector or exit optics. In the interferometer used in this laboratory, a 2 mm aperture was placed before the detector (Chapter II) to ensure that only the central fringe of the interferogram is observed. Therefore, the detector optics will be the limiting factor for the throughput. In this case, the throughput is not affected by the introduction of the monochromator into the FTS measurement system.

To actually obtain spectrochemical information with WSS-FTS the procedure is straightforward. A particular

spectral window can be chosen by simply setting the monochromator to the approximate wavelength, as shown in Figure 39. In Figure 39a, the multielement spectrum measured by the solar blind PMT is shown. To select the analysis of zinc, for example, the monochromator is set to approximately 214 nm. The resultant spectrum, in which the ZnI 213.8 nm line is observed, is shown in Figure 39b. Spectrochemical information from other spectral regions has been excluded by the monochromator.

To attain multielement analysis, slew-scanning between spectral windows is easily accomplished, as demonstrated in Figure 40. By simply changing the monochromator setting, different spectral windows, and consequently, different elements can be measured. In Figure 40, several different 4 nm windows are illustrated. It is evident from this figure that some simultaneous multielement capabilities still remain. For example, in the 228 nm spectral window, emission lines for both cadmium and nickel are observed.

Another consideration with the WSS-FTS system is the length of the transform or of the interferogram necessary to encode the spectrochemical information. Normally, in this laboratory, a double-sided interferogram of length 4096 points is acquired. The question arises as to whether this length is necessary for a 4 nm optical window

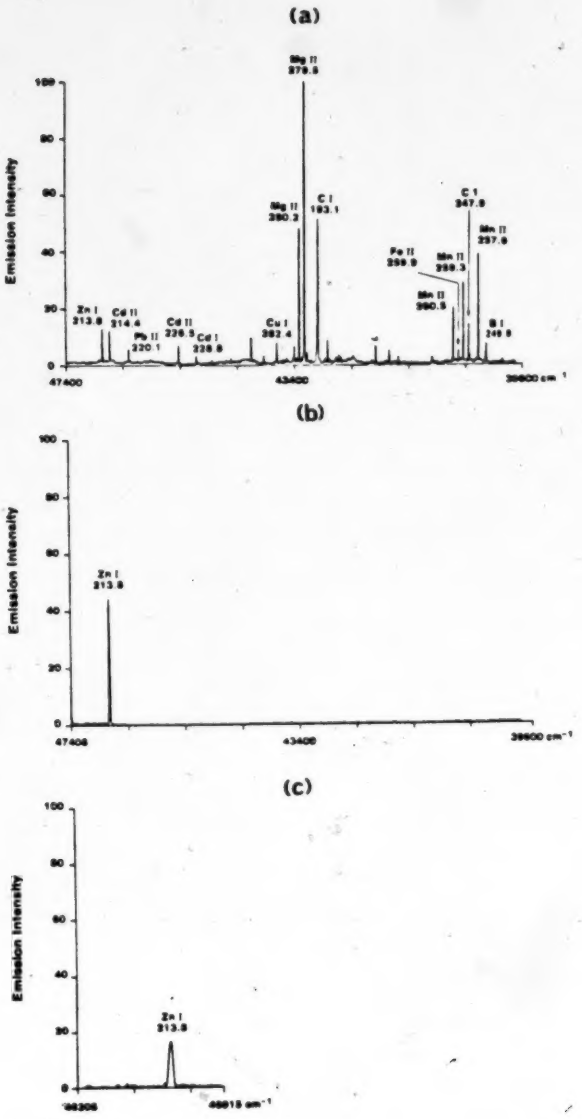

Figure 39. Emission spectra as measured by FTS and WSS-FTS: (a) multielement spectrum (Figure 32), (b) 214 nm window - 4096 point transform and (c) 214 nm window - 256 point transform.

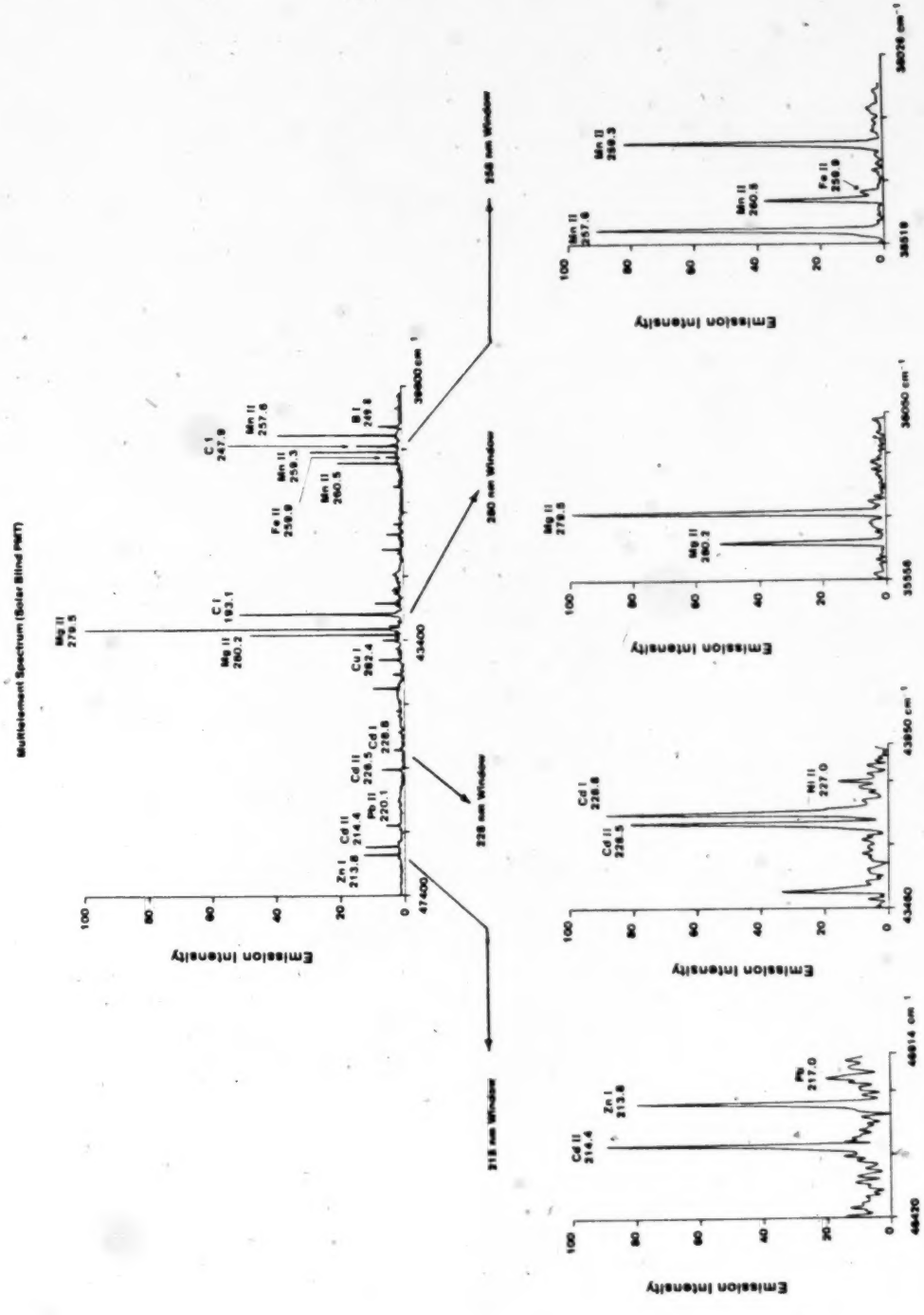

Figure 40. Windowed slew-scan capabilities of WSS-FTS.

and what effect shorter interferograms would have on the resultant spectra. It is important to maintain the current resolution of the interferometer. To acquire shorter interferograms then, it would be necessary to sample every nth laser clock pulse, in effect employing a ÷n counter. The alternative approach is to sample every laser clock pulse, as was previously done, but not acquire as many points. This, of course, will reduce the resolution of the interferometer by reducing the maximum optical path difference between the two arms of the interferometer.

The ÷n approach would consequently appear to be more practical. In Figure 39c, the resultant spectrum for a 256-point interferogram of the 214 nm spectral window, is illustrated. Utilizing the same interferogram as that used to obtain the 4096-point spectrum in Figure 39b, it was possible to software select every sixteenth point in order to generate a 256 point interferogram of identical resolution. The spectra in both Figure 39b and 39c have been plotted on the same intensity scale. Several points are apparent in these spectra. Firstly, because the number of resolution elements is decreased in the shorter interferograms, a signal-to-noise decrease can be noted as the length of the interferogram decreases. This S/N decrease is proportional to the square root of n. For a

256 point interferogram, a S/N decrease of four is expected. No quantitative calculations were performed to verify this factor. However, the noise in the baseline does appear greater with respect to the emission line intensities in the 256 point spectrum as compared to the original 4096 point spectrum.

A more important consideration is that, in a qualitative sense, no atomic spectrochemical information is lost in the shorter transforms. As is to be expected, there is no apparent degradation of the resolution between the two spectra. The final factor is aliasing. The increase in the degree of aliasing as the length of the interferogram is decreased is apparent in Figure 40.

Consider, for example, the 215 nm spectral window illustrated in Figure 40. Wavelengths in the 215 nm region of the multielement spectrum (top of Figure 40) increase from left to right. In the 256 point spectrum of the 215 nm spectral window, the relative ordering of wavelengths has changed. In this spectrum, the ZnI line at 213.8 nm appears between the CdII 214.4 nm and PbII 217.0 nm lines, indicating an increase in the degree of aliasing.

As discussed in both Chapter I and Chapter III, aliasing can be used to advantage. In the case of a 4096 point interferogram, a 7901.4 cm^{-1} bandpass can be

properly sampled. For a 256 point interferogram, only a 493.8 cm^{-1} bandpass can be properly sampled. It is clear that the number of aliasing windows or regions in the ultraviolet and visible spectral regions is quite large for the ÷16 sampling rate. In Table 25, the aliasing regions for the 180 to 300 nm spectral window at both a ÷8 and ÷16 clocking rate are shown. Aliasing tables for the ÷4 and ÷2 clocking rates have been documented in Yuen's thesis [38] and will not be repeated in this thesis. From Table 25 it is clear that to accurately determine the true wavelength of a spectral line over a large spectral window for a 256 point spectrum, for example that covered in this table, would be an almost impossible task. However, with the 4 nm spectral window in the WSS-FTS system, correct line identification becomes relatively straightforward. The monochromator provides the approximate wavelength range. For any one spectral window, only a couple of aliasing regions are applicable, facilitating line identfication.

It would appear, then, that a 256 point interferogram and transform is sufficient to adequately measure atomic spectrochemical information with the WSS-FTS measurement system. This size of interferogram reduces the computation time and memory space necessary to produce a spectrum.

Table 25

Aliasing Regions for ÷8 and ÷16 Clocking Rates

÷16		÷8		÷1	
cm^{-1}	μm	cm^{-1}	μm	cm^{-1}	μm
31605.6-32099.4	0.3164-0.3115	31605.6-33593.3	0.3164-0.3068	31605.6-39507.0	0.3164-0.2531
32593.3-32099.4	0.3068-0.3115				
33581.0-33087.1	0.2978-0.3022	33581.0-32593.3	0.2978-0.3068		
33581.0-34074.8	0.2978-0.3022				
33581.0-34074.8	0.2978-0.2935	33581.0-34568.6	0.2978-0.2893		
34568.6-34074.8	0.2893-0.2935				
34568.6-35062.5	0.2893-0.2852	35556.3-34568.6	0.2812-0.2893		
35556.3-35062.5	0.2812-0.2852				
35556.3-36050.1	0.2812-0.2774	35556.3-36544.0	0.2812-0.2736		
36544.0-36050.1	0.2736-0.2774				
36544.0-37037.8	0.2736-0.2700	37531.7-36544.0	0.2664-0.2736		
37531.7-37037.8	0.2664-0.2700				
37531.7-38025.5	0.2664-0.2630	37531.7-38519.3	0.2664-0.2576		
38509.3-38025.5	0.2596-0.2630				
38519.3-39013.2	0.2596-0.2563	39507.0-38519.3	0.2531-0.2596		
39507.0-39013.2	0.2531-0.2563				
39507.0-40000.8	0.2531-0.2500	39507.0-40494.7	0.2531-0.2469	47408.4-39507.0	0.2109-0.2531
40494.7-40000.8	0.2469-0.2500				
40494.7-40988.5	0.2469-0.2440	41482.4-40494.7	0.2411-0.2469		
41482.4-40988.5	0.2411-0.2440				
41482.4-41976.2	0.2411-0.2382	41482.4-42470.0	0.2411-0.2355		
42470.0-41976.2	0.2355-0.2382				
42470.0-42963.9	0.2355-0.2328	43457.7-42470.0	0.2301-0.2355		
43457.7-42963.9	0.2301-0.2328				

Table 25 (Cont'd.)

Aliasing Regions for ÷8 and ÷16 Clocking Rates

÷16		÷8		÷1	
cm^{-1}	μm	cm^{-1}	μm	cm^{-1}	μm
43457.7-43951.5 44445.4-43951.5	0.2301-0.2275 0.2250-0.2275	43457.7-44445.4	0.2301-0.2250		
44445.4-44939.2 45433.1-44939.2	0.2250-0.2225 0.2201-0.2225	45433.1-44445.4	0.2201-0.2250		
45433.1-45926.9 46420.7-45926.9	0.2201-0.2177 0.2154-0.2177	45433.1-46420.7	0.2201-0.2154		
46420.7-46914.6 47408.4-46914.6	0.2154-0.2132 0.2109-0.2132	47408.4-46420.7	0.2109-0.2154		
47408.4-47902.2 48396.1-47902.2	0.2109-0.2088 0.2066-0.2088	47408.4-48396.1	0.2109-0.2066	47408.4-55309.8	0.2109-0.1808
48396.1-48889.9 49383.8-48889.9	0.2066-0.2045 0.2025-0.2045	49383.8-48396.1	0.2025-0.2066		
49383.8-49877.6 50371.4-49877.6	0.2025-0.2005 0.1985-0.2005	49383.8-50371.4	0.2025-0.1985		
50371.4-50865.3 51359.1-50865.3	0.1985-0.1966 0.1947-0.1966	51359.1-50371.4	0.1947-0.1985		
51359.1-51852.9 52346.8-51852.9	0.1947-0.1929 0.1910-0.1929	51359.1-52346.8	0.1947-0.1910		
52346.8-52840.6 53334.4-52840.6	0.1910-0.1892 0.1875-0.1892	53334.5-52346.8	0.1875-0.1910		
53334.4-53828.3 54322.1-53828.3	0.1875-0.1858 0.1841-0.1858	53334.5-54322.1	0.1875-0.1841		
54322.1-54816.0 55309.8-54816.0	0.1841-0.1824 0.1808-0.1824	55309.8-54322.1	0.1808-0.1841		

It is desirable in any measurement system to be able to obtain essentially instantaneous results. That is, the results should be available shortly after the data acquisition step has been completed. With the computer available in this laboratory, real-time transformations of 4096 point interferograms are not possible. The Fourier transformation of 4096 points takes approximately two minutes. A shorter interferogram might allow real-time, that is on the reverse scan of the moving mirror, transformations. The spectral information would then be available essentially as soon as the data acquisition step is completed.

One other possibility with WSS-FTS is zoom resolution. By using a ÷16 counter, either under software or hardware control, it is possible to obtain higher resolution spectra without drastically increasing the memory space and computation time necessary to obtain these spectra. For example, increasing the resolution by a factor of sixteen, that is, increasing the distance the moving mirror travels by the same amount, yields an interferogram of length 4096 points - similar to the interferograms obtained for the multielement spectra.

The largest trade-off with WSS-FTS is the partial loss of simultaneous multielement measurement capabilities of the conventional FTS measurement system. To

qualitatively measure emission in the entire ultraviolet and visible spectral region, data acquisition would be considerably more time-consuming, since the emission spectrum of each small spectral window must be separately measured. This problem can be partially resolved by measuring the spectrum at zero order. In this case, most light incident into the monochromator is reflected, rather than dispersed, through the monochromator to the exit slit. Although the intensity of the exit radiation is reduced in comparison to the incident radiation, a qualitative simultaneous analysis of the entire spectral region is possible.

In quantitative analysis, it is usually necessary to analyze for a few elements, less than twenty, for any one analysis unless otherwise noted. As mentioned previously, it is possible to measure more than one within the same spectral window. In addition, changing spectral windows is readily accomplished by simply slew-scanning the monochromator to the approximate wavelength of the desired spectral window. In the case of spectral interferences, it is possible to quickly and easily choose an alternate analytical line free of spectral interferences. Often, in analyses utilizing the ICP, sample preparation is the rate determining step. The additional time necessary to acquire data with WSS-FTS as compared to FTS, might not be significant in most situations.

WSS-FTS should improve the quantitative capabilities of FTS, both by decreasing dynamic range limitations and by eliminating the apparent increase in noise in one spectral window caused by emission lines in other spectral windows. In this chapter, the effectiveness of WSS-FTS as a qualitative and quantitative tool for the measurement of emission in the ICP will be demonstrated. The spectral region examined in this chapter ranges from the vacuum ultraviolet, 180 nm, to the beginning of the near-infrared, 925 nm.

C. Windowed Slew-Scanning Capabilities

The spectra presented in this section were calculated from 256 point interferograms. As mentioned previously, changing spectral windows in WSS-FTS is easily accomplished by simply slew-scanning the monochromator to the appropriate wavelength. It is possible, as well, to simultaneously measure emission for more than one element in some spectral windows. Background spectral information can also be acquired simultaneously with the emission lines of interest within the same spectral window.

1. Emission from a Multielement Solution

For all spectra in this section, emission from the 10 ppm sixteen element multielement solution described in

Chapter V was measured. No attempt was made to characterize all possible spectral windows. Rather, spectral windows useful for the quantitative analysis of the sixteen elements in the multielement solution were chosen. Spectra have been arranged in order of increasing wavelength for the multielement solution. However, all spectra containing emission of one particular element are presented consecutively regardless of the spectral windows involved, for the purpose of clarity. Spectra at wavelengths shorter than 290 nm were measured using the solar blind PMT. At longer wavelengths, the 1P28 PMT was used as the detector.

For the multielement solution, only wavelengths longer than 200 nm were considered. In Figure 41a, the spectrum of the 200 nm spectral window is presented. Only one emission line, the zinc 202.6 nm line, is apparent. The 214 nm spectral window illustrated in Figure 41b, can be utilized for the analysis of three elements, lead, zinc and cadmium, simultaneously. Another example of a spectral window in which analysis of more than one element is possible is the 228 nm spectral window (Figure 41c). In this spectrum, the nickel II line at 227.0 nm was observed, in addition to the cadmium II line at 226.5 nm and the cadmium I line at 228.8 nm. It is important to note that several emission lines observed in these three

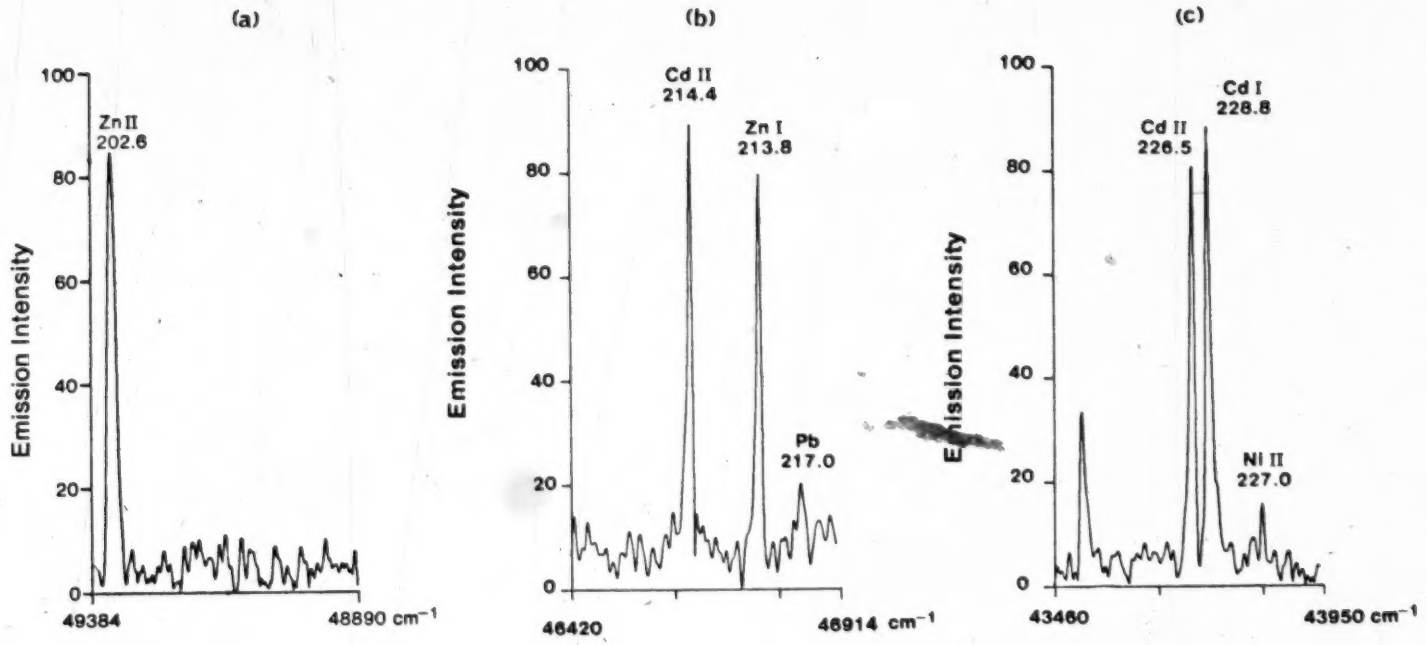

Figure 41. Emission spectra (256 points) of the spectral windows: (a) 202 nm, (b) 215 nm and (c) 228 nm.

spectral windows, in particular the zinc 202.6 nm line, lead at 217.0 nm and nickel at 227.0 nm, were not observed in the multielement solar blind spectrum (Figure 32) presented in Chapter V. In fact, it was not possible to determine a detection limit for nickel because of the absence of nickel emission lines in that spectrum. From the three spectra shown in Figure 41, it is apparent that WSS-FTS is successful in reducing dynamic range problems in addition to reducing the noise disadvantages of the conventional FTS measurement system.

In Figure 42, both the 256 point and 4096 point spectra of the 250 nm spectral window are illustrated. In the 256 point spectrum (Figure 42b) the boron doublet at 249.8 is observed as is the carbon line at 247.9 nm. However, in the 4096 point spectrum, shown in Figure 42a, a molecular band is also observed. This band can be assigned to the nitrous oxide bandhead at approximately 248 nm and arises from air entrainment in the ICP. Its presence is not apparent in the 256 point spectrum. In the acquired interferogram (4096 points), broadband information is contained mostly at the center of the interferogram, while atomic or line information is found in the wings of the interferogram. At the ÷16 sampling rate, the information in the center of the interferogram is essentially missed, leading to a loss of

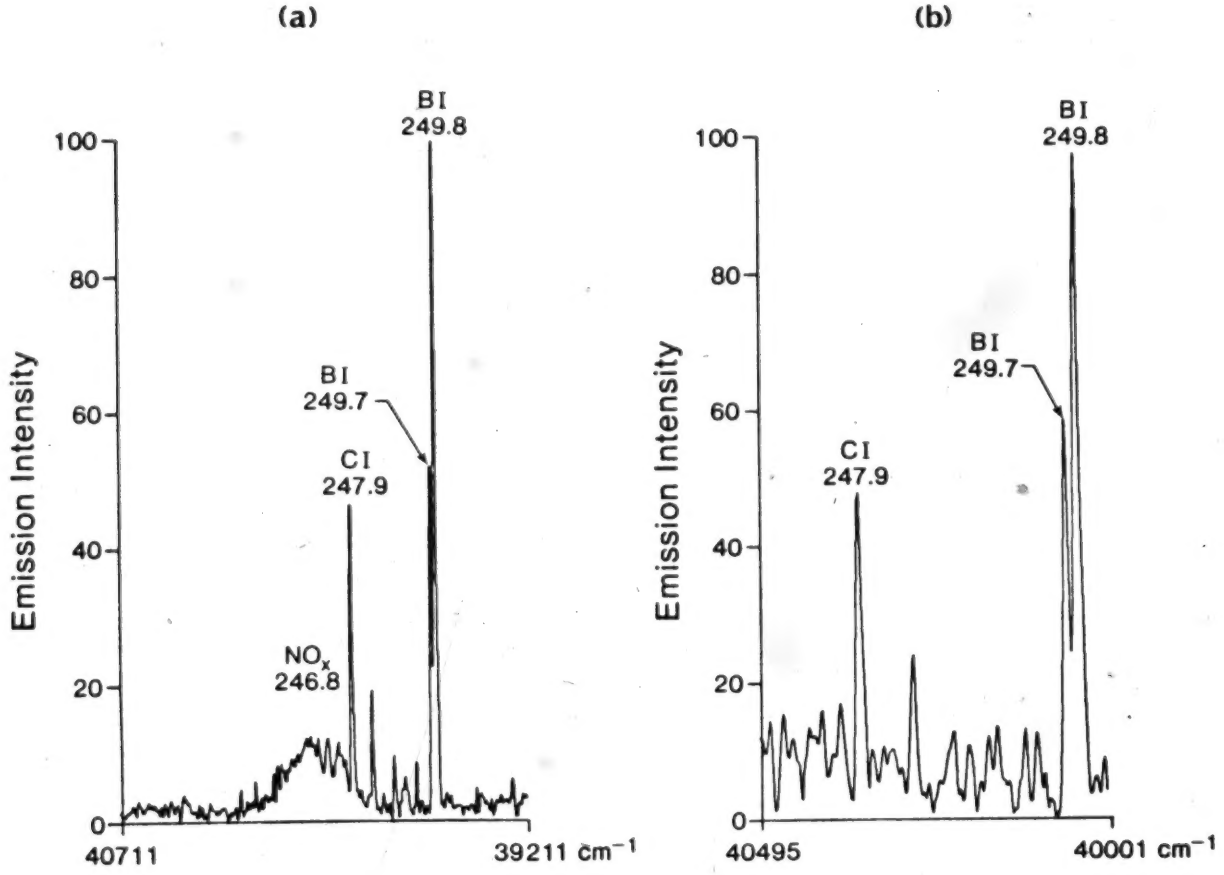

Figure 42. Emission spectra of the 250 nm spectral window: (a) 4096 point transform and (b) 256 point transform.

spectrochemical information. This is not a serious problem when atomic species are being analyzed, but would become exceptionally important if molecular species were under examination.

In the 259 nm spectral window (Figure 43), both manganese and iron emission lines are observed. In the 4096 point spectrum (Figure 43b), all three lines of the manganese triplet at 260 nm are measured and two iron lines at 259.9 nm and 258.6 nm are apparent. In the multielement spectrum (Figure 32) the observation of the iron line at 258.6 nm was precluded by the spectral overlap of the aliased carbon line at 247.9 nm. This spectral interference is not observed in the WSS-FTS system since the carbon line is outside the wavelength region covered by the 259 nm spectral window. In the 256 point spectrum, illustrated in Figure 43a, the iron line at 258.6 nm was again not observed. The decrease in the signal-to-noise ratio in the 256 point spectrum as compared to the 4096 point spectrum, described earlier in this chapter, has caused the disappearance of the iron line into the baseline noise.

The magnesium doublet at 279.5 and 280.2 nm is shown in Figure 44a. No other atomic lines were observed in the 280 nm spectral window. In the 288 nm spectral window, Figure 44b, emission due to both silicon and magnesium was

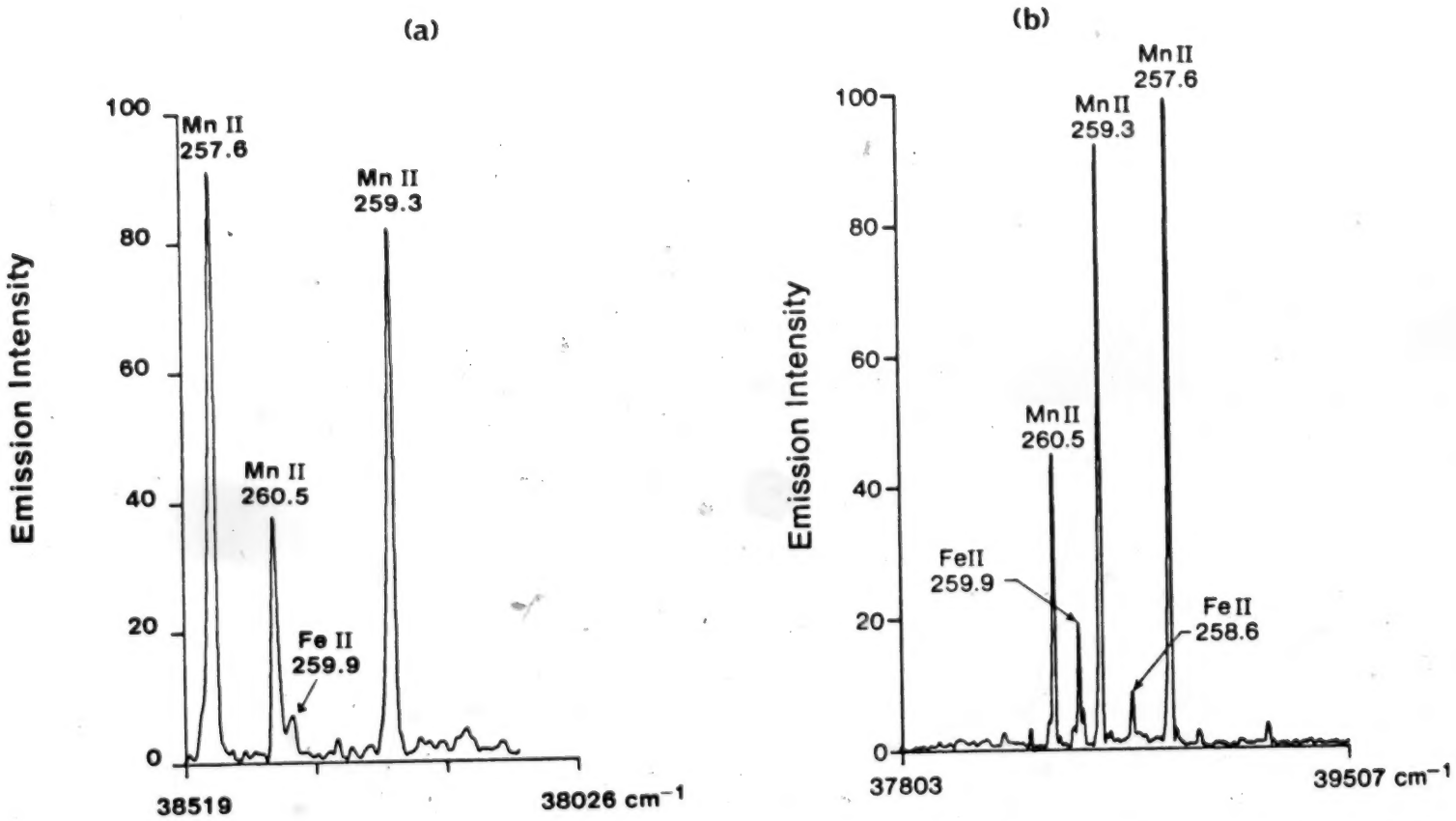

Figure 43. Emission spectra of the 259 nm window: (a) 256 point transform and (b) 4096 point transform.

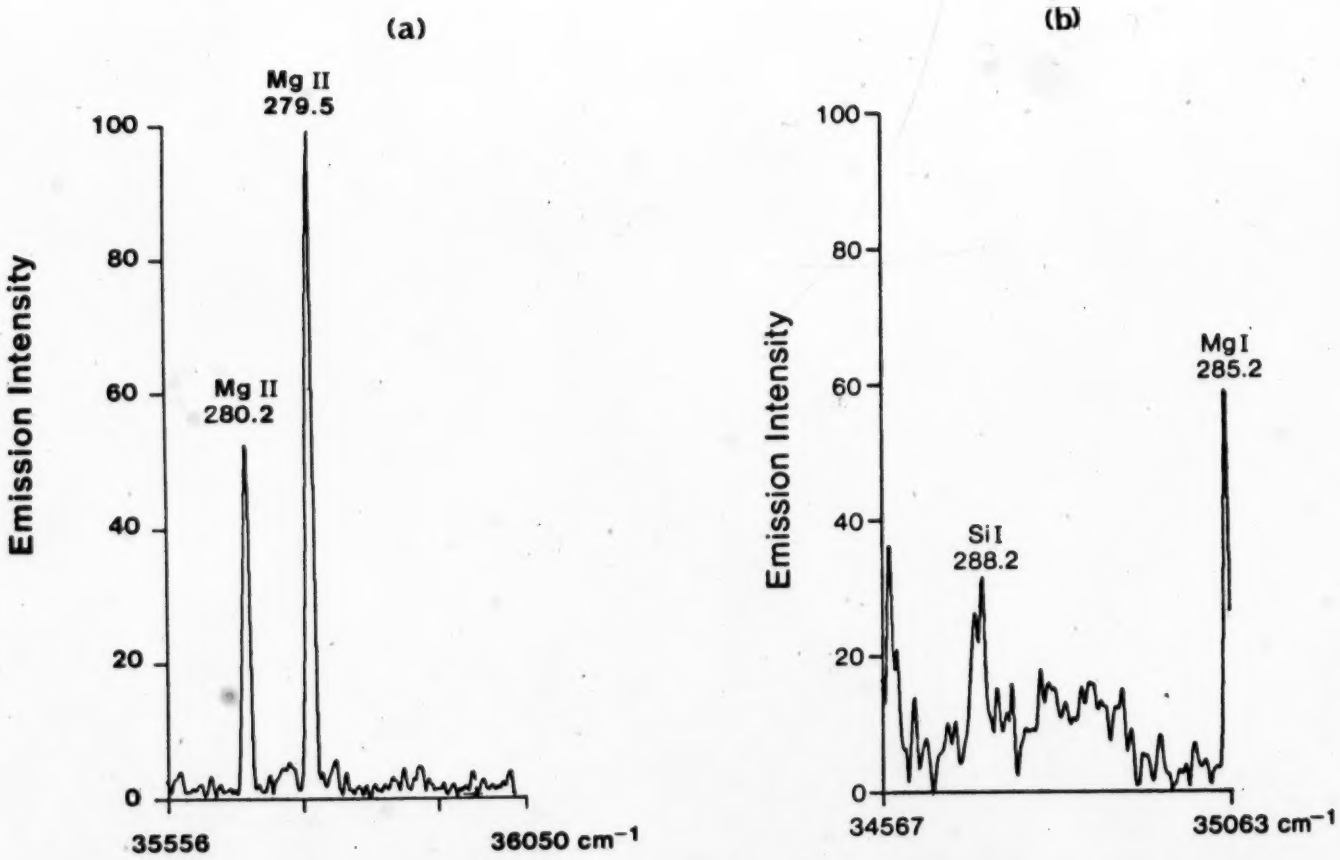

Figure 44. Emission spectra (256 points) of the spectral windows: (a) 280 nm and (b) 285 nm.

measured. The silicon doublet at 288.12 nm, not observed with conventional FTS, is only partially resolved at the current resolution of WSS-FTS. One interesting point noticed in Figure 44b is that the magnesium peak at 285.2 nm does not return completely to the baseline in this spectrum. The aliasing point for this spectral region occurs at the position of the magnesium peak causing the magnesium line to be partially folded over onto itself. This problem arises more often with WSS-FTS, in which 256 point transforms are utilized, because of the large number of aliasing regions (Table 25) and could cause erroneous values for both wavelength and intensity depending on the exact position of the aliasing point.

In Figure 45a, the 310 nm spectral window is illustrated. In this window, both vanadium and aluminum emission lines should be observed. However, the aluminum line at 309.3 nm was not visible in this spectrum. By changing the spectral window to one centered around 307 nm, it was possible to measure aluminum emission at 309.3 nm while eliminating the measurement of the dynamic range limiting vanadium emission lines. This spectral window is illustrated in Figure 45b. Neither aluminum or vanadium emission in this spectral window were noted in the multielement spectrum (Figure 33) measured with the 1P28. Another example of an elemental emission line not

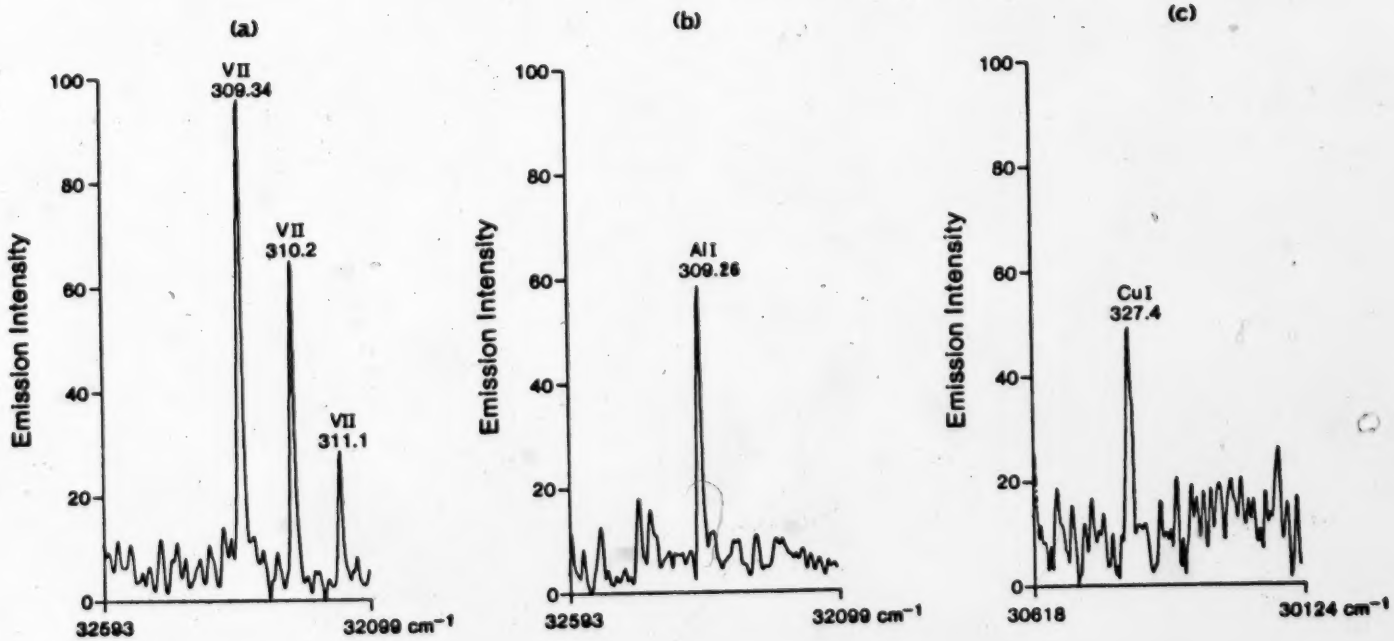

Figure 45. Emission spectra (256 points) of the spectral windows: (a) 310 nm, (b) 308 nm and (c) 325 nm.

observed in conventional FTS, is the copper line at 327.4 nm. In WSS-FTS, this line was clearly evident in the 328 nm spectral window, as illustrated in Figure 45c. A similar situation is present in this spectrum as in the boron spectrum shown in Figure 42. The copper emission line occurs on the edge of a hydroxyl band centered at approximately 328 nm. However, in the 256 point spectrum presented in Figure 45c, there is little evidence for the presence of this hydroxyl band.

In analytical determinations of aluminum in the ICP, the strong calcium emission lines at 393.3 and 396.8 nm interfere with the determination of aluminum using the strong aluminum line at 396.2 nm. This can be seen in the spectrum of the 395 nm spectral window shown in Figure 46a. The aluminum line at 396.2 nm is not observed. With WSS-FTS a simple solution exists. By decreasing the slit width of the monochromator to 100 μm, it is possible to eliminate the calcium interference. The aluminum line can then be measured as shown in Figure 46b. In this case, the throughput into the interferometer is drastically reduced. As well, more precise wavelength alignment of the monochromator is necessary. But it does provide a solution to the calcium emission interference. An alternative approach is to choose another aluminum line for the analysis. For example, the weaker aluminum line

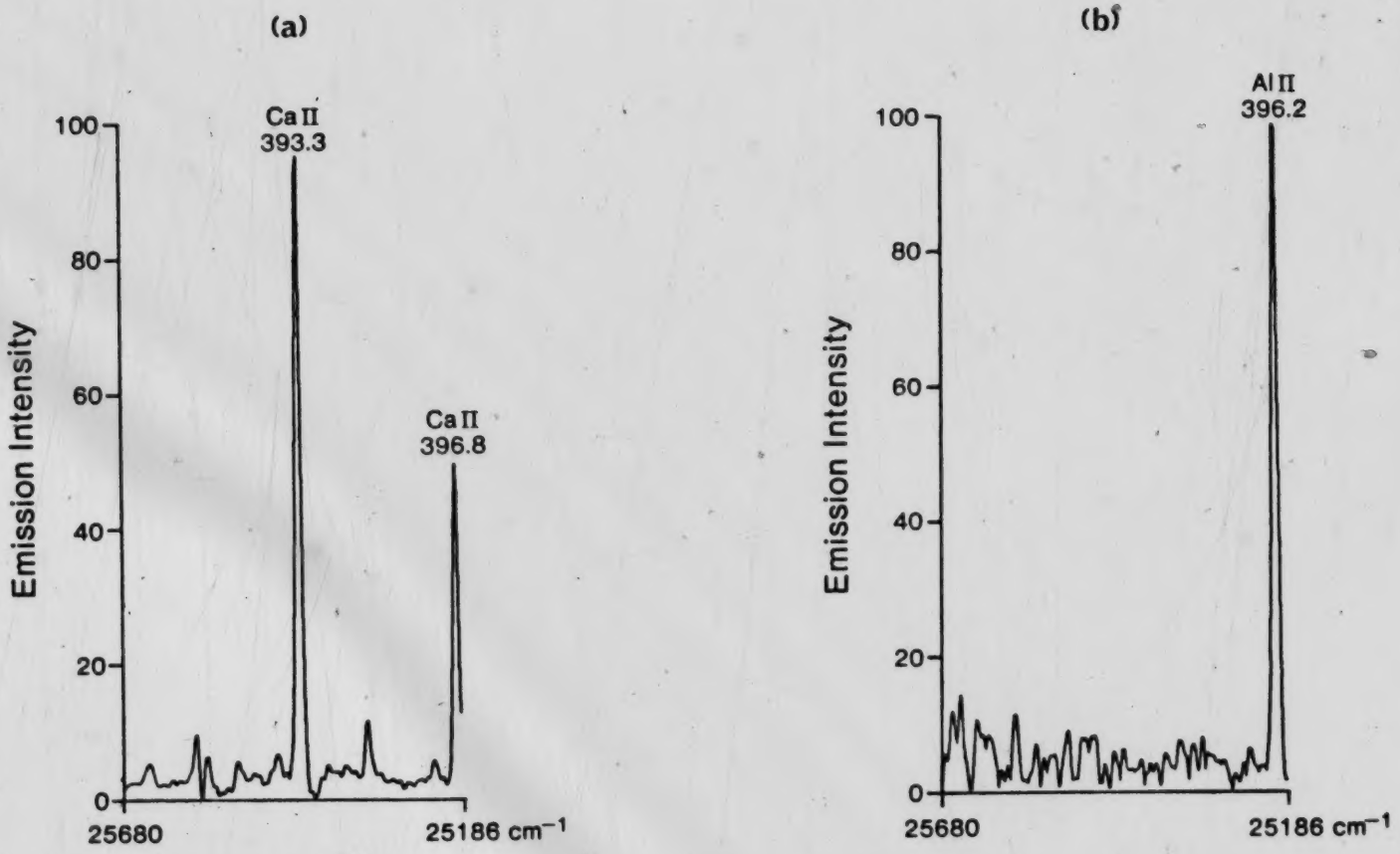

Figure 46. Emission spectra (256 points) of the 396 nm spectral window: (a) 2 mm slits and (b) 100 μm slits.

at 309.32 nm, illustrated in Figure 45b could be utilized for the quantitative determination of aluminum.

In Figure 47 the spectra of spectral windows containing emission from the elements barium, sodium and potassium are presented. In these spectra, the complex argon spectrum in the visible and near infrared spectral regions (Figure 47b) becomes apparent. In Figure 47a only the barium emission line at 455.4 nm was observed.

The spectral window, 765 nm, in which the potassium emission line at 766.5 nm falls, is outside the spectral response of the 1P28 photomultiplier tube used for the visible spectral region. Figure 47c shows the spectrum of this window. A silicon photodiode was used as the detector for this spectral window.

Emission lines observed for each element in the sixteen element multielement solution that were not measured with the conventional FTS system have been tabulated in Table 26. As in other spectra measured, experimental wavelengths are in agreement with literature wavelengths.

2. Emission at Wavelengths Below 200 nm

For nonmetal elements, for example sulphur, phosphorus and carbon, their resonance emission lines fall in the wavelength region below 200 nm, the vacuum ultraviolet spectral region. From the multielement

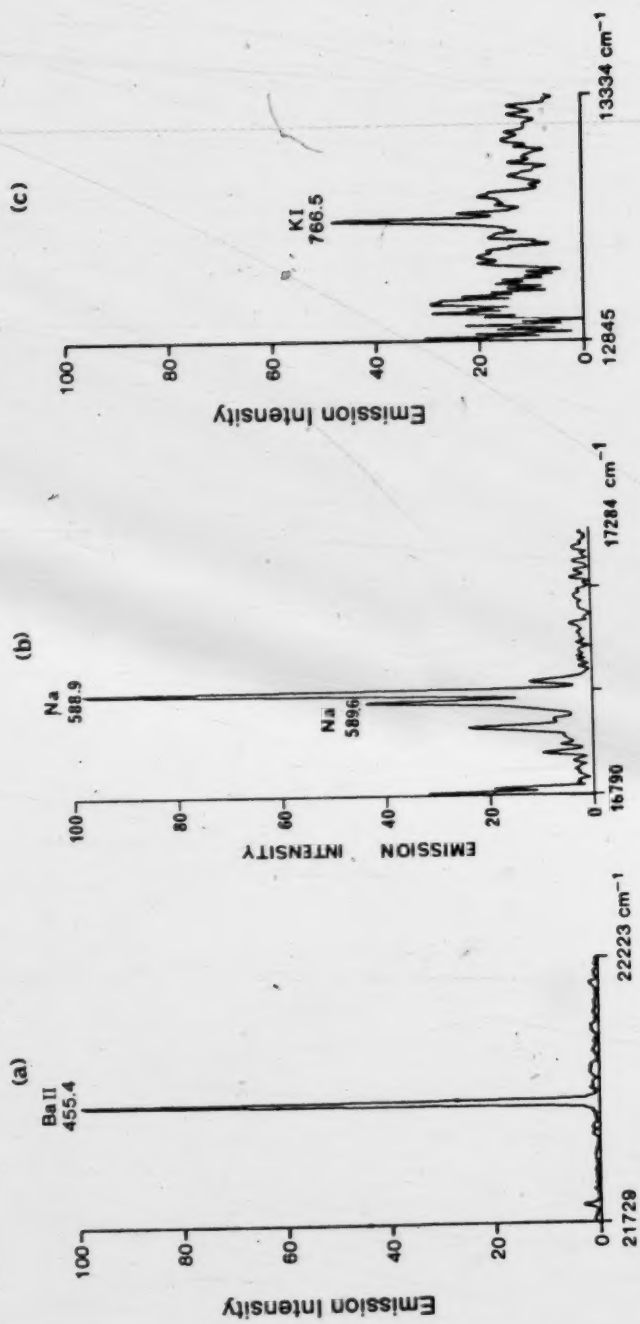

Figure 47. Emission spectra (256 points) of the spectral windows: (a) 455 nm, (b) 590 nm and (c) 766 nm.

Table 26

Emission Lines Measured by WSS-FTS But

Not Observed in FTS

Element	Experimental Wavenumber (cm^{-1})	Experimental Wavelength (nm)	Literature[75] Wavelength (nm)
Al	25244.9	396.12	396.15
	32335.3	309.26	309.28
B	47848.3	208.95	208.96
Cu	30539.9	327.44	327.40
Fe	38665.3	258.63	258.59
K	13047.3	766.44	766.49
Na	16977.4	589.02	589.00
	16962.4	589.54	589.59
Ni	43535.0	229.70	229.75
	43252.6	231.20	231.23
Pb	46089.3	216.97	217.00
Si	34700.5	288.18	288.16
	34421.0	290.52	290.57
V	32326.9	309.34	309.31
	32237.3	310.20	310.23
	32152.3	311.02	311.07
	32068.8	311.83	311.84

spectrum measured with the solar blind PMT (Figure 32), the carbon 193.1 nm line present in this spectrum illustrates that the spectral response of the interferometer at wavelengths below 200 nm is still acceptable.

For measurement in the spectral region between 180 nm and 200 nm, it is necessary to employ either a vacuum or inert gas flushed instrument. With the current instrument, it would be very difficult to construct a vacuum system.

To enable measurement of wavelengths below 190 nm, a pipe to allow purging of the entire optical system was constructed. Flexible plastic tubing (Dundas-Jafine Industries Ltd., Toronto, Ontario) was spray-painted a flat-black colour and attached between the optical components in the measurement system. One argon gas inlet was used to purge the monochromator, a second purged the actual ICP torch box and a third inlet was used to purge the connecting piping. It was not necessary to purge the interferometer since nitrogen was used to float the air bearing in the moving mirror assembly.

In order to determine the analytical usefulness of this spectral region, a 10000 ppm solution of phosphorus as the compound $(NH_4)_2PO_4$ was aspirated into the plasma. Although the phosphorus resonance line at 178.3 nm was not

observed, several alternate emission lines were measured. The spectrum of this spectral window is shown in Figure 48. No emission lines of either nitrogen or oxygen were observed. Phosphorus emission lines are tabulated in Table 27.

In the spectrum of DMSO measured with the conventional FTS system (Chapter III) in the ultraviolet spectral region, only the two intense carbon lines at 193.1 nm and 247.9 nm were observed. With the WSS-FTS measurement system, it was possible to observe weaker sulphur and oxygen emission lines in the spectral region below 200 nm (Figure 49). In the spectral window centered at 193 nm, Figure 49a, only the carbon 193.1 nm emission line was observed. In the spectrum of the 190 nm spectral window, illustrated in Figure 49b, two oxygen lines at 192.0 nm and 192.1 nm, in addition to the same carbon line, were observed. The sulphur resonance line, with a wavelength of 180.6 nm was identified in the 180 nm spectral window (Figure 49c). In addition to this line, the sulphur lines at 182.6 nm and 182.1 nm were observed in this spectrum.

The spectral response of WSS-FTS does appear to be decreasing in the wavelength region below 190 nm. This decrease in sensitivity can be attributed to several factors. Response could possibly be increased with an

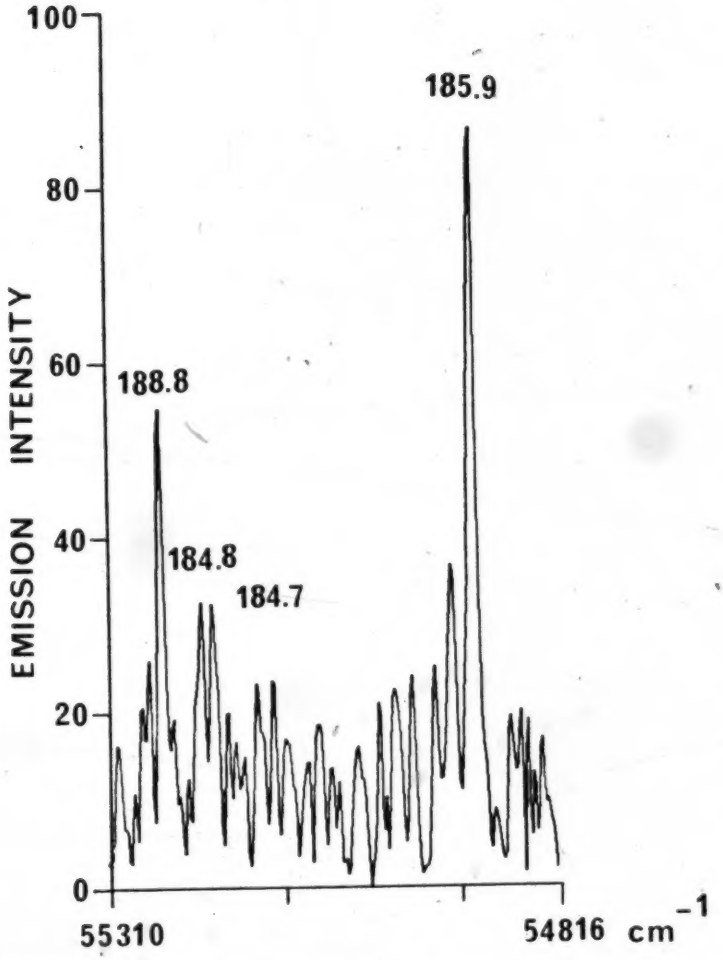

Figure 48. Emission spectrum (256 points) of 10000 ppm phosphorus in the 185 nm spectral window.

Table 27

Emission Lines Observed Below 200 nm

Element	Experimental		Literature[75]
	Wavenumber (cm^{-1})	Wavelength (nm)	Wavelength (nm)
C	51786.6	193.10	193.07
O	52083.3	192.04	192.00
	52061.6	192.12	192.08
S	55367.9	180.62	180.73
	54914.9	182.10	182.04
	54782.5	182.54	182.63
P	54147.7	184.68	184.72
	54077.4	184.84	184.92
	53772.1	185.97	185.94
	52960.5	188.82	188.86

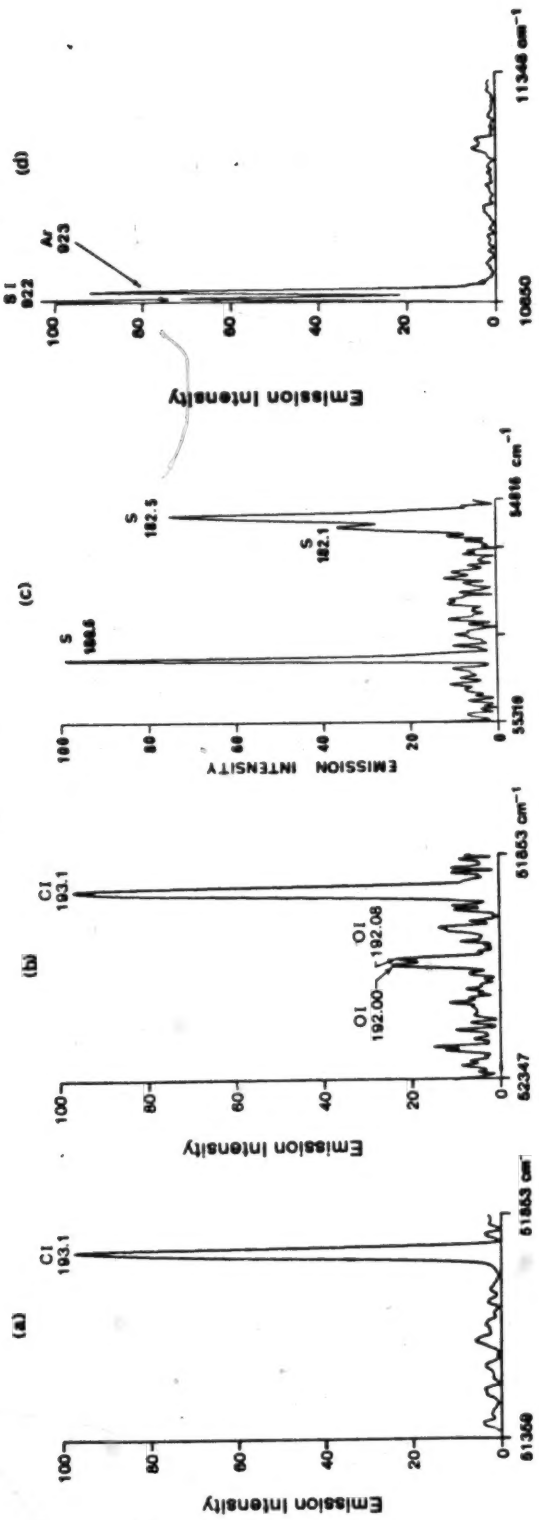

Figure 49. Emission spectra (256 points) of DMSO in the spectral windows: (a) 193 nm, (b) 190 nm, (c) 180 nm and (d) 923 nm.

improved purging system. A second important factor is the stability of the moving mirror drive system. Small variations in the mirror drive become increasingly important as the wavelength decreases. Improvement in the stability of the drive system would almost certainly enhance the response of WSS-FTS at these short wavelengths.

All wavelengths measured below 200 nm have been corrected to vacuum wavelengths. Experimental wavelengths for sulphur, carbon, oxygen and phosphorus are presented in Table 27. Experimental wavelengths were again found to be in agreement with literature wavelengths.

In Chapter III, several sulphur emission lines in the near-infrared spectral region were identified, the most intense being the sulphur triplet at 923 nm. Because of the dynamic range limitations caused by the complex argon background spectrum, the conventional FTS system was not utilized for the analytical determination of sulphur. WSS-FTS could possibly prove to be useful in this spectral region as well as in the ultraviolet and visible regions of the spectrum. The spectrum of the 923 nm window for a 10000 ppm aqueous sulphur solution is illustrated in Figure 49d. The first peak of the sulphur triplet, at 921.7 nm, and the interfering argon line at 922.8 nm, are apparent. It is difficult, even with WSS-FTS, to

eliminate the argon interference due to its close proximity to the sulphur lines. To accomplish this, a much higher resolution interferometer would be necessary.

In this section and in the preceding one, the capabilities of WSS-FTS as a qualitative tool have been demonstrated. Spectral response between 180 nm to 925 nm has been illustrated. In any measurement system, it is also important to be able to correct for background interferences; that is, background subtraction must be viable.

D. Background Subtraction with WSS-FTS

In this section, the background subtraction capabilities of WSS-FTS will be illustrated. The utility of WSS-FTS as an analytical tool will be diminished if the spectral window needs to be exactly identical for the measurement of the background and analyte spectra. That is, it should be possible to slew-scan between spectral windows at the beginning of a series of analyses and acquire background spectra for each window. The analyses can then be performed for each sample. Precise alignment of the monochromator at each spectral window should not be necessary for either the background or the analyte spectrum. Otherwise, the purpose of introducing WSS-FTS has been defeated. To demonstrate background subtraction

with WSS-FTS, the analyte spectra in all cases were measured by setting the monochromator to a spectral window containing the analyte emission of interest. The background spectra were then measured by deliberately changing the spectral window by approximately 0.5 nm.

In the analysis of aqueous solutions in the ICP, the determination of copper at low concentrations using the 327.4 nm line is interfered with by the hydroxyl band at 326.1 nm. Although the 256 point spectrum of the 327 nm spectral window (Figure 45c) does not show the presence of the hydroxyl band, it is clearly present in the 4096 point spectrum (Figure 50a). In the background spectrum of this spectral window (Figure 50b) the hydroxyl band and the two weak emission lines at 324.6 and 323.8 are visible. Background subtraction was performed in the spectral domain and the result is illustrated in Figure 50c. The noise structure on the hydroxyl band in the background and analyte spectra was slightly different, causing some negative spikes (below the average level of the baseline) in the background subtracted spectrum. All three spectra shown in Figure 50 have been plotted on the same intensity scale.

In Figure 42, the 249 nm spectral window was illustrated. In this spectral window, a nitrous oxide band at 248 nm was observed. The intensity of the nitrous

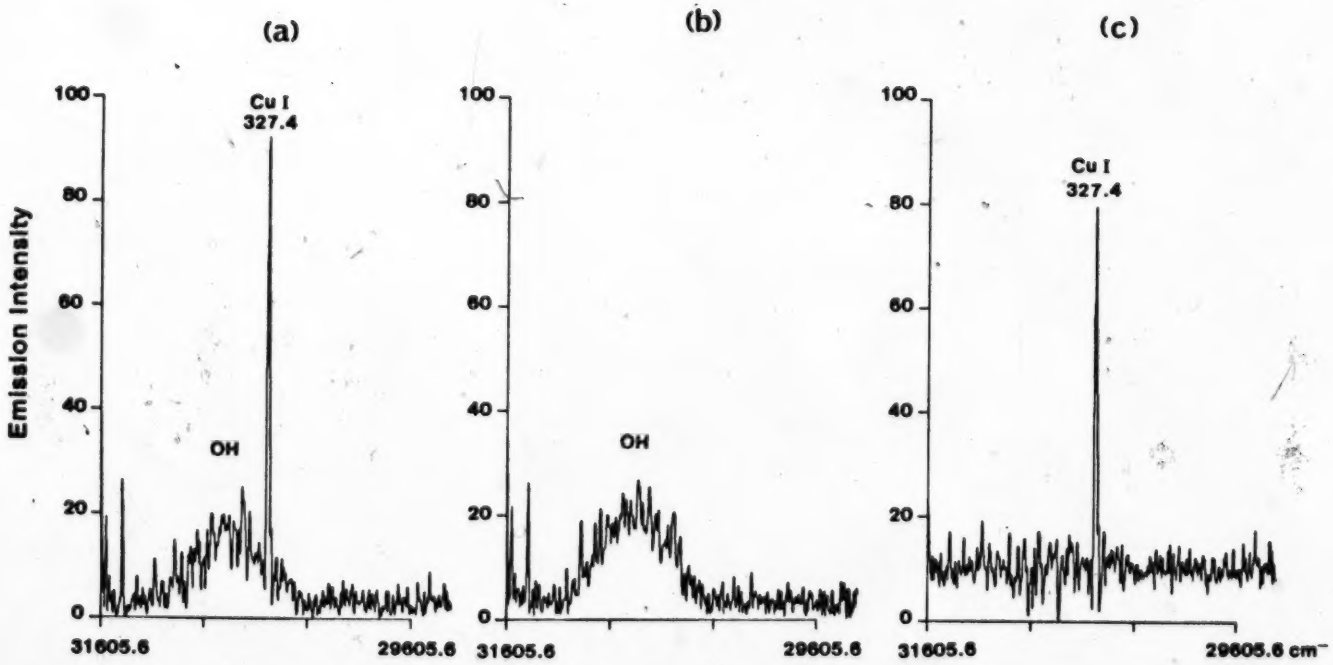

Figure 50. Background subtraction of the hydroxyl band in the 327 nm window: (a) unsubtracted spectrum, (b) background spectrum and (c) subtracted spectrum.

oxide band was weak enough that analysis of boron at 249.8 nm was not affected. To exaggerate the nitrous oxide band in this spectral window and in others, a small amount of air, less than one percent, was introduced into the coolant flow of the plasma. It has been shown [100] that introduction of air into the ICP increases markedly the intensity of nitrous oxide bandheads in the ultraviolet spectral region. The maximum intensities of these bandheads occur at the wavelengths 204.7, 214.9, 226.2, 236.3 and 247.1 nm. It was felt that the background subtraction capabilities of WSS-FTS would be successfully proven if the nitrous oxide band interferences in several of these spectral windows could be essentially eliminated by background subtraction.

With the addition of air into the plasma coolant, the nitrous oxide band intensity in the 250 nm spectral window increased markedly (Figure 51a). The boron doublet at 249.8 nm appeared weakly on the edge of the nitrous oxide band. Figure 51c illustrates the background subtracted spectrum. Background subtraction was not as successful in this instance as it was for the 327 nm window. However, the nitrous oxide band intensity is very weak in the background subtracted spectrum in comparison to the original spectrum (Figure 51a). The carbon emission line at 247.9 nm is apparent in both the background and

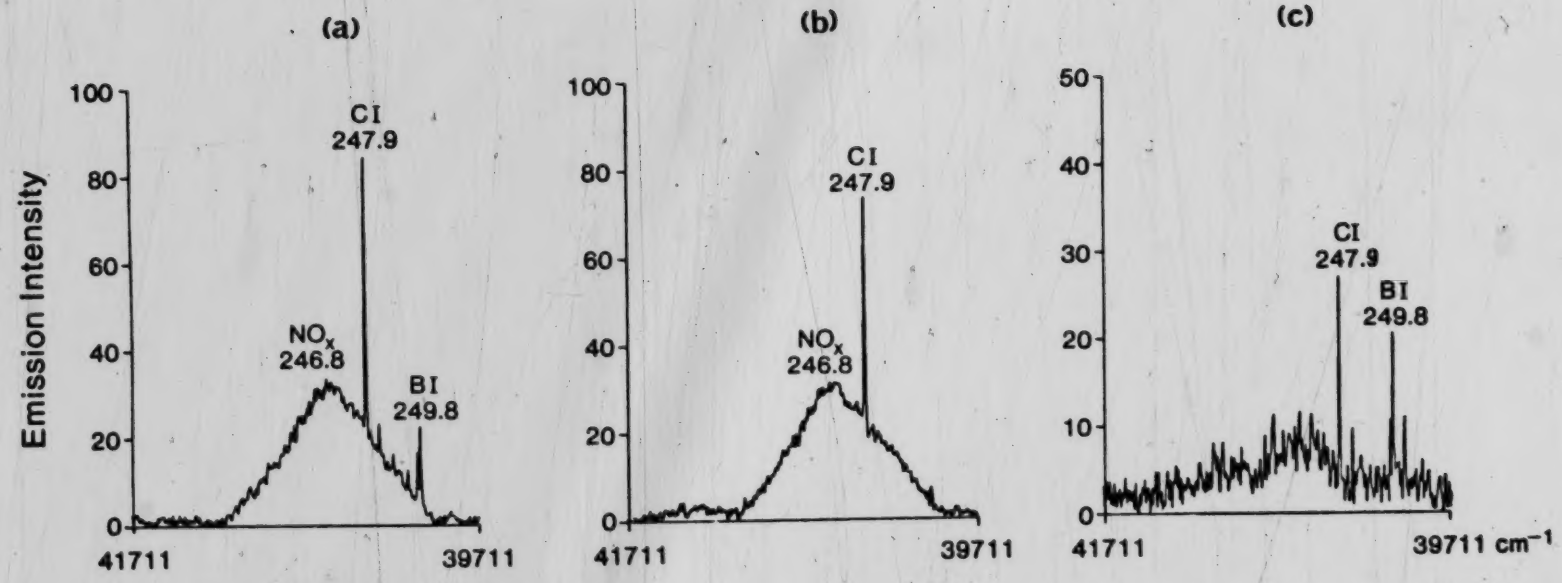

Figure 51. Background subtraction in the 250 nm spectral window: (a) unsubtracted spectrum, (b) background spectrum and (c) subtracted spectrum.

unsubtracted spectra (Figures 51b and 51a) since it is an impurity in argon tanks. In addition, some of the elements in the multielement solution were dissolved as their metal carbonates. It is to be expected that the carbon line would still be present in the background subtracted spectrum, which is indeed the case (Figure 51c).

It is possible to perform background subtraction in the time domain as well as in the spectral domain. In the following two examples, subtraction of the background interferogram from the analyte interferogram was performed. The resultant interferogram was then transformed to obtain the background subtracted spectrum.

In Figure 52, the 215 nm spectral window containing emission lines of both cadmium and zinc is illustrated. Again, 4096 point spectra are necessary to fully observe the broadband nitrous oxide peak. Analyte and background spectra are shown in Figure 52a and 52b. The subtracted spectrum (Figure 52c) shows little evidence of the nitrous oxide band of the unsubtracted background.

In both the copper and boron spectral windows, the presence of molecular emission was not apparent in the 256 point spectral windows. A slightly different case is noted in the 256 point spectra for the 215 nm spectral window. Both the background subtracted and unsubtracted

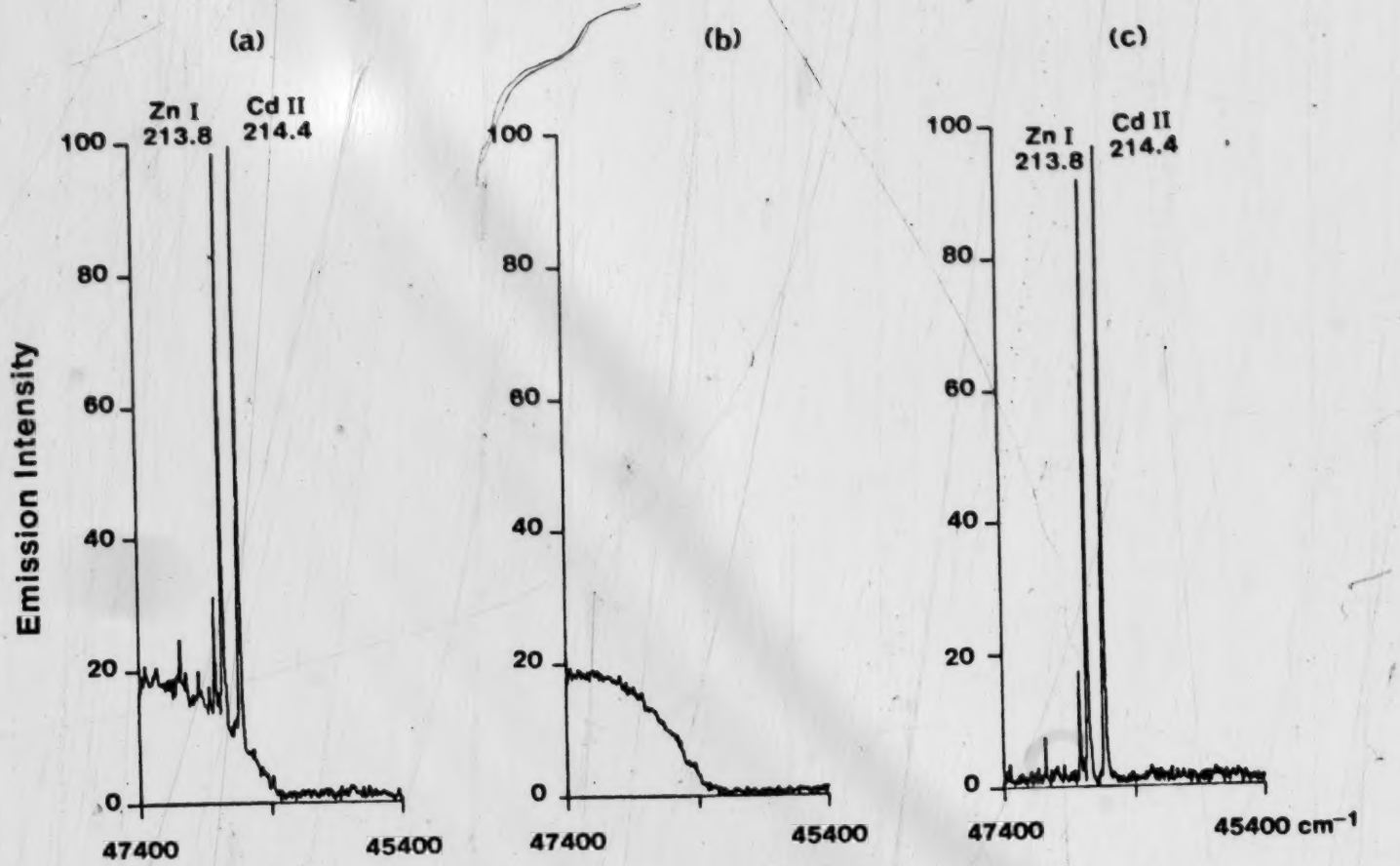

Figure 52. Background subtraction in the 215 nm spectral window, 4096 point spectra: (a) unsubtracted spectrum, (b) background spectrum and (c) subtracted spectrum.

256 point spectra are shown in Figure 53. In Figure 53a, the background subtracted spectrum, both the cadmium and zinc emission lines are observed. However, in the unsubtracted 256 point spectrum shown in Figure 53b, the spectrum is offset from the zero baseline. Although the structure or shape of the nitrous oxide band is not observed in this spectrum, the presence of a broadband spectral feature is indicated.

The final example of background subtraction with the WSS-FTS measurement system involves the 231 nm spectral window (Figure 54). In this spectral window, the intensity of the nitrous oxide band at approximately 229 nm is much weaker than that in the 215 nm and 249 nm spectral windows. In this spectral window, the atomic emission lines observed include the cadmium 228.8 nm line and the nickel 229.7 nm line. Background subtraction was performed in the time domain and was again successful in eliminating the nitrous oxide interference (Figure 54). Having ascertained the qualitative and background subtraction capabilities of WSS-FTS, it is also necessary to demonstrate quantitative determinations with this instrument.

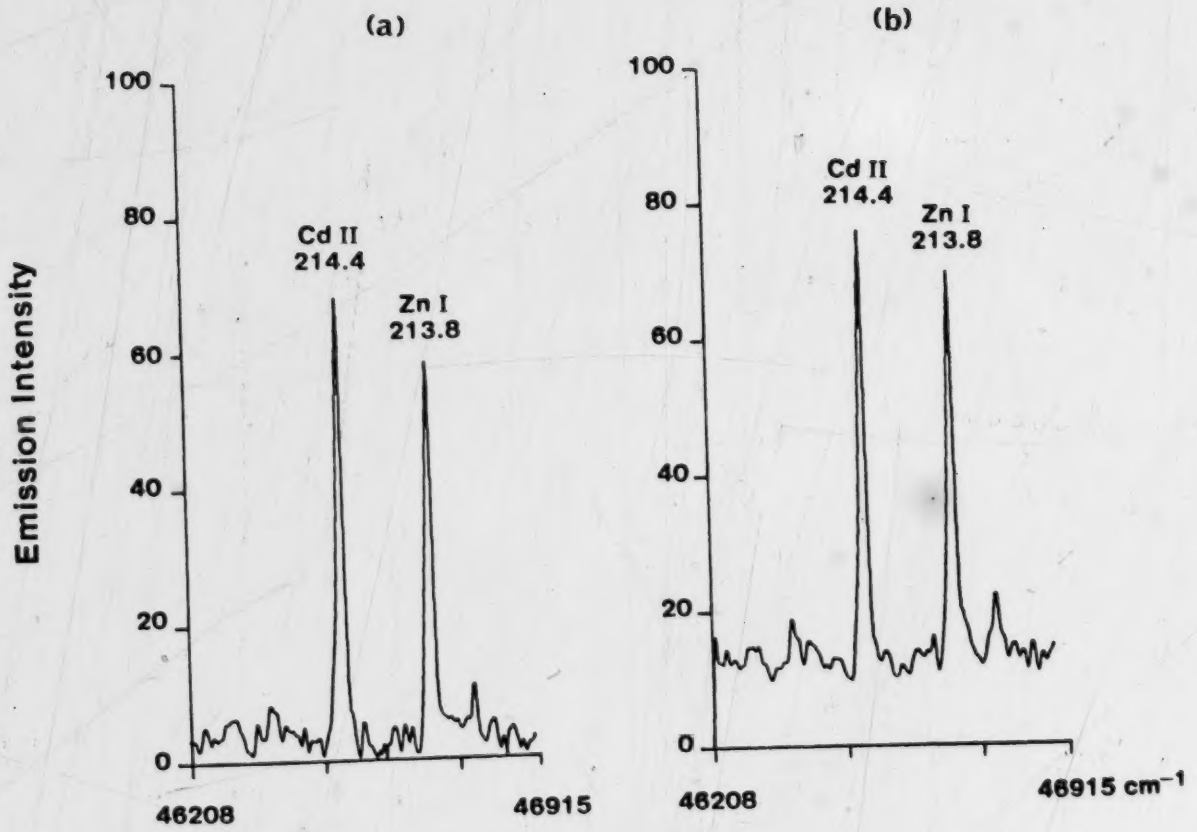

Figure 53. Background subtraction in the 215 nm spectral window, 256 point spectra: (a) subtracted spectrum and (b) unsubtracted spectrum.

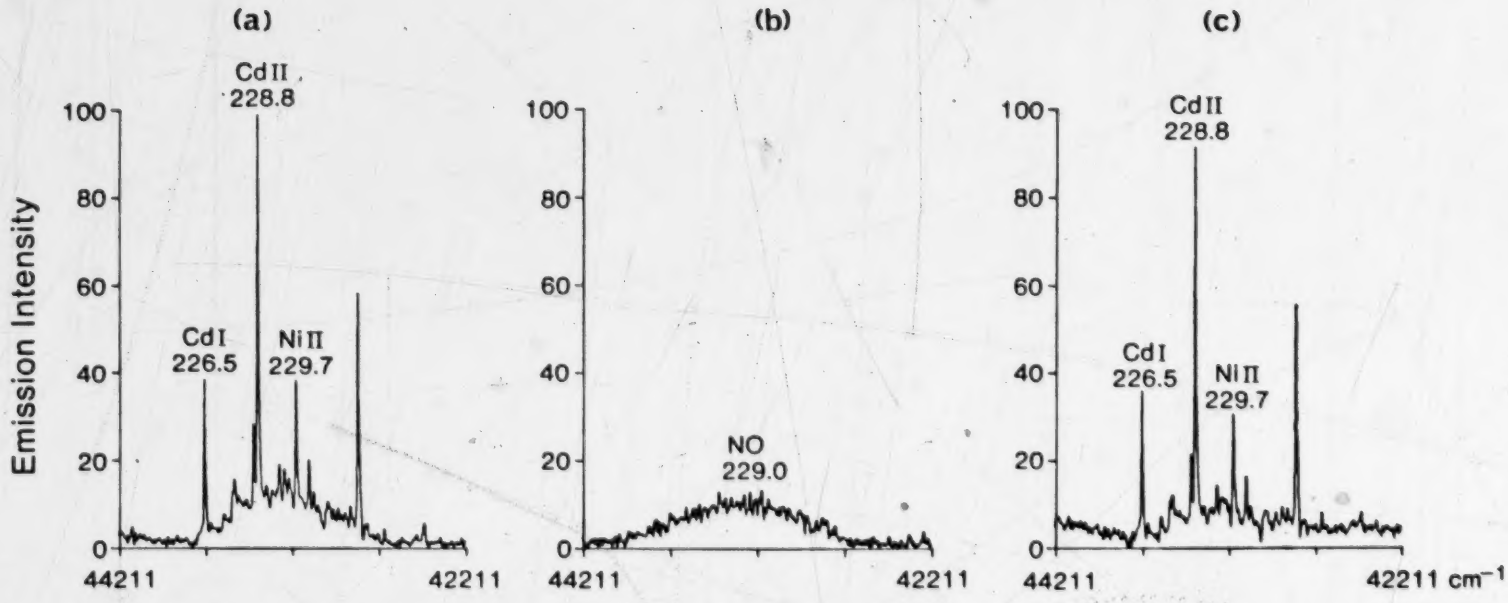

Figure 54. Background subtraction in the 231 nm spectral window: (a) unsubtracted spectrum, (b) background spectrum and (c) subtracted spectrum.

E. Effect of Magnesium on the Determination of Zinc

In order to determine the effectiveness of WSS-FTS in reducing the noise and dynamic range problems, the effect of magnesium concentration on the analytical determination of zinc was again studied. The standard deviation study reported in the last chapter, in the absence of the monochromator, was repeated with the monochromator in the measurement system.

The 4096 point emission spectrum (Figure 55) of a 100 ppm zinc and magnesium solution was measured with the monochromator at zero order. Although the three major magnesium lines in this spectral region are apparent in this spectrum, only the zinc emission line at 213.8 nm is weakly visible. The weak intensities are due to losses in transmission through the monochromator at zero order. Figure 56 shows the 4096 point emission spectrum of the same solution, with the monochromator set at 214 nm. All conditions were kept identical and the spectra in Figure 55 and Figure 56 are plotted on identical emission intensity scales. Only one emission line, zinc at 213.8 nm is present, as expected, in the 214 nm spectral window. The difference in intensities of the zinc emission line in the two spectra, as previously explained, is due to transmission losses in the monochromator. However, a real difference in the noise in the baselines

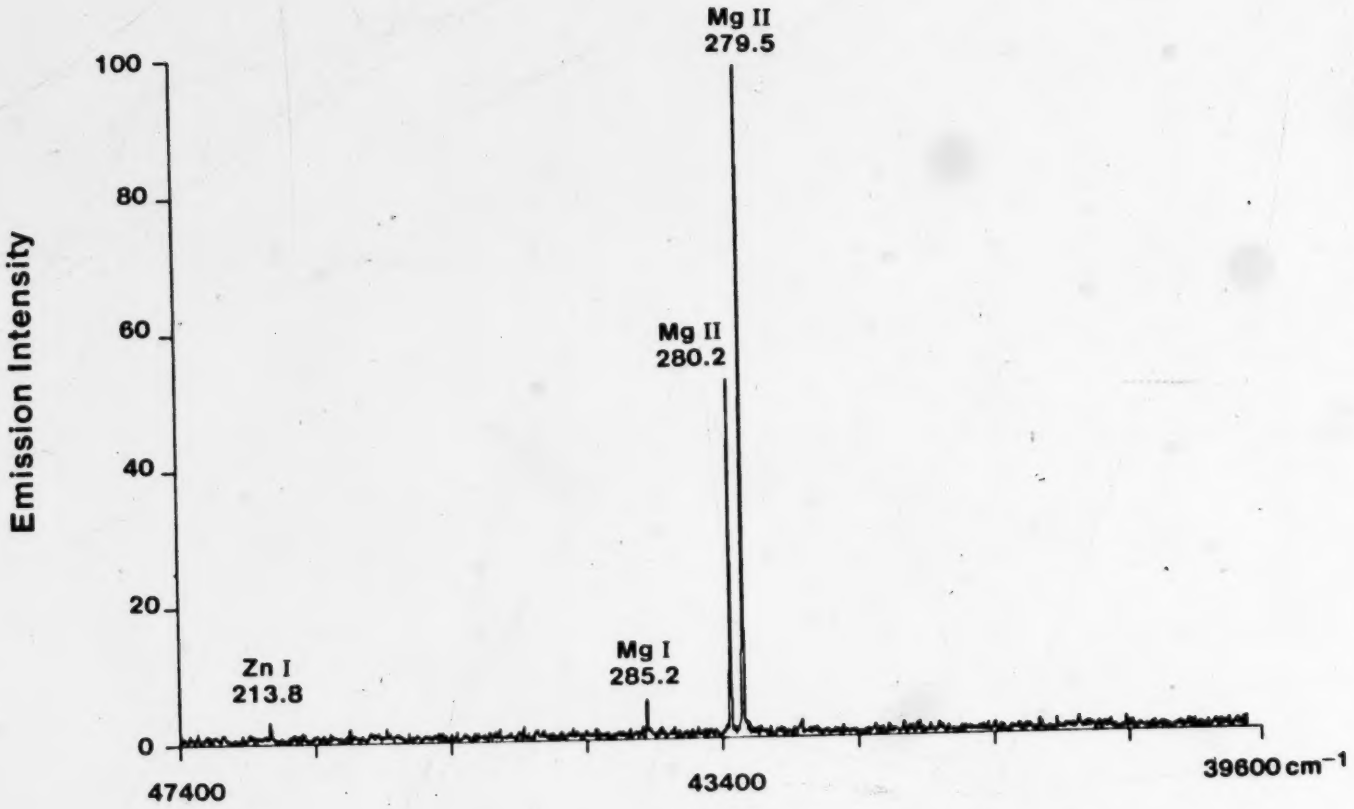

Figure 55. Zero-order emission spectrum of a 100 ppm zinc and magnesium solution.

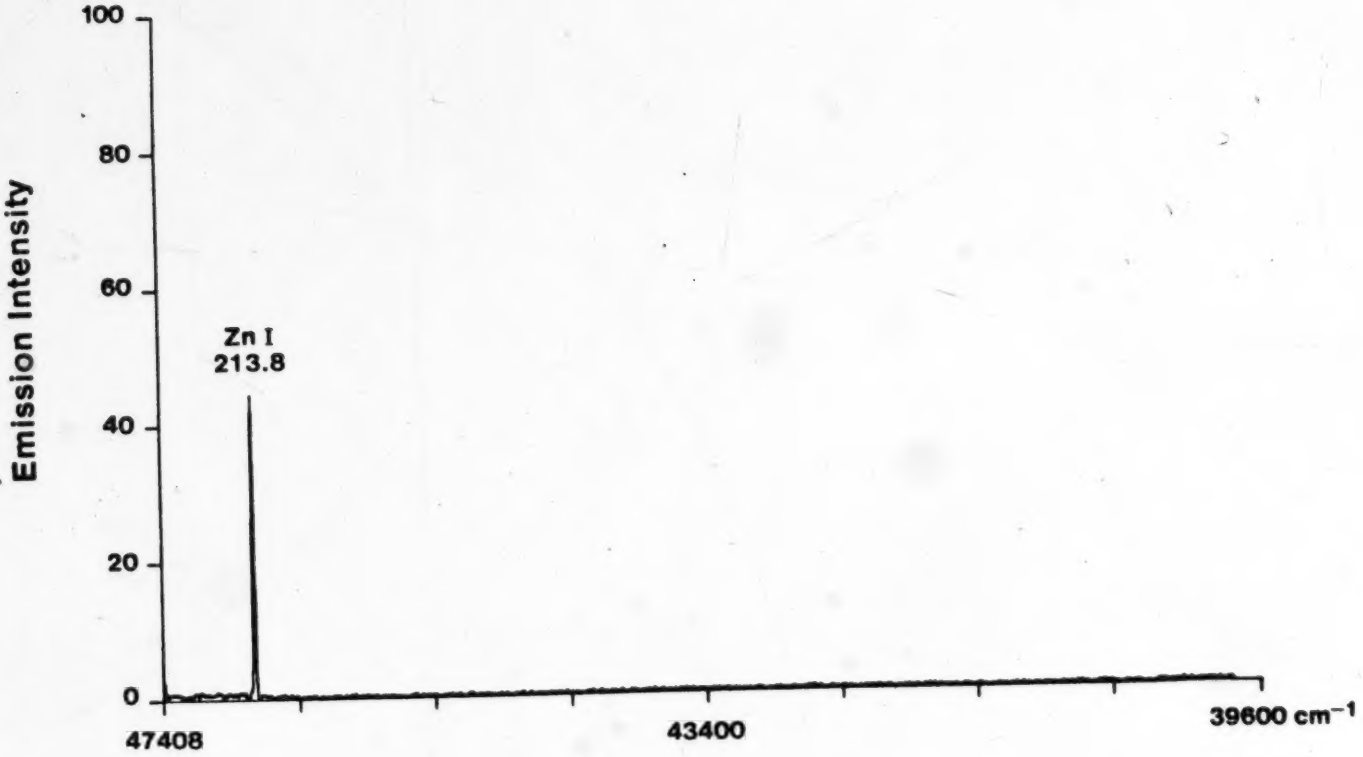

Figure 56. Emission spectrum of a 100 ppm zinc and magnesium solution in the 214 nm spectral window.

of the two spectra can be observed. The noise in the spectrum of the 214 nm window is considerably reduced in comparison to that observed in the zero order spectrum. Qualitatively, WSS-FTS appears then to be effective in reducing the noise limitations of the FTS measurement system.

In a more quantitative fashion, standard deviations of the identical points in the spectrum (4096 points) as described in the last chapter were determined for spectra measured in the 214 nm spectral window. Again, three different solutions with varying magnesium concentrations were aspirated into the ICP. Each solution contained 100 ppm zinc and either 0, 100 or 500 ppm magnesium. The standard deviations obtained were markedly different than those measured in the same study in the absence of the monochromator. In Figure 57 the relationship between the background standard deviation and magnesium concentration with and without the monochromator is illustrated for the spectral point number 116. Without the monochromator, there is a strong dependence of the standard deviation on the magnesium concentration. However, with the monochromator at the 214 nm window, the background standard deviation is virtually independent of the concentration of magnesium in the solutions and is similar in magnitude to the standard deviation of the 100 ppm Zn,

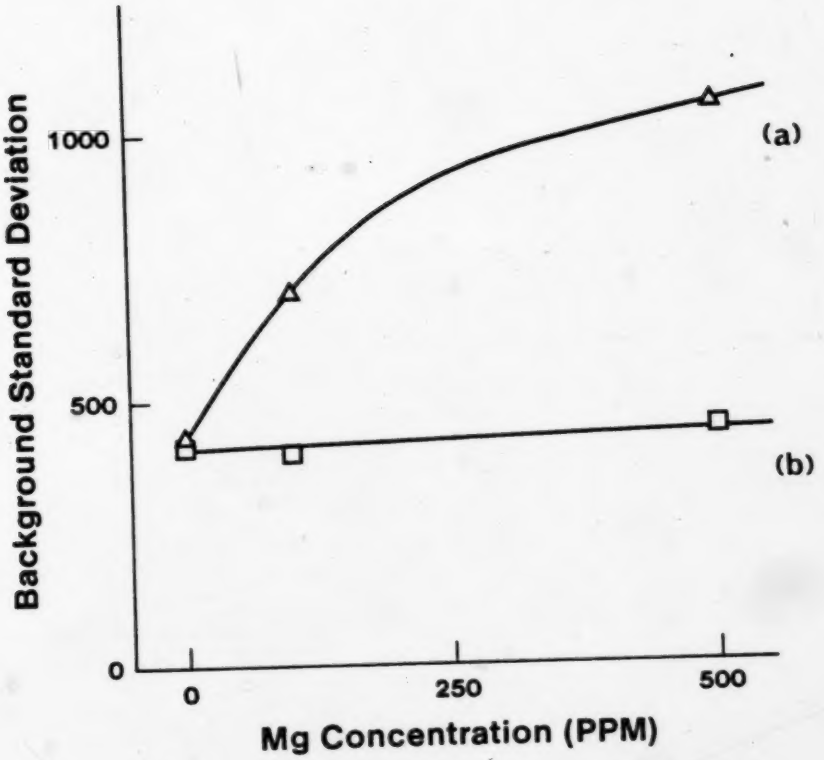

Figure 57. Standard deviations of the baseline point 116 in the presence of varying magnesium concentrations: (a) without monochromator and (b) with monochromator.

0 ppm Mg solution. Table 28 illustrates the standard deviation of the background versus point number in the spectra for these three solutions for: 1) without the monochromator, 2) for the 214 nm spectral window and 3) the 280 spectral window. Again, the standard deviation in the spectrum of the 214 nm window is independent of magnesium concentration. For comparison purposes, the standard deviation of a distilled water background emission spectrum has been included in Table 28. In the spectra measured in the 214 nm spectral window, the standard deviation is higher in the vicinity of the zinc 213.8 nm line than it is in regions far removed from that line. It would be expected that the noise at frequencies within the spectral window would be higher than at frequencies outside that spectral window since restricting the optical bandpass will also limit noise at other frequencies. However, even in the spectral region outside the 214 nm window, the standard deviation of the background does not diminish to the level of the standard deviation of the distilled water emission spectrum. This supports the theory that noise in the FT domain is at least to some extent distributed over the entire spectrum.

Behaviour of the background standard deviation of the spectra in the 280 nm spectral window which includes the intense magnesium lines at 279.5 nm and 280.2 nm is

Table 28

Standard Deviations of the Background as a Function of Magnesium Concentration with WSS-FTS

Point Number	Standard Deviation									
	500 ppm Mg			100 ppm Mg			0 ppm Mg			
	0-order	280 nm window	214 nm window	0-order	280 nm window	214 nm window	0-order	280 nm window	214 nm window	distilled water
116	1042	690	465	701	532	401	452	227	422	235
321	1142	600	508	585	521	423	446	269	476	254
416	1153	632	525	653	567	417	501	307	483	294
2080	1494	1020	279	836	669	297	357	254	247	268
2184	2364	1782	248	970	794	302	392	295	291	233
3516	1172	927	258	693	562	294	399	276	263	278

similar to that obtained for the spectra measured in the absence of the monochromator. Although the standard deviations are smaller in magnitude than those measured by FTS, they are still much higher than those obtained in the 214 nm spectral window. This is indicative of a shot noise or flicker noise limited situation in which the noise is proportional to the signal intensity. Since the zinc emission lines are much weaker than the two intense magnesium lines, a lower noise level would indeed be expected for the 214 nm window than for the 280 nm spectral window.

WSS-FTS has definitely proven to be effective in reducing the noise problem apparent in conventional FTS in the ultraviolet and visible regions of the spectrum. The quantitative abilities of WSS-FTS should therefore represent a marked improvement over those of FTS.

F. Quantitative Analysis with WSS-FTS

Detection limits for all elements were calculated as the concentration necessary to give a signal intensity of twice the standard deviation of a distilled water background for the appropriate spectral window. To ensure complete elimination of noise from outside the spectral window of interest, the frequency bandpass of the Krohn-hite electronic filter, described in Chapter II, was

limited to include only those frequencies contained in each spectral window. All detection limits were determined using 4096 point interferograms of the 10 ppm multielement solution described in Chapter V.

The 256 point spectra were not utilized due to the poorer S/N ratio previously described in those spectra as compared to the 4096 point spectra. As well, comparison between detection limits obtained with conventional FTS and with WSS-FTS are facilitated, since it was necessary to use 4096 point spectra with the FTS measurement system. It is also possible to rationalize use of the 4096 point spectra on a consideration of current computer technology. In contrast to the computer available in this laboratory which cannot transform a 4096 point interferogram on the reverse scan of the moving mirror, state-of-the-art computer technology can easily accomplish this. Transformation of a 4096 point interferogram would, with such a system, be trivial in comparison to the same process with the computer used in this study.

The detection limits obtained with WSS-FTS as the measurement system are presented in Table 29. Included in this table, in addition to the detection limits, are the analytical wavelength and the detector used in each analysis. For the analysis of aluminum, two wavelengths were used to determine a detection limit. For the

Table 29

Detection Limits as Measured with WSS-FTS

Element	Wavelength (nm)	Detection Limits (ppb) 1P28	RF66	Si	% RSD
Al	396.2	99			0.6
	309.3	82			1.2
B	249.7		10		1.0
Ba	455.4	0.9			0.5
Ca	393.3	0.4			0.7
Cd	226.4		8		0.6
	214.3		12		0.8
Cu	324.7	19			1.5
Fe	259.9	11	6		0.9
K	766.5			95	2.1
Mg	279.1	7	4		0.9
Mn	257.6	12	7		1.0
Na	589.6	135			2.3
Ni	226.9		26		1.6
Pb	216.9		26		1.3
	220.7		18		0.8
Si	288.1	32			1.8
V	309.2	5			1.1
Zn	213.8		7		0.6

aluminum 396.15 nm line, it was necessary to close the entrance and exit slits of the monochromator to 100 μm to avoid spectral interferences from the two neighbouring calcium lines. The detection limit obtained for aluminum was slightly poorer with this analytical line than for that calculated using the weaker 309.3 nm emission line as the analytical wavelength. This difference could possibly be attributed to the loss in throughput created by decreasing the slit widths in the monochromator.

It was possible to determine detection limits for iron, magnesium and manganese with both the 1P28 and the solar blind PMT (Table 29) at the same analytical wavelength. For these three elements, with analytical wavelengths shorter than 300 nm, detection limits were consistently poorer with the 1P28 PMT than with the solar blind PMT as the detector. The increases in the measured detection limits can be attributed to the decrease in the spectral response of the 1P28 PMT at wavelengths below 300 nm in comparison to the solar blind PMT.

For the alkali metals, sodium and potassium, detection limits were poor. In the plasma, the spatial profile [5] for these elements is different than those of other metals. Consequently, the optimum viewing zone for sodium and potassium emission in the plasma is higher, approximately 20 mm above the load coil, than that chosen

for this study. This could be a contributing factor in the poor detection limits obtained for these elements.

In addition to detection limits, an important parameter is the relative standard deviation, a measure of precision, of the signal intensity used to calculate the detection limits. Relative standard deviations have been calculated for all sixteen elements and have been included in Table 29. Relative standard deviations ranged between 0.5% for barium and 2.3% for sodium, compared to the 3% to 5% relative standard deviations obtained with the conventional FTS measurement system.

In addition to the multielement solution, detection limits were determined for sulphur at both 180.7 nm and at 921.7 nm. For the vacuum wavelength, a detection limit of 18.6 ppm was obtained. This detection limit is comparable to, but not significantly better than, the detection limit reported in Chapter IV for the monochromator-silicon photodiode measurement system and is orders of magnitude poorer than the 20 ppb detection limits reported [106] for the 180.73 nm sulphur line. In the near-IR region, the detection limit measured with WSS-FTS and a silicon photodiode was 226 ppm. This detection limit is significantly poorer than those attained at 180.7 nm and the best results reported in Chapter IV. The dynamic range limitations imposed by the neighbouring argon line

(Figure 49) could possibly account for most of this discrepancy.

G. Conclusions

A comparison of detection limits obtained with the conventional FTS system and with the technique of WSS-FTS is shown in Table 30. Without exception, the detection limits obtained with the WSS-FTS measurement system were superior to those of the FTS measurement system. In addition, detection limits were obtained for some elements, in particular iron, nickel, sodium and vanadium, that were not even observed in the multielement spectra measured with the conventional FTS system. Potassium was excluded from Table 30 since its emission line at 766 nm was outside the spectral range measured with the FTS system.

A more important type of comparison might be between detection limits measured by WSS-FTS and by other types of measurement systems for ICP emission. In comparison to detection limits obtained with the photodiode array spectrometer [59] developed in this laboratory, WSS-FTS yields improved detection limits. For example, with the PDA spectrometer, detection limits for nickel and zinc were 300 and 50 ppb while with WSS-FTS as the measurement system, detection limits were 26 and 6 ppb, representing an order of magnitude improvement.

Table 30

A Comparison of Detection Limits Obtained by Conventional FTS and WSS-FTS

Element	DETECTION LIMITS (PPB)			
	1P28		R166	
	WSS-FTS	FTS	WSS-FTS	FTS
Al	82	-		
B			10	62
Ba	0.9	77		
Ca	0.4	16		
Cd			8	48
Cu	19	-		
Fe	11	-	6	-
Mg	7	58	4	5
Mn	12	145	7	17
Na	135	-		
Ni		-	26	-
Pb			18	130
Si	32	-		
V	5	-		
Zn			7	37

In comparison to the "state-of-the-art" detection limits, as represented by the commercial ICP instrument available in this laboratory, WSS-FTS compared favourably. Results are tabulated for both measurement systems in Table 31. Only elements for which the same analytical wavelengths were used in both instruments have been included in this table. Although the detection limits obtained with the commercial instrument were consistently superior to those measured with WSS-FTS, in most cases the detection limits were similar in magnitude. With the exception of copper, manganese and sodium, the detection limits measured by WSS-FTS were within a factor of two or three of those measured with the commercial instruments. For both sodium and manganese, the detection limits were an order of magnitude different. No explanation for this discrepancy is apparent. Although the viewing zone in the ICP was not the optimum zone for the analysis of sodium and potassium, a similar viewing zone was utilized in the commercial instrument. If this were a factor, the detection limit for potassium would have been an order of magnitude poorer as well.

WSS-FTS has proven to be successful in reducing the problems of the conventional FTS measurement system in the ultraviolet and visible spectral regions in both a

Table 31

Comparison Between Detection Limits Obtained by WSS-FTS and by a Commercial ICP Instrument

Element	Detection Limits (ppb)	
	WSS-FTS	ARL 34000
B	10	3
Ba	0.9	0.7
Cd	8	2
Cu	19	3
Fe	6	2
K	95	89
Mn	7	0.7
Na	135	14
Si	32	23
Zn	7	4

qualitative and quantitative sense. In fact, the quantitative capabilities of this instrument are comparable to those of a commercial instrument (Table 31), thus providing a viable alternative to the direct reader based measurement system.

The simultaneous wavelength measurement capability of WSS-FTS within a particular spectral window facilitates the identification of spectral interferences, while at the same time, the slew-scanning capability of this instrument provides a facile method of alternate analytical wavelength selection.

Both background and analyte emission can be easily measured with WSS-FTS and the background subtraction capabilities in both the frequency and time domain have been demonstrated. It is important to note that the spectral window for the background and the analyte emission spectra can be different by as much as 0.5 nm and still attain successful background subtraction.

The main drawback to this approach is the increase in data acquisition time. The time necessary for data acquisition for one element is identical to the time necessary to acquire the multielement spectra with conventional FTS. In that same period of time, a direct reader instrument easily provides quantitative information for ten to fifteen elements.

It is felt that the applicability of windowed slew-scan Fourier transform spectrometry to the measurement of atomic spectrochemical information has been amply demonstrated in this chapter. In the future, WSS-FTS should prove to be a viable alternative to conventional dispersive-based measurement systems employed for the measurement of ICP emission.

CHAPTER VII

SUMMARY

The Fourier transform spectrometer has been shown in this thesis to be a viable alternative for the measurement of atomic spectrochemical information.

In the near-infrared spectral region, a qualitative investigation of emission from the ICP provided spectral information previously unobserved with the ICP. Both the ICP background spectra, for 100% argon and several mixed gas ICP's, and analyte emission spectra for nonmetal elements were characterized in this region. Several potentially useful analytical lines for the elements carbon, sulphur, oxygen, chlorine and bromine, were identified.

With the spectral information provided by the interferometer, a quantitative determination of sulphur was carried out using a monochromator-based detection system with several different detectors. A monochromator-silicon photodiode combination was found to be most effective. A detection limit of 20 ppm was calculated with this detection system.

For trace analysis, the near-infrared spectral region has limited usefulness for analyses with the ICP. However, it is often necessary to analyze for nonmetal elements at relatively high concentration levels, in the order of one percent. At these concentration levels, analysis in the near-infrared region can be effectively employed.

Conventionally, measurement of emission of the ICP in the ultraviolet and visible spectral regions has been accomplished using dispersive-based measurement systems. The possibility of a signal-to-noise disadvantage has discouraged most researchers from attempting FTS in these spectral regions.

With an interferometer especially developed for the ultraviolet spectral region, emission from the ICP was measured. Response of the interferometer was found to extend to 180 nm in the vacuum ultraviolet region and to at least 925 nm in the near-infrared region of the spectrum.

For quantitative analysis, the conventional FTS measurement system was found to have limited capabilities in the ultraviolet and visible spectral regions. Both noise and dynamic range limitations have been presented and discussed. To circumvent these problems, a new instrument, a windowed slew-scan Fourier transform

spectrometer, has been introduced. This instrument combines the advantages of the interferometer and the slew-scanning monochromator while limiting their disadvantages.

WSS-FTS, capable of simultaneously measuring emission in any 4 nm spectral window, was found to be effective in reducing both the dynamic range and the noise limitations of conventional FTS. Flexibility of the instrument is provided by the slew-scanning monochromator while accurate wavelength identification and simultaneous multielement measurement is provided by the interferometer. The spectral characteristics and capabilities of this instrument were presented. Detection limits were calculated with WSS-FTS that were comparable to those obtained with a commercial direct reader based ICP instrument.

Although slew-scanning between spectral windows was accomplished manually for the purpose of this research, automatic microprocessor-controlled slew-scanning could be easily implemented. This would facilitate the measurement of both background and analyte emission spectra. Elements of interest in any particular analysis could be chosen and the appropriate spectral windows could be implemented under software control. Automation could go one step further. By measuring the entire spectral region at zero

order, a qualitative determination of elements in the sample could be accomplished. Based on this information, the computer or microprocessor could choose the appropriate spectral windows to obtain quantitative information. With the shorter transforms necessary for WSS-FTS, it should also be possible to perform real-time or "on-the-fly" transforms. This was actually attempted with the PDP-11/10 available in this laboratory. However, even with a 256 point transform, data could only be taken on every fourth scan of the moving mirror. Acquisition of a newer and faster computer would allow real-time transforms. In this case, the spectral information would be available immediately after data acquisition had been completed.

The current configuration of WSS-FTS is probably not the optimum configuration. As mentioned previously, there are a large number of optical surfaces involved in this instrument, which reduces the throughput into the interferometer. As well, it should be possible to devise a more compact version of WSS-FTS. Although this would not be an overly expensive instrument to construct, a more compact system should also decrease the cost of the instrument.

Future configurations of WSS-FTS could incorporate a decrease in the number of optical surfaces. For example,

in the instrument developed in this laboratory, a collimating lens was placed after the monochromator. But within the monochromator itself (Figure 37), collimated light is available after the grating. Modification of the monochromator to redirect this collimated light directly into the interferometer would decrease by one the number of optical surfaces in WSS-FTS. A schematic of this instrument is illustrated in Figure 58.

An even simpler, more compact instrument could be conceived. This system is depicted in Figure 59 and would eliminate completely the need for lenses in the optical coupling between the ICP and the interferometer. In this instrument, only the dispersive element from the monochromator, the grating, would be necessary. An off-axis parabolic mirror could be utilized to provide collimated light incident from the source to the grating. Light diffracted at the grating would then be incident directly into the interferometer. Positioning of the grating, to measure emission in the desired spectral window, would be difficult at first, but would become easier as the positions for different spectral windows were identified. This would provide a very compact instrument with a minimum number of optical surfaces, thus minimizing the decrease in throughput.

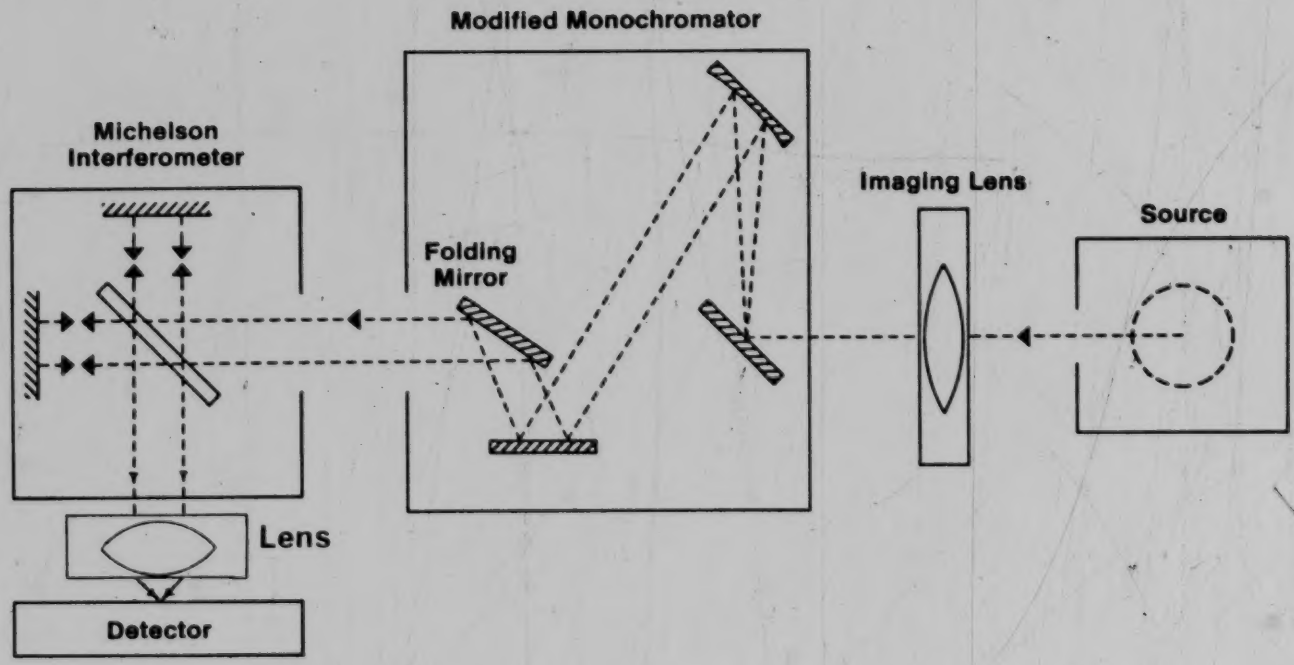

Figure 58. Schematic diagram of a WSS-FTS instrument with a modified monochromator.

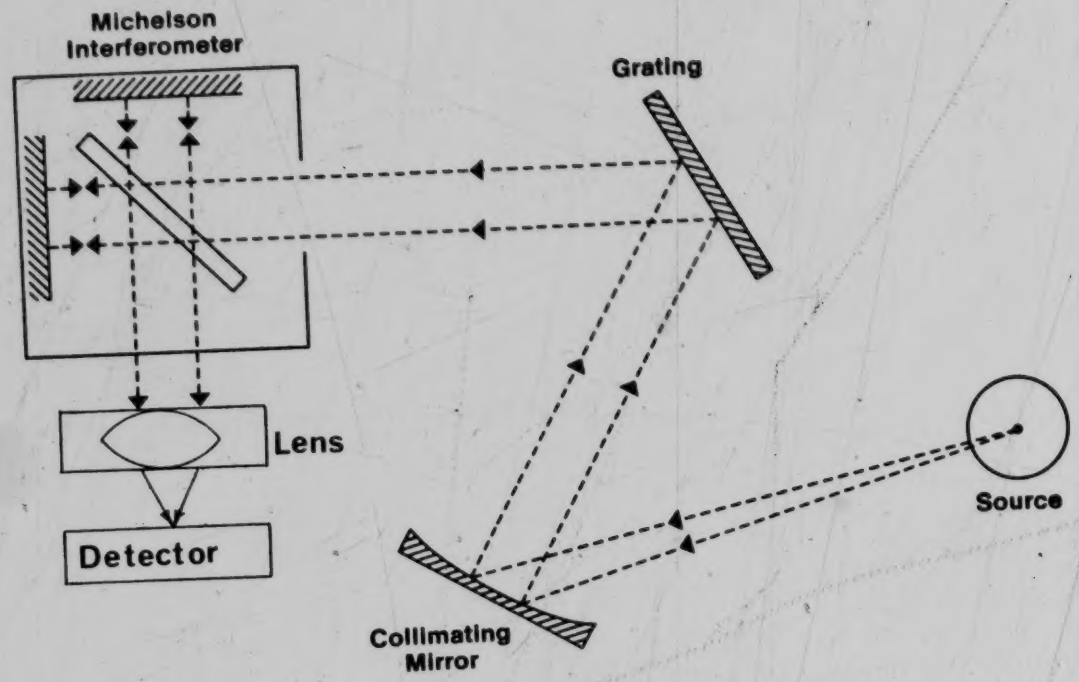

Figure 59. Schematic diagram of a WSS-FTS instrument incorporating only a grating and collimating optics.

The potential of windowed slew-scan Fourier transform spectrometry to compete favourably with conventional dispersive-based measurement systems for the measurement of ICP emission has been demonstrated in this thesis. Its low cost, flexibility and excellent measurement capabilities will promote and enhance the use of Fourier transform spectrometry as an atomic spectrochemical measurement system in the ultraviolet and visible regions of the spectrum.

FOOTNOTE

1. For energy transitions between two electron configurations, there is usually more than one transition between any two configurations. For example, for a 3^2S to 3^2P configuration, there are two transitions: $3^2S_{1/2}$ to $3^2P_{3/2}$ and $3^2S_{1/2}$ to $3^2P_{1/2}$. Often, the resolution of the interferometer was insufficient to resolve these different transitions. In these cases, the literature wavelength quoted in the wavelength tables is an average of the wavelengths associated with each transition.

BIBLIOGRAPHY

1. V.A. Fassel, Anal. Chem. 51, 1290A (1979).
2. G.R. Kornblum and L. de Galan, Spectrochim. Acta 29B, 249 (1974).
3. P.W.J.M. Boumans and F.J. de Boer, Spectrochim. Acta 32B, 365 (1977).
4. M.W. Blades and G. Horlick, Appl. Spectrosc. 34, 969 (1980).
5. M.W. Blades and G. Horlick, Spectrochim. Acta 36B, 881 (1981).
6. Y. Nojiri, K. Tanabe, H. Uchida, H. Haraguchi, K. Fuwa and J.D. Winefordner, Spectrochim. Acta 38B, 61 (1983).
7. P.W.J.M. Boumans and F.J. de Boer, Spectrochim. Acta 30B, 309 (1975).
8. R.K. Winge, V.A. Fassel, R.N. Kniseley, E. DeKalb and W.J. Haas, Spectrochim. Acta 32B, 327 (1977).
9. R.N. Merryfield and R.C. Lloyd, Anal. Chem. 51, 1965 (1979).
10. G.F. Wallace, Atomic Spectrosc.2, 87 (1981).
11. N. Furuta and G. Horlick, Spectrochim. Acta 37B, 53 (1982).

12. G.R. Kornblum and L. de Galan, Spectrochim. Acta 32B, 71 (1977).

13. R.D. Reeves, S. Nikdel and J.D. Winefordner, Appl. Spectrosc. 34, 477 (1980).

14. B. Smets, Analyst 105, 482 (1980).

15. A.M. Gunn, D.L. Millard and G.F. Kirkbright, Analyst 103, 1066 (1978).

16. D.R. Hull, Ph.D. Thesis, University of Alberta, 1981.

17. J.W. Carr and G. Horlick, Spectrochim. Acta 37B, 1 (1982).

18. W.E. Pettit and G. Horlick, 8th Annual FACCS Conference, Philadelphia, PA., 1981, Paper No. 54A.

19. W.E. Pettit and G. Horlick, Pittsburgh Conference on Analytical Chemistry and Applied Spectroscopy, Atlantic City, 1983, Paper No. 151.

20. V.A. Fassel, Anal. Chem. 51, 1290A (1979).

21. P.N. Keliher and C.C. Wohlers, Anal. Chem. 48, 333A (1976).

22. A. Strasheim, M.E. Thain, N.M. Walters, C. Claase, H.G.C. Human and N.P. Ferreira, Spectrochim. Acta, in press.

23. R.G. Evans and G. Horlick, Pittsburgh Conference on Analytical Chemistry and Applied Spectroscopy, Atlantic City, 1982, Paper No. 441.

24. R.G. Evans and G. Horlick, CIC Conference, Calgary, 1983, Paper No. AN7-2.

25. G. Horlick, Appl. Spectrosc. 30, 113 (1976).

26. Y. Talmi and R.W. Simpson, Appl. Opt. 19, 1401 (1980).

27. N. Furuta, Ph.D. Thesis, University of Tokyo, 1979.

28. D.G. Mitchell, K.W. Jackson and K.M. Aldous, Anal. Chem. 45, 1215A (1973).

29. M.F. Tompsett, G.F. Amelio and G.E. Smith, Appl. Phys. Lett. 17, 111 (1970).

30. G. Horlick, 10th International Conference on Atomic Spectroscopy, Amsterdam, 1983, Paper No. 391.

31. A.L. Gray, Analyst 100, 289 (1975).

32. R.S. Houk, V.A. Fassel, G.D. Flesch, H.J. Svec, A.L. Gray and C.E. Taylor, Anal. Chem. 52, 2283 (1980).

33. R.S. Houk, H.J. Svec and V.A. Fassel, Appl. Spectrosc. 35, 380 (1981).

34. D.J. Douglas and J.B. French, Anal. Chem. 53, 37 (1981).

35. D.J. Douglas and E.S.K. Quan, Pittsburgh Conference on Analytical Chemistry and Applied Spectroscopy, Atlantic City, 1983, Paper No. 402.

36. D.J. Douglas, E.S.K. Quan and R.G. Smith, Spectrochim. Acta 38B, 39 (1983).

37. G. Horlick, Ph.D. Thesis, University of Illinois, 1969.

38. W.K. Yuen, Ph.D. Thesis, University of Alberta, 1978.

39. R.H. Hall, Ph.D. Thesis, University of Alberta, 1979.

40. G.H.C. Freeman, Opt. Commun. 14, 274 (1975).

41. G.H.C. Freeman, Opt. Commun. 4, 66 (1971).

42. W.A. Hilton, Amer. J. Phys. 40, 629 (1972).

43. T.L. Chester and J.D. Winefordner, Anal. Chem. 49, 113 (1977).

44. L. Mertz, Transformations in Optics, John Wiley and Sons, Inc., New York, 1965.

45. P. Connes and G. Michel, Appl. Opt. 14, 2067 (1975).

46. J.W. Brault, J. Opt. Soc. Amer. 66, 1081 (1976), 1976 Annual Meeting, Paper No. TuJ3.

47. J. Davis and T.M. Rynne, Amer. J. Phys. 45, 166 (1977).

48. H. Buijs, Pittsburgh Conference on Analytical Chemistry and Applied Spectroscopy, Atlantic City, 1983, Paper No. 898.

49. H. Buijs, CIC Conference, Calgary, 1983, Paper No. PH 11-1.

50. B.A. Palmer, L.M. Faires and R. Engleman, Pittsburgh Conference on Analytical Chemistry and Applied Spectroscopy, Atlantic City, 1983, Paper No. 401.

51. L.M. Faires, B.A. Palmer and R. Engleman, Pittsburgh Conference on Analytical Chemistry and Applied Spectroscopy, Atlantic City, 1983, Paper No. 403.

52. L.M. Faires, B.A. Palmer and R. Engleman, Pittsburgh Conference on Analytical Chemistry and Applied Spectroscopy, Atlantic City, 1983, Paper No. 404.

53. R. Engleman, L.M. Faires and B.A. Palmer, Pittsburgh Conference on Analytical Chemistry and Applied Spectroscopy, Atlantic City, 1983, Paper No. 405.

54. H.R. Griem, Plasma Spectroscopy, McGraw-Hill, New York, 1964.

55. P.R. Griffiths, Chemical Infrared Fourier Transform Spectroscopy, John Wiley and Sons, New York, 1975.

56. J. Chamberlain, The Principles of Interferometric Spectroscopy, John Wiley and Sons, New York, 1979.

57. A. Girard and P. Jacquinot, Advanced Optical Techniques, A.C.S. Van Heel, editor, North Holland Publishing Co., Amsterdam, 1967, pp. 71-109.

58. M.H. Tai and M. Harwit, Appl. Spectrosc. 30, 68 (1976).

59. E.D. Salin and G. Horlick, Anal. Chem. 52, 1578 (1980).

60. J.D. Winefordner, R. Avni, T.L. Chester, J.J. Fitzgerald, L.P. Hart, D.J. Johnson and F.W. Plankey, Spectrochim. Acta 31B, 1 (1976).

61. T. Hirschfeld, Appl. Spectrosc. 30, 68 (1976).

62. A.S. Filler, J. Opt. Soc. Am. 63, 589 (1973).

63. T.L. Chester, J.J. Fitzgerald and J.D. Winefordner, Anal. Chem. 48, 793 (1976).

64. R.F. Knacke, Appl. Opt. 17, 684 (1978).

65. P. Luc and S. Gerstenkorn, Appl. Opt. 17, 1327 (1978).

66. S. Marra and G. Horlick, CIC Conference, Calgary, 1983, Paper No. PH 26-3.

67. W.K. Yuen and G. Horlick, Anal. Chem. 49, 1446 (1977).

68. Y. D'astous and M. Blanchard, Am. J. Phys. 50, 464 (1982).

69. G. Horlick and G.M. Hieftje, "Correlation Methods in Chemical Data Measurement" in Contemporary Topics in Analytical and Clinical Chemistry, Vol. 3, D.M. Hercules, G.M. Hieftje, L.R. Snyder and M.A. Evenson, Eds., Plenum, New York, 1978.

70. R.C. Ng and G. Horlick, Spectrochim. Acta 36B, 529 (1981).

71. R.C. Ng and G. Horlick, Spectrochim. Acta 36B, 543 (1981).

72. G. Horlick, R.H. Hall and W.K. Yuen, "Atomic Emission Spectrochemical Measurements with a Fourier Transform Spectrometer" in Fourier Transform

Infrared Spectroscopy, Vol. III, J.R. Ferraro, L.J. Basile and A. Mantz, Eds., Academic Press Inc., New York, 1982, pp. 37-81.

73. R.R. Williams, unpublished data.

74. L.A. Leventhal, 6502 Assembly Language Programming, Osborne/McGraw-Hill, Berkeley, California, 1979.

75. A.N. Zaidel, V.K. Prokof'er, S.M. Raiskii, V.A. Slavnyi and E.Ya. Schreider, Table of Spectral Lines, IFI/Plenum Publishers, New York, 1970, 3rd edition.

76. D.L. Windsor and M.B. Denton, J. Chrom. Sci. 17, 492 (1979).

77. D.L. Windsor and M.B. Denton, Appl. Spectrosc. 32, 366 (1978).

78. A.J. McCormack, S.S.S. Tong and W.D. Cooke, Anal. Chem. 37, 1470 (1965).

79. C.A. Bache and D.J. Lisk, Anal. Chem. 37, 1477 (1965).

80. C.A. Bache and D.J. Lisk, Anal. Chem. 39, 786 (1967).

81. B.D. Quimby, P.C. Uden and R.M. Barnes, Anal. Chem. 50, 2112 (1978).

82. R.H. Dagnall, S.J. Pratt, T.S. West and R. Deans, Talanta 16, 797 (1969).

83. D.L. Windsor and M.B. Denton, Anal. Chem. 51, 1116 (1979).

84. S.J. Northway, R.M. Brown and R.C. Fry, Appl. Spectrosc. 34, 338 (1980).

85. R.M. Brown and R.C. Fry, Anal. Chem. 53, 532 (1981).

86. S.J. Northway and R.C. Fry, Appl. Spectrosc. 34, 332 (1980).

87. S.K. Hughes and R.C. Fry, Appl. Spectrosc. 35, 493 (1981).

88. S.K. Hughes and R.C. Fry, Anal. Chem. 53, 1111 (1981).

89. R.C. Fry, S.J. Northway, R.M. Brown and S.K. Hughes, Anal. Chem. 52, 1716 (1980).

90. S.K. Hughes, R.M. Brown and R.C. Fry, Appl. Spectrosc. 35, 396 (1981).

91. M.W. Blades and M. Decker, Pacific Conference on Chemistry and Spectroscopy 1982, San Francisco, California, Paper No. 91 (1982).

92. M.W. Blades and P. Hauser, submitted for publication.

93. E.A. Stubley and G. Horlick, Pittsburgh Conference on Analytical Chemistry and Applied Spectroscopy, Atlantic City, 1982, Paper No. 425.

94. E.A. Stubley and G. Horlick, Appl. Spectrosc., in press.

95. S. Bashkin and J.O. Stoner, Jr., Atomic Energy Levels and Grotrian Diagrams, Vol. 1 and 2, North Holland, Amsterdam, 1975.

96. P.E. Charters and J.C. Polanyi, Can. J. Chem. 38, 1742 (1960).

97. E.H. Choot and G. Horlick, Pittsburgh Conference, Atlantic City, New Jersey, Paper No. 124 (1981).

98. S. Greenfield, I.L. Jones, H.M. McGeachen and P.B. Smith, Anal. Chim. Acta 74, 225 (1975).

99. A. Montaser and J. Mortazavi, Anal. Chem. 52, 225 (1980).

100. E.H. Choot, Ph.D. Thesis, University of Alberta, 1983.

101. J. Jarosz and J.M. Mermet, J. Quant. Spectrosc. Radiat. Transfer 17, 237 (1977).

102. R.D. Gordon and G.W. King, Can. J. Phys. 39, 252 (1961).

103. G. Henrion, D. Marquardt and G. Rietz, Z. Chem. 18, 263 (1978).

104. R.G. Winkel, J.L. Hunt and M.J. Clouter, J. Chem. Phys. 50, 1298 (1969).

105. M.E. Jacox and D.E. Milligan, J. Chem. Phys. 53, 2688 (1970).

106. T. Shimanouchi and I. Suzuki, J. Mol. Spectrosc. 6, 227 (1961).

107. R.M. Belchamber, Ph.D. Thesis, University of Alberta (1981).

108. R.M. Belchamber and G. Horlick, Spectrochim. Acta 37B, 17 (1982).

109. D. Wallace, Alberta Research Council, private communication.

110. J.G. Speight and S.E. Moschopedis, "The Influence of Crude Oil Composition on the Nature of the Upgrading Process: Athabasca Bitumen", 1st International Conference on the Future of Heavy Crude and Tar Sands, Edmonton, Alberta, 1979.

111. ASTM method D2747-72.

112. Jarrell-Ash Inc., "Analysis of Coal and Coal Fly Ash by Inductively Coupled Argon Plasma", Applications Note No. A21, 1982.

113. T. Hayakawa, F. Kikui and S. Ikeda, Spectrochim. Acta 37B, 1069 (1982).

114. H.N. Olsen, Phys. Rev. 124, 1703 (1961).

115. A. Batal, J. Jarosz and J.M. Mermet, Spectrochim. Acta 36B, 983 (1982).

116. E.A. Stubley and G. Horlick, CIC Conference, Calgary, 1983, Paper No. PH 26-4.

APPENDIX I

APPENDIX I

AIM 65 CONTROL PROGRAM FOR THE INTERFEROMETER

The program listed here was written in the AIM 65 assembly language. A flow chart (Figures 60 and 61) has been included to aid in understanding the program. It might also be helpful to refer to Figure 5 and the program description in Chapter II. Some comments have been included in the program listing to make interpretation easier.

```
* = $0900        ; program starting address

LDA #$A0         ; sets timer 2 to count laser pulses
                 ; on PB6
STA $A00B        ; and timer 1 to generate pulses on
                 ; PB7.

LDA #$11         ; sets so that interrupts occur on
STA #A00C        ; positive transitions of CA1 and CB1

LDA #$03         ; initialize port A
STA $A003
STA $A001        ; set start and stop flags (Bit 0 and
                 ; 1 on Port A) high.

LDA #$80         ; initialize port B
STA $A002
STA #A000        ; dummy write to clear interrupts

LDX #$00         ; initialize for indexed addressing
LDY #$00

LDA #$FF         ; initialize timer 2 and start
                 ; counting
STA $0040,X      ; load with maximum delay count
STA $0050,Y
```

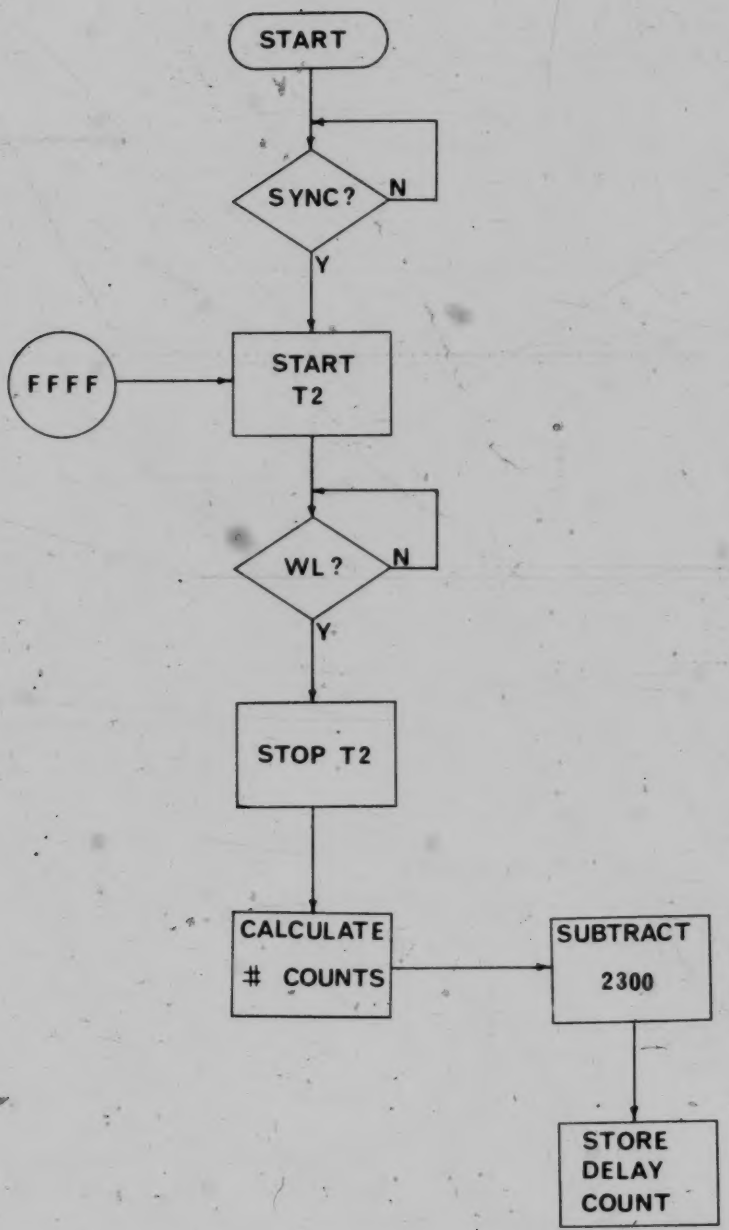

Figure 60. Flow chart for the initial portion of the program to generate the control signals for the PDP-11/10.

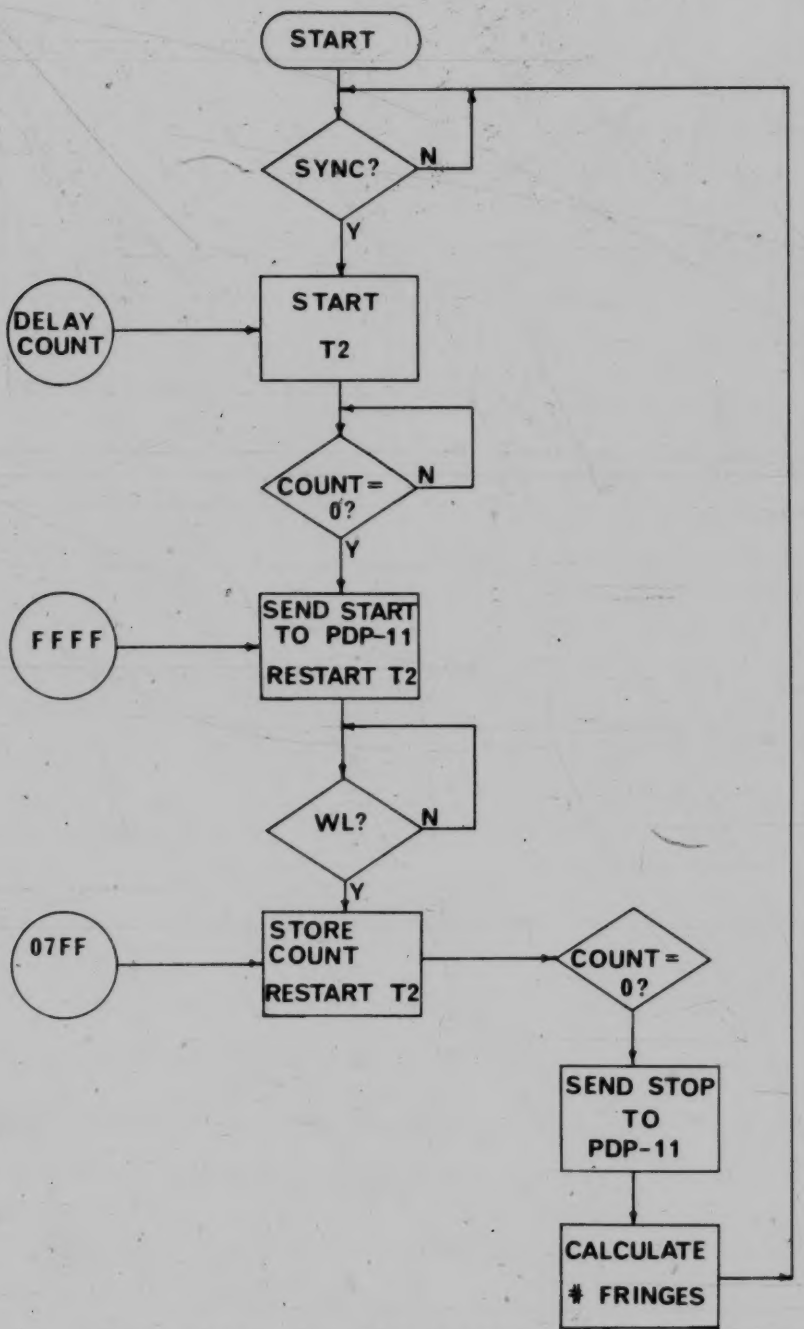

Figure 61. Flow chart for the program used to generate the control signals for the PDP-11/10.

```
        JSR SYNC        ; wait for sync pulse on CA1
        JSR WL          ; count pulses between zync and white
                        ; light
        JSR SUBTR       ; figure out delay count
        LDA $0050,Y
        SBC #$80

        STA $0040,X
        LDA $0050,Y
        SBC #$09
        STA $0050,Y     ; store delay count
                        ; are now ready to generate stop and
                        ; start
START   JSR SYNC        ; wait for interrupt of sync pulse
        LDA $A001       ; clears interrupts

PULSE   LDA #$20        ; check for end of delay count
        BIT $A00D
        BEQ PULSE
        LDA #$01        ; send start pulse (PA1) to PDP-11
        STA $A001
        LDA #$FF        ; start timer 2 counting again
        STA $A008
        STA $A009
        INX
        INY
        JSR WL          ; wait for white light
        LDA #$FF        ; load timer 2 with 2047 (2048
        STA $A008       ; counts)
        LDA #$07
        STA $A009
        LDA $A001       ; clear interrupts

STOP1   LDA #$20        ; check for end of 2048 counts
        BIT $A00D
        BEQ STOP1

        LDA $A001       ; send stop pulse (PA0) to PDP-11
        STA #A004       ; load timer 1 with count
        LDA #$04        ; for length of start and stop pulses
        STA $A005
STOP2   LDA #$40
        BIT $A00D
        BEQ STOP2
        LDA #$03        ; terminate stop and start pulses
        STA $A001
        JSR SUBTR       ; figure out # of data points
        LDA $0050,Y     ; acquired
        ADC #$08
```

```
        STA $0050,Y
        DEX
        DEY
        JMP START       ; return for next scan

SYNC    LDA #$02        ; wait for sync
        BIT $AOOD
        BEQ SYNC
        LDA $0040,X     ; load timer 2 with delay
        STA $A008       ; count
        LDA $0050,Y
        STA $A009
        LDA $A000
        LDA $A001
        RTS

WL      LDA #$10        ; wait for white light
        BIT $A00D
        BEQ WL
        LDA $A008       ; stop timer 2
        STA $0040,X
        LDA $A009
        STA $0040,Y
        LDA $A001
        LDA $A000
        RTS
SUBTR   SEC             ; to figure out number of
        LDA #$FF        ; counts timer 2 has counted
        SBC $0040,X
        STA $0040,X
        LDA #$FF
        SBC $0050,Y
        STA $0050,Y
        RTS
FINI    BRK
```